CHEMICAL ABUNDANCES OF OPEN CLUSTERS USING *THE CANNON*: APPLICATION TO IMPROVE CALIBRATION OF ASTEROSEISMIC AGES

by

AMY E. RAY

Bachelor of Science, 2013
Mississippi State University
Mississippi State, MS

Master of Science, 2017
Mississippi State University
Mississippi State, MS

Submitted to the Graduate Faculty of the
College of Science and Engineering
Texas Christian University
in partial fulfillment of the requirements
for the degree of

Doctor of Philosophy

December 2022

CHEMICAL ABUNDANCES OF OPEN CLUSTERS USING *THE CANNON*: APPLICATION TO IMPROVE CALIBRATION OF ASTREOSEISMIC AGES

by

Amy E. Ray

Dissertation Approved:

Peter M. Frinchaboy III

Kat Barger

Yuri Strzhemechny

Hana Dobrovolny

For The College of Science and Engineering

ACKNOWLEDGEMENTS

I would like to thank Dr. Frinchaboy for being an excellent advisor.

Thank you fellow graduate students, my committee, my parents, and my puppy Andromeda "Annie" Ray.

I would like to acknowledge grant support for this research from the National Science Foundation (AST-1311835 & AST-1715662).

Funding for SDSS-III has been provided by the Alfred P. Sloan Foundation, the Participating Institutions, the National Science Foundation, and the U.S. Department of Energy Office of Science. The SDSS-III web site is http://www.sdss3.org/.

SDSS-III is managed by the Astrophysical Research Consortium for the Participating Institutions of the SDSS-III Collaboration including the University of Arizona, the Brazilian Participation Group, Brookhaven National Laboratory, Carnegie Mellon University, University of Florida, the French Participation Group, the German Participation Group, Harvard University, the Instituto de Astrofisica de Canarias, the Michigan State/Notre Dame/JINA Participation Group, Johns Hopkins University, Lawrence Berkeley National Laboratory, Max Planck Institute for Astrophysics, Max Planck Institute for Extraterrestrial Physics, New Mexico State University, New York University, Ohio State University, Pennsylvania State University, University of Portsmouth, Princeton University, the Spanish Participation Group, University of Tokyo, University of Utah, Vanderbilt University, University of Virginia, University of Washington, and Yale University.

Funding for the Sloan Digital Sky Survey IV has been provided by the Alfred P. Sloan Foundation, the U.S. Department of Energy Office of Science, and the Participating Institutions. SDSS-IV acknowledges support and resources from the Center for High-Performance Computing at the University of Utah. The SDSS web site is www.sdss.org.

SDSS-IV is managed by the Astrophysical Research Consortium for the Participating Institutions of the SDSS Collaboration including the Brazilian Participation Group, the Carnegie Institution for Science, Carnegie Mellon University, the Chilean Participation Group, the French Participation Group, Harvard-Smithsonian Center for Astrophysics, Instituto de Astrofísica de Canarias, The Johns Hopkins University, Kavli Institute for the Physics and Mathematics of the Universe (IPMU)/University of Tokyo, Lawrence Berkeley National Laboratory, Leibniz Institut für Astrophysik Potsdam (AIP), Max-Planck-Institut für Astronomie (MPIA Heidelberg), Max- Planck-Institut für Astrophysik (MPA Garching), Max-Planck- Institut für Extraterrestrische Physik (MPE), National Astronomical Observatories of China, New Mexico State University, New York University, University of Notre Dame, Observatário Nacional/MCTI, The Ohio State University, Pennsylvania State University, Shanghai Astronomical Observatory, United Kingdom Participation Group, Universidad Nacional Autónoma de México, University of Arizona, University of Colorado Boulder, University of Oxford, University of Portsmouth, University of Utah, University of Virginia, University of Washington, University of Wisconsin, Vanderbilt University, and Yale University.

This work has made use of data from the European Space Agency (ESA) mission *Gaia* (https://www.cosmos.esa.int/gaia), processed by the *Gaia* Data Processing and Analysis Consortium (DPAC, https://www.cosmos.esa.int/web/gaia/dpac/consortium). Funding for the DPAC has been provided by national institutions, in particular the institutions participating in the *Gaia* Multilateral Agreement.

This research made use of Astropy, a community-developed core Python package for Astronomy (Astropy Collaboration, 2018).

Contents

List of Figures

List of Tables

List of Common Acronyms and Terms in Astronomy

- Metals – All elements heavier than hydrogen and helium
- Metallicity – The mass fraction of metals in a star with respect to hydrogen
  - [Fe/H] – Often used as a proxy for metallicity in stellar spectroscopic studies
  - $[\mathrm{Fe/H}] = \log(\mathrm{Fe/H})_{\mathrm{star}} - \log(\mathrm{Fe/H})_{\odot}$
- dex – Decimal exponent (deprecated)
  - Unit used for abundance value (e.g. [Fe/H] = 0.06 dex)
- LTE – Local Thermal Equilibrium
  - Statistical thermal equilibrium
- Å – Angstrom; 10^{-10} m
- λ – Wavelength, usually in Å
- ly – 1 lightyear = 9.46 x 10^{12} km
- kpc – 1000 parsecs; 1 parsec (pc) = 3.262 ly
- Main Sequence star – Star fusing hydrogen (H) to helium (He) in its core
- APOGEE – Apache Point Observatory Galactic Evolution Experiment
- SDSS – Sloan Digital Sky Survey
- J, K_s – The near-infrared magnitudes taken from APOGEE
- $J - K_s$ – Difference between magnitudes, also known as the color index
- IRAF – Image Reduction and Analysis Facility

Chapter 1

Introduction

Three women of the famous Harvard Computers, Cecilia Payne, Annie Jump Cannon, and Henrietta Leavitt, have undoubtedly had some of the biggest influences on modern astronomy today. Payne's doctoral thesis in 1925 was the first to describe abundances of elements in the Sun and other stars based on work by Meghnad Saha (Payne 1925). Despite prominent astronomer Henry Norris Russell opposing her findings and directing her to remove them from her thesis, Payne correctly showed that stars were composed of mostly hydrogen and helium with trace amounts of heavier elements. Annie Jump Cannon, whom Payne collaborated with, was one of the first astronomers to classify stars based on their spectral features and temperatures which gave astronomy the spectral classes still used today of O, B, A, F, G, K, M. Finally, Henrietta Leavitt was the first to describe a period-luminosity relationship for pulsating variable stars known as Cepheids (Leavitt & Pickering 1912). This discovery made it possible for other influential astronomers Edwin Hubble and Harlow Shapley to determine the distance to objects outside of the Milky Way for the first time, expanding the size of the known universe.

The research by these three women is still applicable to current research in astronomy, especially research on the evolution of the Milky Way. Modern spectroscopic studies use the principles founded by Payne and Cannon to examine properties such as the chemical enrichment history of the galaxy. While Leavitt's work is mainly used as one of the fundamental parts of the cosmic distance ladder, she was also one the first to examine radial pulsations in stars by studying how it's light changed over time. This technique is currently used in the field of asteroseismology to determine other pulsation modes in addition to radial pulsations. The pulsation modes themselves allow astronomers to

determine properties of stars such as mass and relative age. In this paper, we combine these principles of spectroscopy as well as asteroseismology to study the ages of stars.

1.1 Spectroscopy

One incredibly important stellar parameter obtained from stars is their chemical abundance or metallicity. It is a measure of the proportion of elements heavier than hydrogen or helium in a star's atmosphere. There are a few ways that these elements are produced. The first is from massive stars. They are able to produce these elements over their short lifetimes in their cores and, when they die, through core collapse supernovae. These elements are dispersed by the supernova into the interstellar medium to be Incorporated into the next generation of stars Lower mass stars can also produce heavier elements if the star becomes a white dwarf and is in a binary system with another star. If the white dwarf accretes mass from the companion it can produce a type Ia supernova that also enriches the surrounding medium, although this has a larger timescale than the massive stars. These heavier elements build up in stars over generations meaning metallicity can begin to yield information on chemical enrichment history and stellar ages. This proportion is commonly expressed as the ratio of iron to hydrogen, or [Fe/H]. The expression is given below as

$$[Fe/H] \equiv \log_{10}\left(\frac{N_{Fe}}{N_H}\right)_{\star} - \log_{10}\left(\frac{N_{Fe}}{N_H}\right)_{\odot}. \tag{1.1}$$

The $\odot$ indicates the value for the Sun and the $\star$ indicates the value for the star in question and N_{Fe} is the number of iron atoms and N_H is the number of hydrogen atoms.

This ratio can be determined by examining iron absorption lines and then comparing to the known solar iron abundance. The unit used to describe metallicity is referred to as the dex, which refers to a 'decade' or 'orders of magnitude'. Stars with a dex of 0 have metallicities the same abundance of the element as the Sun. For a dex of +1.0, stars have a metallicity 10 times greater than that of the Sun, and for a dex of −1.0, it is 1/10th of the Sun's value. Iron is not the only element that is useful. A slightly different comparison is used for the abundance of other elements. These abundances are commonly expressed as the ratio of a certain element to iron, [X/Fe], with regard to the iron to hydrogen ratio,

$$[X/Fe] \equiv \log_{10}\left(\frac{N_X}{N_H}\right)_\star - \log_{10}\left(\frac{N_X}{N_H}\right)_{star} - \quad [Fe/H]_{star}. \tag{1.2}$$

This abundance also has the unit of dex and N_X is the number density of a given element. This switch to be relative to iron is that most elements enrich in roughly equal relative amounts in metal-rich stars, like the Sun, such that any difference in [X/Fe] shows differing enrichment from how the Sun was enriched. However, to be able to track accurately the rate of enrichment over time, we need a way to measure the ages of stars.

Open clusters lie in the disk of the Milky Way and consist of up to several hundred to several thousand stars. They are ideal for studying stellar ages because the stars in an open cluster formed from the same gas cloud at the same time, and the stars are considered to have the same distance from our solar system. Ages of clusters can be determined from what is known as the main sequence turn off. The main sequence is where a star begins fusing hydrogen into helium inside of its core and it is illustrated on

an H-R diagram as a continuous line. Image (1.1) shows the evolution of a cluster where all of the stars begin on the main sequence, and as time continues, the stars move to the right of the main sequence starting from higher mass and going to lower mass.

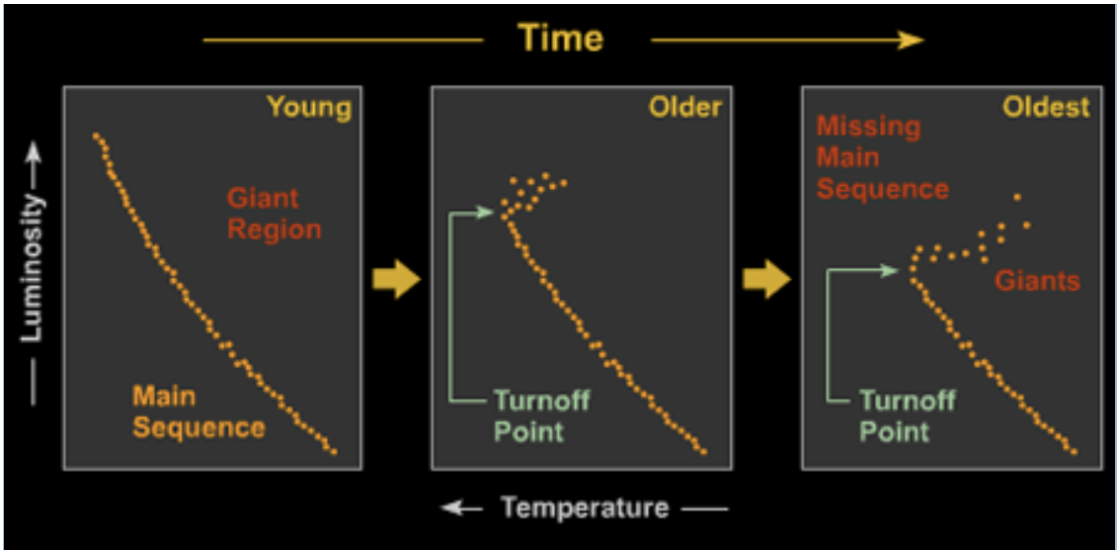

Figure 1.1: Illustration of the evolution of a star cluster. The panel on the left shows a new cluster with all of its stars on the main sequence. As the cluster ages, the higher mass stars begin to move above and to the right of the main sequence. This trend continues as mass decreases and time increases.

The parameters (T_{eff}, log g, and metallcity) are the basis for stellar evolution models. A set of stellar evolution models of different masses, but with a fixed age form an isochrone, or a line of equal age, which can be compared/calibrated against star clusters. Observed distributions of stars are sensitive to log g and T_{eff} therefore model stellar flux distributions can be fit to them to find these parameters.

In order to calibrate cluster age estimates to individual stellar parameters using high-resolution spectroscopy, several characteristics in addition to metallicity, log g or surface gravity (density) and effective surface temperature T_{eff}, need to be determined. These parameters are measured by analysis of individual spectral lines in a star. The first step is to determine how the strength of a spectral line increases with optical depth in a star.

This is called the curve of growth. Next, the equivalent width of a line can be determined and used with the Boltzmann and Saha equations to get elemental abundances. Finding abundances for different ionizations of the same element can better constrain the values for log g and T_{eff}. This method has been used for nearly 100 years, but can be slow and is therefore not feasible for analysis of modern large-scale surveys.

The Cannon is a machine learning method that can quickly determine chemical abundances, log g and T_{eff} for a large number of stars, based on calibration to a well understood training set. How *The Cannon* works is described in Section 2.2.

1.2 Asteroseismology Background

1.2.1 How Asteroseismology Works

Asteroseismology is the study of how waves propagate through stars. There are two different types of waves, pressure (acoustic) waves and gravity waves. For stars like the Sun, pressure waves are commonly found in the outer regions of the star where convection occurs. Gravity waves are found in the inner parts of the star that contain the core and the radiative layer outside of the core (Kurtz et al. 2016). Examples of these two types and where they would be found in a solar-like star are shown in Figure 1.2. This means that if modes of both of these types of waves can be identified for a given star, valuable information about the internal structure can be determined. There are also two different types of modes that occur in stars, radial and non-radial. Both cause the surface of the star to expand and contract which corresponds to the surface of the star becoming

cooler and hotter as well as brighter and dimmer. After observing a star's flux over time, known as either a photometric timeseries or light curve, the light curve can be represented as a power spectrum through Fourier transform. The resulting frequency range can be examined to find where and how the star is oscillating. Examples of a light curve and a power spectrum are shown in Figure 1.3

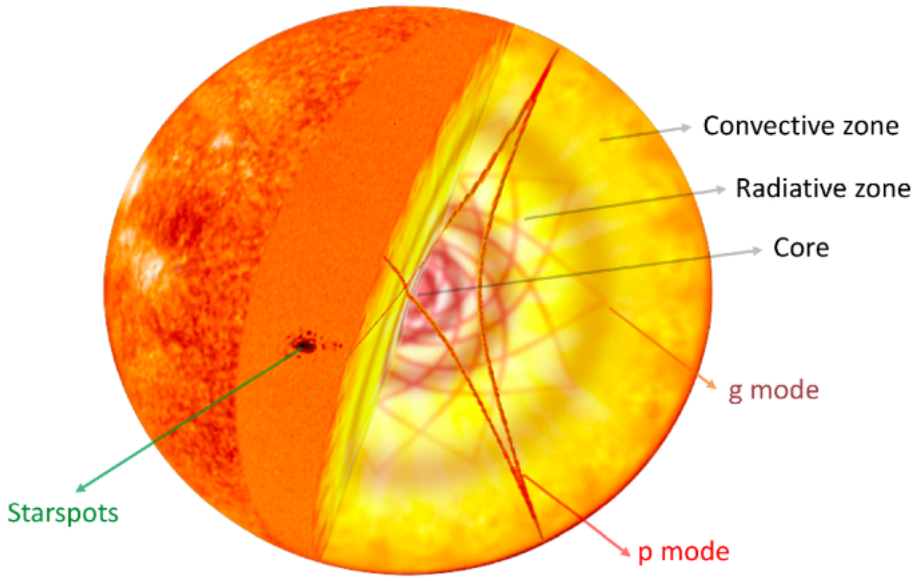

Figure 1.2: This diagram shows where both p modes and g modes are commonly found inside of a star like the Sun. P modes mostly travel in the outer layers where convection is the main energy transportation and g modes primarily travel through the inner layers and the core where radiation transport dominates. This figure is courtesy of (García & Ballot 2019).

Since stars can be approximated as spherically symmetrical objects, resonance frequencies can be described using spherical harmonics. These functions are given by

$$Y_l^m(\theta,\phi) = N_l^m \; P_l^{|m|} \left(\cos\theta\right) e^{im\phi} \; , \tag{1.3}$$

where l is the total number of surface nodes, m is the number of surface nodes that are around the equator, and $l-m$ is the number of nodes that are lines of latitude. Examples

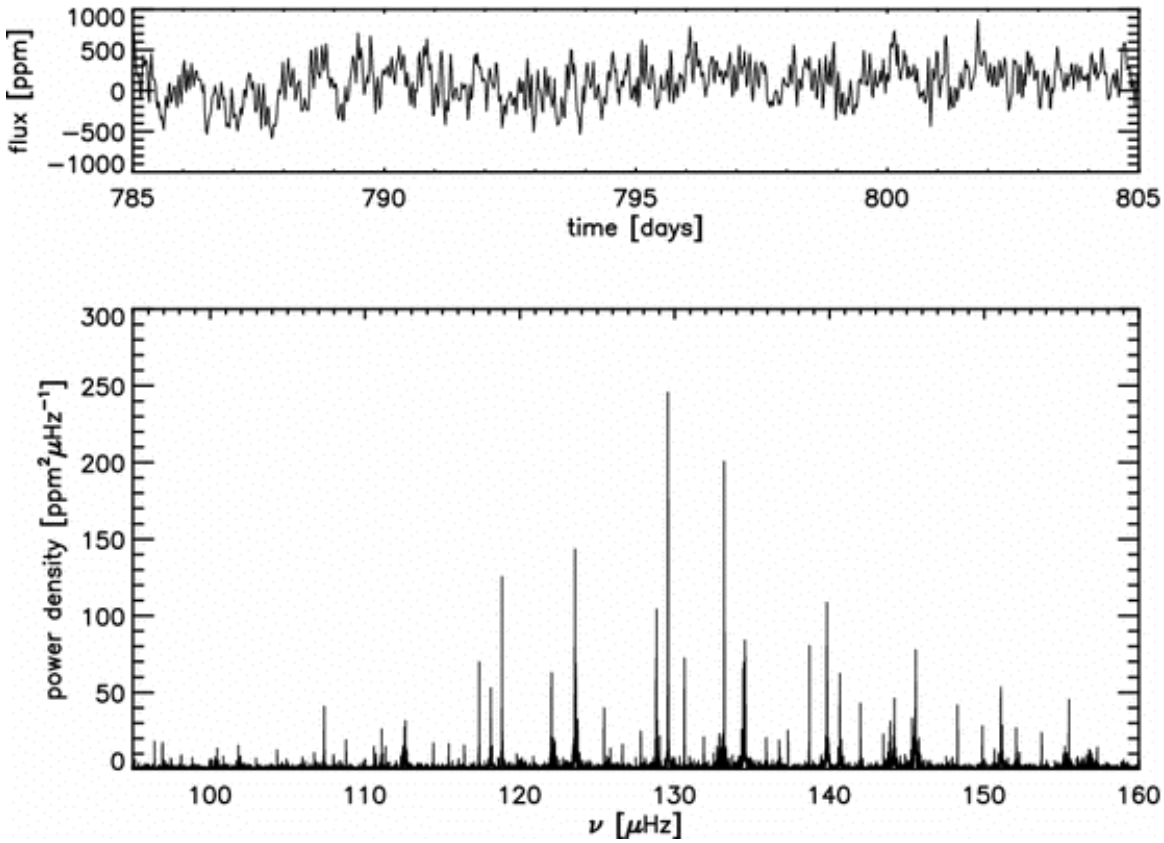

Figure 1.3: An example of a photometric timeseries and associated power spectrum from (Hekker & Christensen-Dalsgaard 2017) for a red giant observed by Kepler. The top panel shows only 20 days of the light curve, and the bottom panel shows where the primary oscillations are after a Fourier transform was done for the entire 1060-day light curve.

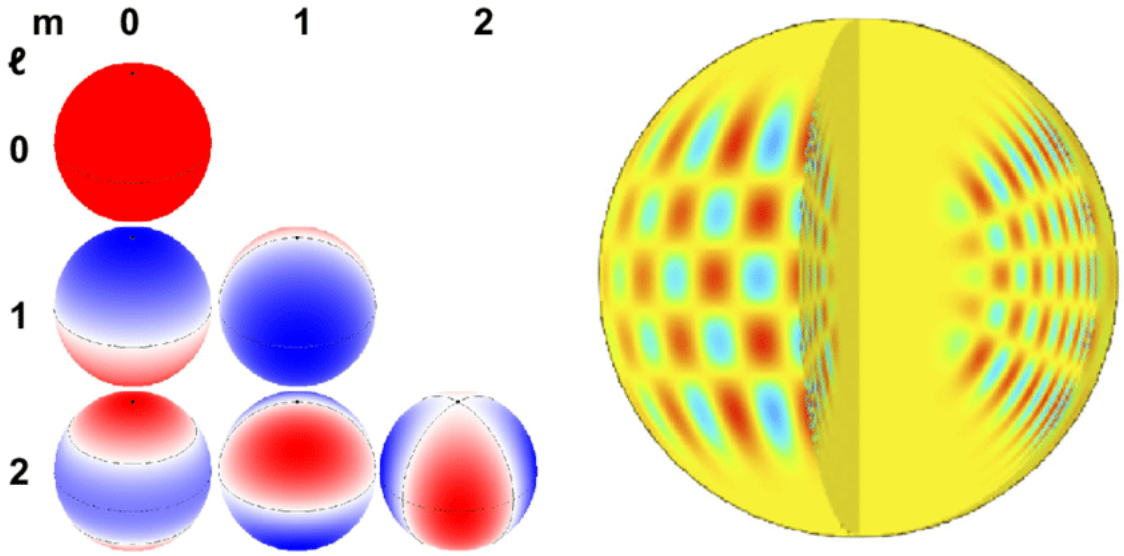

Figure 1.4: Visualization of the different pulsation modes a star can have. On the left are examples of pulsations with increasing orders of l on the vertical and increasing m on the horizontal. The first fundamental radial mode is given by $l = 0$ and $m = 0$ and dipole modes are shown for $l = 1$ and $m = 0, 1$. On the right is a representation of the pulsation for $l = 20$ and $m = 16$. This figure is also from (García & Ballot 2019).

of what the first few pulsation modes look like are shown in Figure 1.4. Values of $l = 0$ and $m = 0$ is the first fundamental radial mode, and it represents the entire surface of a star expanding and contracting radially. This pulsation mode is most notably associated with stars that have significant changes in luminosity and radius such as Cepheids (Kurtz et al. 2016). For $l = 1$ and $m = 0$, this is a non-radial or dipole mode where the north and south poles expand and contract and the equator is a node that stays the same. Another example, $l = 1$ and $m = \pm 1$, is where expansion and contraction of the surface appears to rotate around the equator (Kurtz et al. 2016).

While many different modes of oscillation can be observed in a star's power spectrum, there are two properties of this spectrum that are incredibly important because they are directly related to the mass and radius of a star. The first is $\Delta\nu$, or the separation between frequencies that have the same angular frequency l and are sequential in the

number of radial nodes n. This separation is related to the time it takes a wave to travel from the surface to the core of a star (Christensen-Dalsgaard 1998). The equation for $\Delta\nu$ is shown below,

$$\Delta\nu = \sqrt{\frac{M}{R^3}}. \tag{1.4}$$

The second property of the power spectrum that also scales with the mass and radius of an associated star is the frequency where the pulsations have the highest amplitude, ν_{max}. This relation is given as

$$\nu_{max} \propto \frac{GM/R^2}{\sqrt{T_{eff}}} \propto \frac{g}{\sqrt{T_{eff}}}, \tag{1.5}$$

where g is the surface gravity of a star and $T_{\rm eff}$ is effective temperature. This maximum frequency decreases as the star transitions to a red giant because waves take longer to cross the star since it has increased in size (Kurtz et al. 2016). Once $\Delta\nu$ and ν_{max} are known, and the above relations are substituted into one another, the mass and the radius of a star can be determined. The now separate equations

$$\frac{M}{M_\odot} \simeq \left(\frac{\nu_{max}}{\nu_{max,\odot}}\right)^3 \left(\frac{\Delta\nu_{max}}{\Delta\nu_{max,\odot}}\right)^{-4} \left(\frac{T_{\rm eff}}{T_{\rm eff,\odot}}\right)^{3/2} \tag{1.6}$$

and

$$\frac{R}{R_\odot} \simeq \left(\frac{\nu_{max}}{\nu_{max,\odot}}\right) \left(\frac{\Delta\nu_{max}}{\Delta\nu_{max,\odot}}\right)^{-2} \left(\frac{T_{\rm eff}}{T_{\rm eff,\odot}}\right)^{1/2}, \tag{1.7}$$

are expressed as a ratio of the mass or radius of the star in question to the values for the Sun. Finally, with these stellar parameters a relative age can be estimated.

1.2.2 The NASA/*Kepler* and K2 Missions

The asteroseismic data that will match up with the sample was taken by the *Kepler* space telescope as a part of NASA's K2 mission. Originally, the *Kepler* Mission's primary objective was looking for exoplanets and collected data on roughly 2,800 exoplanet candidates during its lifetime. Along with the exoplanet search, *Kepler* also made observations, in the same field, that contributed to advancements in binary stars (e.g., Sandquist et al. 2016) and asteroseismology (e.g., Gilliland et al. 2010, Huber et al. 2010, Pinsonneault et al. 2014). The K2 mission began after a malfunction disabled two reaction wheels on the telescope that affected it's pointing ability. Engineers were able to find a workaround to this problem, which meant that observations could continue, however the telescope could not continue to point to its original field of view. as part of K2, the spacecraft could be pointed to different fields along the ecliptic plane. This allowed for additional new types of science targets to be observed, including the asteroseismology targets from the Galactic Archaeology Program of K2. Asteroseismic red giants were observed for all of the 19 campaigns of K2 until the spacecraft ran out of fuel and was shut down in the second half of 2018.

The type of data required for asteroseismology is different from spectroscopy. Here, the changes in intensity of the star's light are observed over time, giving a power spectra. For example, red giant targets in Campaign 1 of K2 were observed over 80 days (Stello

et al. 2015). The first important information gained from the power spectra are the frequency separation $\Delta\nu$ and the maximum frequency ν_{max}.

1.3 Goals

Precise stellar ages for field stars or stars that are not gravitationally bound to other stars are still elusive today. If precise ages were able to be determined, they would have a significant impact on our understanding of the history of stellar formation in the Milky Way. It would also provide a basis for understanding stellar formation in other galaxies as well. More accurate ages of halo stars, thought to be the oldest stars in the Milky Way, could provide an even better limit on the age of the universe itself. Determining these ages with better precision is crucial to our understanding of the universe. Current methods to determine age estimates of stars, such as spectroscopy and asteroseismology, individually have very large uncertainties. Combining these two age estimation methods would significantly reduce this uncertainty.

In this dissertation, metallicites and asteroseismology data for a set of open clusters are combined to reduce the uncertainty in age estimates of stars. Open clusters are a good start to constraining the age uncertainties due to the fact that the stars in a cluster are all the same age. To date, there have been no larger scale surveys of open clusters that compare asteroseismology and spectroscopy estimates of stellar ages, due to the limits of area coverage from the *Kepler* mission. *In the original Kepler field there are only 4 open clusters.* The approach in this study we hopped to more than double the number of clusters with high-quality asteroseismology and high-resolution

abundance determinations by observing a sample of 10 open clusters. These clusters were chosen so that they overlapped with *Kepler* 2 (K2) campaign fields. This is because the asteroseismology side of this project will have observations from giant stars in the K2 fields that could also be members of our 10 clusters. By comparing the cluster ages we derive from accurate isochrone fitting, constrained by our measured chemical abundances to ages derived from asteroseismology observations for this larger sample, we reduce the uncertainties in ages.

In Section 2, we present an initial study determining chemical abundances for low signal-to-noise open cluster data. We show that reliably abundances can be determined using a machine learning program known as *The Cannon* (Ness et al. 2015). Some of the same clusters are also analyzed in later sections with newer high resolution and higher signal-to-noise data. Section 3 presents the targeting and analysis of 10 clusters selected to overlap with existing data from the NASA *Kepler-2* mission. We present the reduction and analysis and stellar cluster membership verification. Using our expanded sample of open clusters with asteroseisic observation, we determine a new age-mass-metallicity for determination asteroseismology masses that can be used for determination of ages for "field" or non-cluster stars in Section 4. Finally, in Section 5 we summarize our key results of the age-mass-metallicity calibration and discuss possible future work that is possible as a result of this project.

Chapter 2

Cannon and CTIO spectra

2.1 Cluster Abundances (CTIO/Hydra spectra)

There are several problems in using open clusters to study the properties of the Milky Way. One is the number of open clusters used in individual studies. A way to improve the current knowledge in this area is to increase the number of clusters with known chemical abundances. There are roughly 2000 known open clusters (Cantat-Gaudin et al. 2020), but only a small portion of them have been analyzed chemically. Even the ones with measured abundance values can have substantial uncertainties from study to study (Yong et al. 2005). A few reasons for such large uncertainties are due to varying data quality, the type of data, and different data analysis methods between studies. Another source of uncertainty arises depending on which catalog each survey chose for open cluster distances, as there are several that have determined substantially different distance results as discussed in Donor et al. (2018). This difference translates into widely varying results when attempting to determine a chemical abundance gradient across the disk of the Milky Way. Yong et al. (2012) and Donor et al. (2018; 2020) highlight this problem in their abundance gradient research. Netopil et al. (2016) compiled a homogenized sample of open cluster abundances, but there are still large uncertainties due to different types of observations and resolutions.

In this chapter, we provide updated results from a large uniform sample open clusters previously observed with CTIO/hydra (published in Ray et al. 2022). For this work, we are use *The Cannon*, developed by Ness et al. (2015), which offers a unique way to find stellar parameters without having to use any astrophysical models.

2.2 *The Cannon*

The Cannon is a data-driven approach for determining stellar 'labels' from spectroscopic data. The Cannon is trained from the "known" labels using identified reference stars in the data set. These 'labels' are astrophysical properties of the stars that affect/are in the spectral region measured (e.g., $T_{\rm eff}$, log g, [Fe/H], [Mg/Fe]). *The Cannon* uses continuum-normalized spectra and the provided labels to create a flexible model at each wavelength, which can then be used to apply to date taken in the same dataset (e.g., same instrument and setup). *The Cannon* then can be used to apply this model to derive 'labels' for the remaining survey stars.

The use *The Cannon* on spectroscopic data, there are several reduction sets/corrections that first need to be made, first, standard reduction and wavelength calibration of the data. Secondly, the data need to be corrected to the 'rest' wavelength for the stellar features, so the Doppler velocity of the object/star must be removed.

Our CTIO/Hydra training set 'labels' are taken from the Apache Point Observatory Galactic Evolution Experiment Data Release 16 (APOGEE DR16) system in order to correct the problems with current surveys that were listed above. This sample trained with stars from Donor et al. (2020, also on the APOGEE DR16 system) is designed to form a more extensive dataset for Galactic abundance studies.

2.2.1 Data and Observations

The primary data for this study comes from optical data near the Calcium infrared triplet (7745–8730 Å) taken with the Hydra spectrograph using the Cerro Tololo Inter-American

Observatory (CTIO) 4m telescope. Data was observed on UT 2002 March, 2003 March, 2003 July, and 2003 August. The data reduction and radial velocity and membership analysis of this data was conducted using IRAF[1] standard `ccdproc`, `dohydra`, and `fxcor` routines, which is fully described in Frinchaboy & Majewski (2008).

We have chosen to train *The Cannon* using data from the Sloan Digital Sky Survey's (SDSS; Blanton et al. 2017, Eisenstein et al. 2011) sixteenth data release (DR16; Ahumada et al. 2020, Holtzman et al. 2018, Jönsson et al. 2020) taken as part of the APOGEE (APOGEE 2; Majewski et al. 2017). The APOGEE/DR16 dataset includes about 430,000 stars, collected using two APOGEE spectrographs (Wilson et al. 2012) at Apache Point Observatory (APO; New Mexico Gunn et al. 2006) and Las Campanas Observatory (LCO; Chile Bowen & Vaughan 1973) . For this study data from LCO provides a key overlap with our available training data. The APOGEE data reduction pipeline (Nidever et al. 2015, Holtzman et al. 2018) provides stellar atmospheric parameters and radial velocity measurements, while elemental abundances are provided from the ASPCAP pipeline (García Pérez et al. 2016, Holtzman et al. 2018, Jönsson et al. 2020)

For this study, we have applied *The Cannon* to derive chemical abundances for selected available elements, after applying a cut based on the radial velocity cross-correlation quality Tonry-Davis Ratio ($TDR \geq 11$ Tonry & Davis 1979). After this cut we were able to use 25 stars from 3 clusters that are also observed with APOGEE DR16 in the training set. The Galactic distribution of the clusters in our sample are

[1]IRAF is distributed by the National Optical Astronomy Observatory, which is operated by the Association of Universities for Research in Astronomy, Inc., under cooperative agreement with the National Science Foundation.

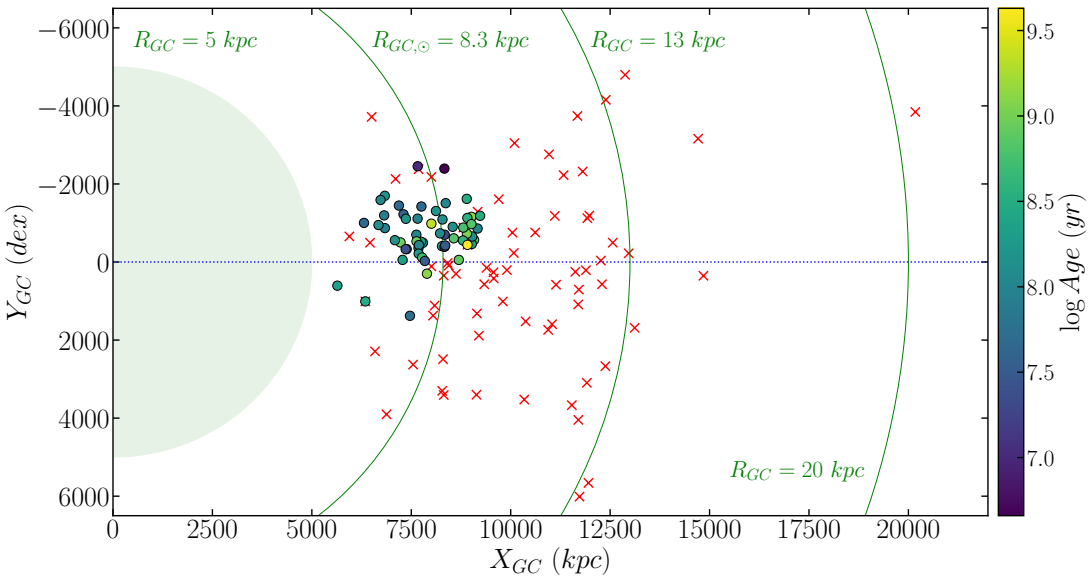

Figure 2.1: Spatial Galactic distribution of open clusters in *this survey* color-coded with ages and R_{GC} distance from Cantat-Gaudin et al. (2020). Also shown are the location of OCCAM-IV DR16-based cluster from Donor et al. (2020) also updated with ages and R_{GC} distance from (Cantat-Gaudin et al. 2020, ; red crosses).

shown in Figure 2.1 using distances from (Cantat-Gaudin et al. 2020) and also showing the positions of the high quality clusters from (Donor et al. 2020).

Additionally, to verify the results from Frinchaboy & Majewski (2008), we also used updated proper motion data from *Gaia* DR2 (Gaia Collaboration et al. 2018) to re-check membership and found no change in membership between the Tycho-2 and Gaia-based proper motion selection.

2.3 Results

Our resultant sample in this study consists of 58 open clusters with 237 member stars of which 35 have no previous spectroscopically determined metallicity measurements. The individual stellar abundance measurements for Fe as well as the α-elements magnesium, silicon, and oxygen, plus the odd-Z element aluminum. Signal-to-noise (S/N) for all cluster stars is computed at 8000 Å. We find that all of the elements scale relative to iron, in solar abundance ratios, as expected for clusters nearby the Sun and are within the normal of solar neighborhood cluster mean abundances as seen in Donor et al. (2020).

2.3.1 Comparison to Other Surveys

The Santos et al. (2009) survey provided iron abundances for 13 open clusters using high-resolution spectra. There were 8 clusters that overlapped with this survey, and their values are listed in Table 2.1. To better illustrate how the two surveys compare, we constructed a one-to-one plot of iron abundances from *The Cannon* vs. values from three significant studies, including Santos et al. (2009), which is shown in Figure 2.2. All of the cluster values from Santos et al. (2009) lie within the average uncertainties, although our values were slightly more metal-poor.

The next comparison was to the Reddy et al. (2013a) and Reddy et al. (2015a) studies. Both examined a total of 12 clusters using high-resolution spectra. Here, there was also an overlap of 7 clusters between this survey and the combined Reddy surveys. The values for each are shown in Table 2.1. These clusters are also shown on the one-to-one plot Figure 2.2. The values obtained by Reddy et al. (2013a; 2015a) were more

metal-poor than the values determined using *The Cannon*. Reddy et al. (2013a) and Reddy et al. (2015a) have been found to be slightly more metal-poor with respect to most measurements other high-resolution measurements, as summarized in Donor et al. (2018) and seen in Figure 2 from Reddy et al. (2016) in their comparison to previous literature results.

The last spectroscopic survey compared to was by Netopil et al. (2016). They examined 172 clusters with a variety of data including low, medium, and high-resolution spectra as well as photometric data. The 12 clusters that overlapped had iron abundances determined from high-resolution spectra. All of the iron abundances are listed in Table 2.1 and the one-to-one plot Figure 2.2, which shows that the majority of the iron abundances are consistent and most clusters lie within the scatter range from *The Cannon*. There are two outliers which are discussed in §2.3.2.

Table 2.1: Average open cluster iron abundance for open clusters in common between *this study* and literature studies.

	This Study		**Other Studies**		
Cluster Name	**Stars**	**[Fe/H] (dex)**	**Stars**	**[Fe/H] (dex)**	**Citation**
IC 2581	1	-0.10 ± 0.27	1	$-0.34 \pm \cdots$	Luck (1994)
IC 4651	9	$+0.04 \pm 0.09$	3	$+0.01 \pm 0.01$	Santos et al. (2009)
			18	$+0.12 \pm 0.04$	Netopil et al. (2016)
			5	$+0.12 \pm 0.05$	Pace et al. (2008).
			3	$+0.11 \pm 0.01$	Carretta et al. (2004a)
IC 4756	3	-0.05 ± 0.16	3	$+0.02 \pm 0.02$	Santos et al. (2009)
			9	-0.02 ± 0.01	Bagdonas et al. (2018)
			12	-0.01 ± 0.10	Ting et al. (2012)
			2	$+0.01 \pm \cdots$	Pace et al. (2010a)
NGC 1662	3	$+0.04 \pm 0.16$	2	-0.10 ± 0.06	Reddy et al. (2013a, 2015a)
			2	-0.11 ± 0.01	Netopil et al. (2016).
NGC 2354	10	-0.12 ± 0.09	2	-0.19 ± 0.04	Reddy et al. (2013a, 2015a)

Continued on next page

	This Study		**Other Studies**		
Cluster Name	**Stars**	**[Fe/H] (dex)**	**Stars**	**[Fe/H] (dex)**	**Citation**
			2	−0.18 ± 0.02	Netopil et al. (2016)
NGC 2423	8	+0.10 ± 0.10	3	+0.14 ± 0.06	Santos et al. (2009)
			3	+0.08 ± 0.05	Netopil et al. (2016)
NGC 2447	17	−0.06 ± 0.07	3	−0.08 ± 0.01	Donor et al. (2020)
			3	−0.10 ± 0.03	Santos et al. (2009)
			3	−0.13 ± 0.05	Reddy et al. (2013a, 2015a)
			4	+0.07 ± 0.03	Netopil et al. (2016)
			12	−0.17 ± 0.05	da Silveira et al. (2018)
NGC 2482	5	+0.07 ± 0.12	1	−0.07 ± 0.04	Reddy et al. (2013a, 2015a)
			1	−0.07 ± ···	Netopil et al. (2016)
NGC 2527	3	−0.11 ± 0.16	2	−0.11 ± 0.04	Reddy et al. (2013a, 2015a)
NGC 2516	3	−0.09 ± 0.16	2	+0.05 ± 0.11	Netopil et al. (2016)
NGC 2539	9	−0.08 ± 0.09	3	+0.13 ± 0.03	Santos et al. (2009)
			2	−0.06 ± 0.04	Reddy et al. (2013a, 2015a)
			4	−0.02 ± 0.08	Netopil et al. (2016)
			12	−0.03 ± 0.07	Martinez et al. (2020)
NGC 2548	3	+0.12 ± 0.16	95	−0.06 ± 0.01	Sun et al. (2020)
NGC 2567	6	−0.07 ± 0.11	3	−0.04 ± 0.08	Netopil et al. (2016)
NGC 2682	10	+0.09 ± 0.09	32	+0.01 ± 0.03	Donor et al. (2020)
			3	+0.00 ± 0.01	Santos et al. (2009)
			3	−0.08 ± 0.04	Reddy et al. (2013a, 2015a)
			27	+0.03 ± 0.05	Netopil et al. (2016)
			6	+0.03 ± 0.04	Pace et al. (2008)
NGC 3680	6	−0.05 ± 0.11	3	−0.04 ± 0.01	Santos et al. (2009)
			10	−0.01 ± 0.06	Netopil et al. (2016)
			6	−0.06 ± 0.07	Peña Suárez et al. (2018)
			11	−0.03 ± 0.02	Mitschang et al. (2012)
			2	+0.04 ± 0.03	Pace et al. (2008)
NGC 5617	6	−0.04 ± 0.11	2	−0.18 ± 0.02	De Silva et al. (2015)
NGC 5822	3	+0.01 ± 0.16	3	+0.05 ± 0.04	Santos et al. (2009)
			7	+0.08 ± 0.08	Netopil et al. (2016)
			11	−0.09 ± 0.06	Peña Suárez et al. (2018)
			3	+0.15 ± 0.08	Pace et al. (2010b)
			7	+0.08 ± 0.08	Luck (1994)
NGC 6067	1	+0.03 ± 0.27	5	+0.19 ± 0.05	Alonso-Santiago et al. (2017)

Continued on next page

	This Study		**Other Studies**		
Cluster Name	**Stars**	**[Fe/H] (dex)**	**Stars**	**[Fe/H] (dex)**	**Citation**
NGC 6134	2	+0.00 ± 0.19	8	+0.11 ± 0.07	Netopil et al. (2016)
			6	+0.15 ± 0.07	Carretta et al. (2004b)
NGC 6281	7	−0.06 ± 0.10	2	+0.06 ± 0.06	Netopil et al. (2016)
NGC 6405	6	−0.06 ± 0.11	44	+0.07 ± 0.03	Kılıçoğlu et al. (2016)
NGC 6603	1	+0.05 ± 0.27	7	+0.34 ± 0.15	Carrera et al. (2015)
NGC 6705	3	+0.01 ± 0.16	12	+0.12 ± 0.04	Donor et al. (2020)
			21	+0.12 ± 0.09	Netopil et al. (2016)

The remaining clusters with iron abundances from smaller high-resolution studies were also examined for inconsistencies. Table 2.1 lists all of the values for [Fe/H] determined by *The Cannon*, the [Fe/H] values from the literature, and the type of data that was used. Most of the clusters fall within the range of scatter again (Table 2.1); however, 3 clusters were not. Reasons for why these values do not appear to agree are discussed in §2.3.2.

The cluster NGC 2682 is one of the most well studied open clusters, therefore it was used as a calibration cluster. It also has an average [Fe/H] value determined from APOGEE DR16 data from Donor et al. (2020) making it a significant check on how well *The Cannon* produced values. The average [Fe/H] from Donor et al. (2020) was 0.01±0.03, and this survey found a value of 0.09 ± 0.16. Additionally, the five other studies compared to in this paper with [Fe/H] determined for NGC 2682 (Santos et al. 2009, Reddy et al. 2013a; 2015a, Netopil et al. 2016, Pace et al. 2008) agree within the uncertainties.

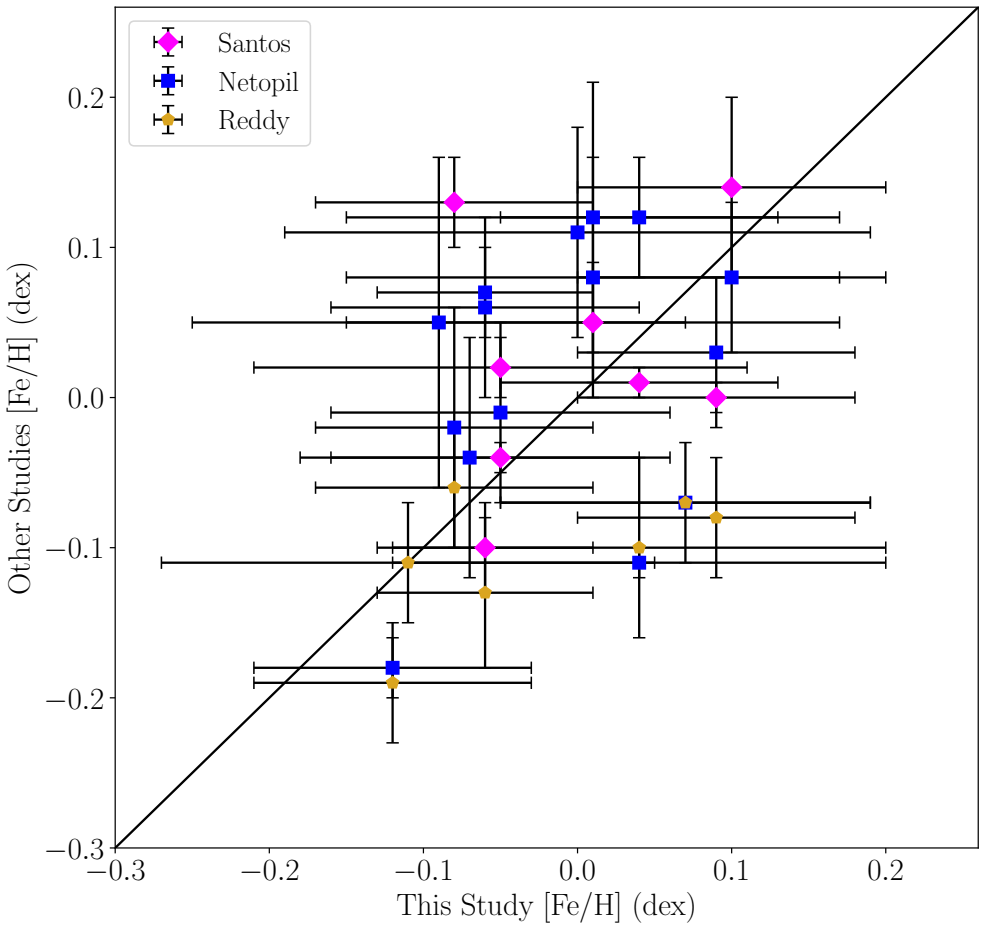

Figure 2.2: A comparison of average [Fe/H] values for in common open clusters from *this survey* and from the literature compilation in Tables 2.1. Magenta clusters are from Santos et al. (2009), blue clusters are from Netopil et al. (2016), and orange clusters are from Reddy et al. (2013a; 2015a).

2.3.2 Discrepancies

There were 3 clusters that were almost outside of the acceptable scatter when compared to the literature values, which are significant given our larger uncertainties due to the lower S/N of this study. This section discusses possible reasons why there were differences in iron abundance values.

The value obtained for NGC 6705 was within the uncertainty of Donor et al. (2020), however it was more metal-poor. This is likely due to Donor et al. (2020) having four times the number of member stars used for average abundance analysis as well as higher resolution, higher-S/N spectra than this study. The same is also true when compared to the results of (Netopil et al. 2016)

For NGC 1662, both Reddy et al. (2015b) and Netopil et al. (2016) had values that were in agreement and for reference, these values are listed in Tables 6 and 7. The value for NGC 1662 from this study was more metal-rich than both Reddy et al. (2015b) and Netopil et al. (2016) and the comparison is shown in Figure 4. Each of these studies used high-resolution spectra of two stars where we used medium-resolution spectra of three stars.

The cluster NGC 2482 showed similar discrepancies to NGC 1662. Reddy et al. (2013b) and Netopil et al. (2016) found more metal-poor values for this cluster and each only used one star for the average abundance analysis compared to five stars used in this study, therefore cluster membership of the other studies may be the reason for such a large offset. This comparison is also shown in Figure 2.2.

Chapter 3

Star Clusters with Asteroseismic Masses

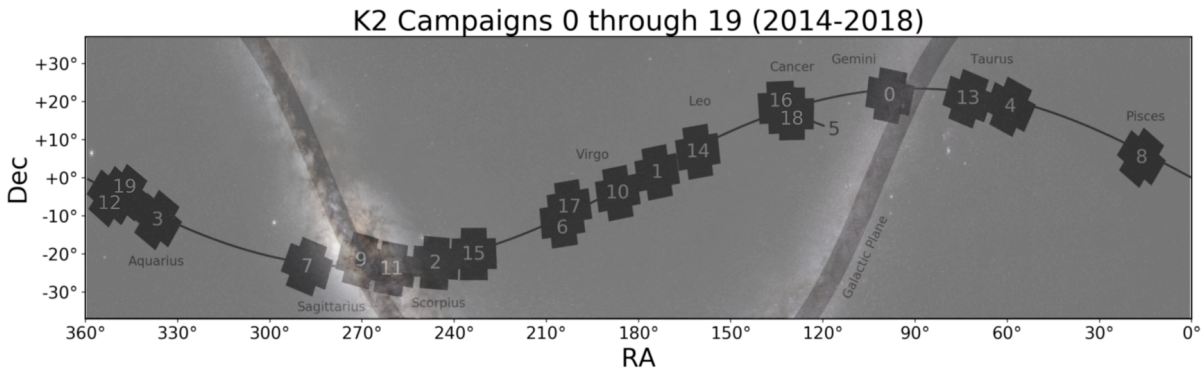

Figure 3.1: K2 Campaign fields with respect to the Galactic Plane.

3.1 K2 Fields with Open Clusters

To find the open clusters for this survey, the entire Optically Visible Open Clusters and Candidates Catalog or Dias Catalog (Dias et al. 2002) was queried. Since we collaborated with the Kepler 2 (K2) asteroseismology study, we had to find clusters that were also in the fields of the K2 campaign fields, see Figure 3.1. Once the K2 fields were compared to the Dias Catalog, the total potential cluster sample was determined to be 59. Next, the sample was further vetted to see which clusters contained individual asteroseismology targets within a circle defined by twice the cluster's radius. This brought the sample to 24 clusters with at least 10 stars, and 10 clusters in a secondary sample, which are all listed in Table 1. While there were initially 59 clusters that matched, it was difficult to observe this many clusters given the limited time to submit proposals to our preferred telescope, the Multiple Mirror Telescope (MMT). Ultimately, we were able to get spectra for stars in 10 clusters that overlapped with K2 data.

Table 3.1: K2/MMT Open Cluster Sample

Cluster	l[a] (°)	b[a] (°)	Radius[a] (')	Age[a] (Gyr)	R_{gc}[a] (kpc)	R_{guide}[b] (kpc)	μ_α[a] (mas/yr)	μ_δ[a] (mas/yr)	RV (km/s)	[Fe/H] (dex)
Berkeley 29	197.9472	+7.9816	1.7	3.09	20.51	18.10	+0.11±0.02	-1.05±0.02	+25.3±0.1	-0.53±0.02
NGC 1647	180.3675	-16.7923	50.0	0.36	8.88	9.77	-1.03±0.02	-1.52±0.01	-12.9±0.0	-0.19±0.01
NGC 1746	179.1252	-10.4756	18.0	···	···	···	+3.20±0.03	-3.79±0.02	+4.8±0.4	+0.06±0.01
NGC 1758	179.1550	-10.490	0.34	···	···	···	···	···	···	···
NGC 1817	186.6244	+2.1436	22.4	1.12	10.02	10.58	+0.42±0.03	-0.96±0.03	+66.8±1.6	-0.16±0.03
NGC 2158	186.6355	+1.7881	5.3	1.55	12.55	12.37	-0.26±0.02	-1.99±0.02	+27.2±1.8	-0.25±0.02
NGC 2632	205.9525	+32.4278	118.2	0.68	8.41	8.51	-36.42±0.05	-13.04±0.04	+35.3±0.6	+0.14±0.06
NGC 2682	215.6912	+31.9208	19.9	4.27	8.90	9.97	-11.00±0.03	-2.91±0.02	+34.3±1.0	-0.00±0.05
NGC 6791	69.9644	+10.9065	8.2	6.31	7.89	6.47	-0.40±0.01	-2.26±0.02	-46.9±1.2	+0.31±0.04
NGC 6819	73.9815	+8.4811	11.4	2.24	7.97	8.53	-2.87±0.01	-3.93±0.01	+2.6±1.3	+0.03±0.04

[a] Values from (Cantat-Gaudin et al. 2020) .
[b] Values from (Myers et al. 2022) .

3.2 Observations with MMT

The spectroscopic data for the stars in each of the ten clusters was taken using the Multiple Mirror Telescope (MMT; Beckers et al. 1981) in Arizona after successfully applying for time on two separate occasions. This telescope has a 6.5-m primary mirror and is situated at the top of Mt. Hopkins at an elevation of over 8,000 ft. It has an altitude-azimuth (alt-az) mount, meaning it moves on two axes which are perpendicular to the horizon and parallel to the horizon, respectively. The MMT used to be composed of six 1.8-m mirrors that made up the primary mirror, however in 1999 this configuration was replaced by a single 6.5 m mirror. Spectra for each of the stars was collected using an instrument called the Hectochelle spectrograph (Fabricant et al. 2005), which is an echelle spectrograph that observes in the optical wavelength range. It has 240 fibers that are moved by a robot positioner that moves them to the appropriate on-sky locations. One of the major advantages of using the Hectochelle at the MMT is that it can observe multiple objects at once, which made this an ideal choice to observe multiple stars in a cluster at the same time.

Additionally, the Hectochelle had several filters to choose from that covered narrow wavelength ranges in the optical. We selected the CJ 26 filter that covered a wavelength range of 611–644 nm because it allowed, both neutral and ionized Iron lines, Fe `I` and Fe `II`, plus selected α-elements and neutron capture elements, as shown in Table 3.2 [1]. Iron abundances can give information on the overall metal abundance of each star, [Fe/H]. Each of these lines, depending on the strength, are also used to find an estimate of the

[1]Information on the Hectochelle and the CJ 26 filter can be found at https://www.cfa.harvard.edu/mmti

effective temperature T_{eff} and surface gravity g, which were used to derive mass and subsequent age estimates.

Table 3.2: Elements Available using the MMT/Hectochelle CJ 26 filter (6150–6400Å)

# Lines	Element[a]	Wavelengths	Comments
13	**Fe I**	6151Å, 6165Å, 6180Å, 6187Å, 6200Å, 6229Å, 6232Å, 6240Å, 6246Å, 6270Å, 6301Å, 6336Å, 6393Å	
4	**Fe II**	6149Å, 6247Å, 6369Å, 6416Å	
2	**Na I**	6154Å, 6160Å	(edge)
3	**Mg I**	6318Å, 6319Å, 6319Å	
5	**Si I**	6142Å, 6145Å, 6155Å, 6243Å, 6244Å	
4	**Ca I**	6161Å. 6166Å, 6169Å, 6169Å	
3	Sc II	6245Å, 6300Å, 6320Å	
4	Ti I	6261Å, 6303Å, 6312Å, 6336Å	
2	**V I**	6274Å, 6285Å	
4	**Ni I**	6176Å, 6204Å, 6223Å, 6378Å	
1	Zr I	6114Å	(edge)
1	Ba II	6141Å	(iffy)
1	La II	6390Å	
1	Eu II	6437Å	(edge, Si blend)

[a] **Bold** denote elements that overlap with those analyzed by SDSS/APOGEE.

3.3 Data Reduction

After the targets were observed at the MMT, the data was processed by a pipeline for the Hectoechelle instrument (Fabricant et al. 2005). This included standard image processing such as bias corrections and applying the proper wavelength solution. However, one step that had to be done that was omitted from the pipeline was subtracting out the sky spectrum. This was easily done using IRAF which is an image processing tool developed by NOAO/NOIRLab. The next step, also completed using IRAF, was to determine the radial velocities for each star that was observed. Having the radial velocities was crucial

because it is used to shift all of the spectra back to a rest wavelength which is necessary for accurate *The Cannon* values. Radial velocities are also useful in assessing membership of stars in clusters which is discussed in the next section.

To begin the process of determining radial velocities, stars with already known values were selected from APOGEE DR17. These stars composed the standard star set. The standards were first compared to each other in IRAF using `fxcor` to make sure the values produced were similar to the values from DR17. Once this was confirmed, the standard set of stars was applied to the entire set of stars. With metallicites and the reliable radial velocities, cluster membership analysis was performed again to ensure that only cluster members were used in the age-mass-metallicity calibration.

3.4 Cluster Membership Re-Verification

After selecting clusters that were also in K2 fields with asterosiesmic data, the next step was to determine which stars were members of these clusters. To determine which stars to observe, an initial membership assessment using proper motions from Gaia DR2 was performed, similar to that of Donor et al. (2018). This was a 2-D Gaussian fit in proper motion space for stars that fell within two times the cluster radius. Stars that are gravitationally bound in an open cluster will have similar motions when moving through the galaxy. Once the members and non-member field stars were identified, they could be sorted into three groups. The first group are cluster members with K2 asteroseismic masses. These were the highest priority stars that we requested observations for because they would be used in the age-mass-metallicity calibration. The next highest priority

group were non-members with K2 data. They are important because their ages can be determined once the calibration is complete. Finally, the third group were cluster members without K2 data. The members from this group and the first group were all used to determine the metallicity of the ten clusters overall.

While using proper motion alone to assess cluster membership is reliable, a secondary round of membership analysis was done using radial velocities discussed in Section 3.3 and metallicities from *The Cannon* . A one-dimensional Gaussian fit was done for each of these parameters and members were stars with values within 3-sigma of the mean. This process moved several stars from the groups mentioned earlier, members with K2 data and members without K2, into a new group of non-member stars without K2 data. The member stars that remained were used in the age-mass-metallicity calibration and the overall metallicities determined for each cluster.

3.5 *The Cannon* MMT/Hectochelle Abundances

As described in Section 2.2, *The Cannon* had to be trained on a set of reference spectra with known values before it can be used to find metallicities for all of the stars in the sample. The stars in this reference set were chosen based on which ones had stellar parameters determined in the latest APOGEE data release which was DR17. Stars were matched to 8 of the 10 open clusters in our sample. When the reference set was used to train The Cannon, a check had to be performed to determine if the output values made sense. This check was done by creating one-to-one plots for each of the parameters. Displayed in Figure 3.2, these plots showed that the scatter for Teff and log g fit well

with a scatter of 43 K and 0.1 dex, respectively. In Figure 3.3, the scatter for each of the elements was also small meaning that for this high-resolution data set *The Cannon* returned parameters that closely matched the DR17 data. Once *The Cannon* was trained, the next step was to apply the model to the entire sample of stars to determine these parameters for all of the stars in the set of 10 open clusters.

3.6 Asteroseismic sample parameters

The masses for the groups cluster members with K2 data and non-members with K2 data were calculated using ν_{max} and $\Delta\nu$, found from the light curves in Zinn et al. (2022) and Pinsonneault et al. (2018), as well as the effective temperature that was determined with *The Cannon* . The equation used for each stellar mass is given in Section 1.2 which covered the asteroseismology background and shown again here:

$$M_{star} \simeq \left(\frac{\nu_{max}}{\nu_{max,\odot}}\right)^{3}\left(\frac{\Delta\nu_{max}}{\Delta\nu_{max,\odot}}\right)^{-4}\left(\frac{T_{\rm eff}}{T_{\rm eff,\odot}}\right)^{3/2} M_{\odot} \tag{3.1}$$

The solar values for $\nu_{max,\odot}$ and $\Delta\nu_{\odot}$ were 3103.3 μHz and 135.5 μHz, respectively Zinn et al. (2022). The results for all of the asteroseismic stars are shown in Table 4.3. To find the errors on each of the masses, standard error propagation was done using the errors given in Zinn et al. (2022) and Pinsonneault et al. (2018) as well as the errors produced from The Cannon. Both were important for the fit and errors of the fit discussed in the next Chapter.

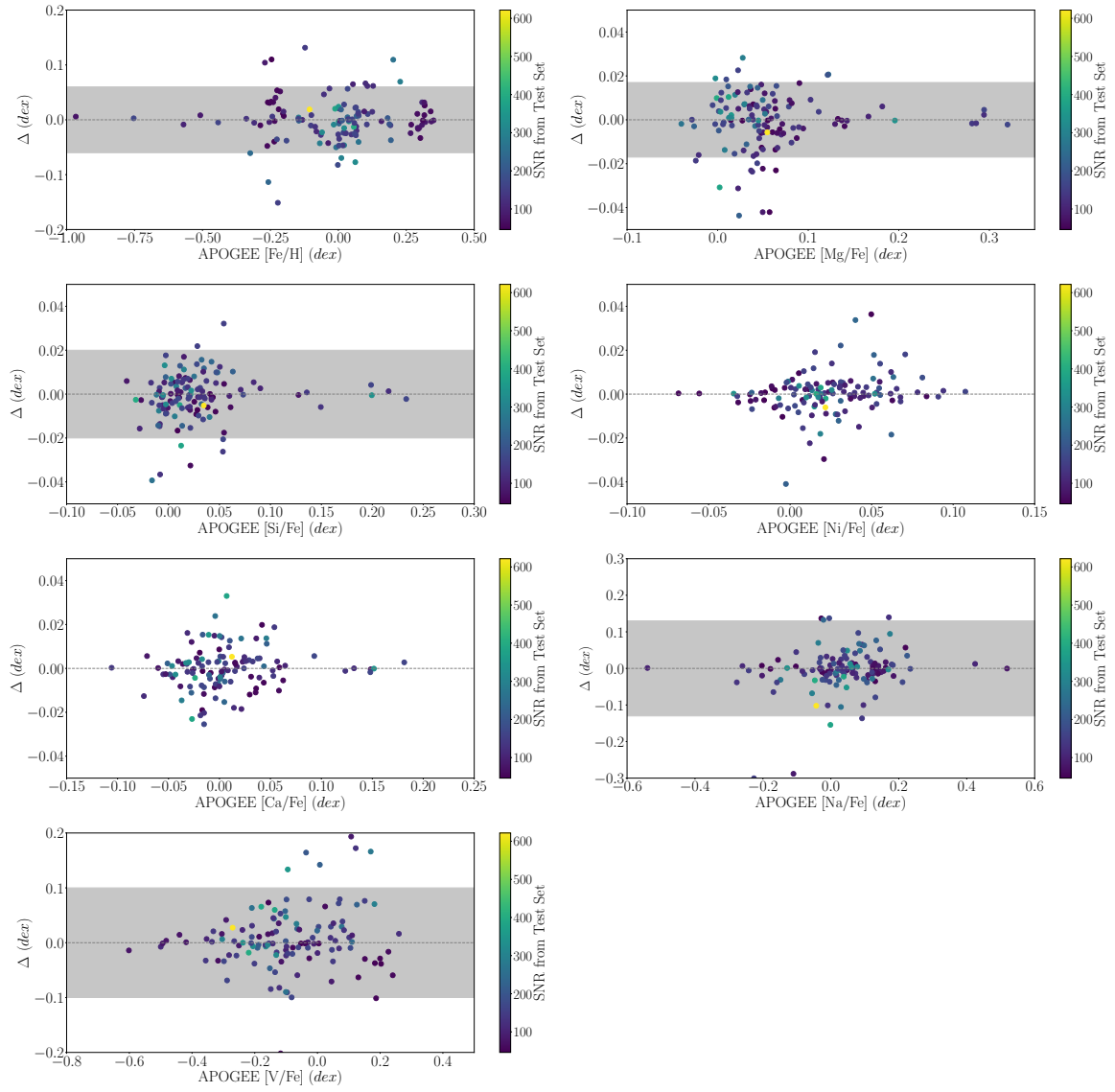

Figure 3.2: A comparison of [Fe/H], [Mg/Fe], [Si/Fe], [Ni/Fe], [Ca/Fe], [Na/Fe,] and [V/Fe] values obtained by *The Cannon* and values obtained using APOGEE DR16 data. The shaded areas represent the acceptable scatter as in 3.3.

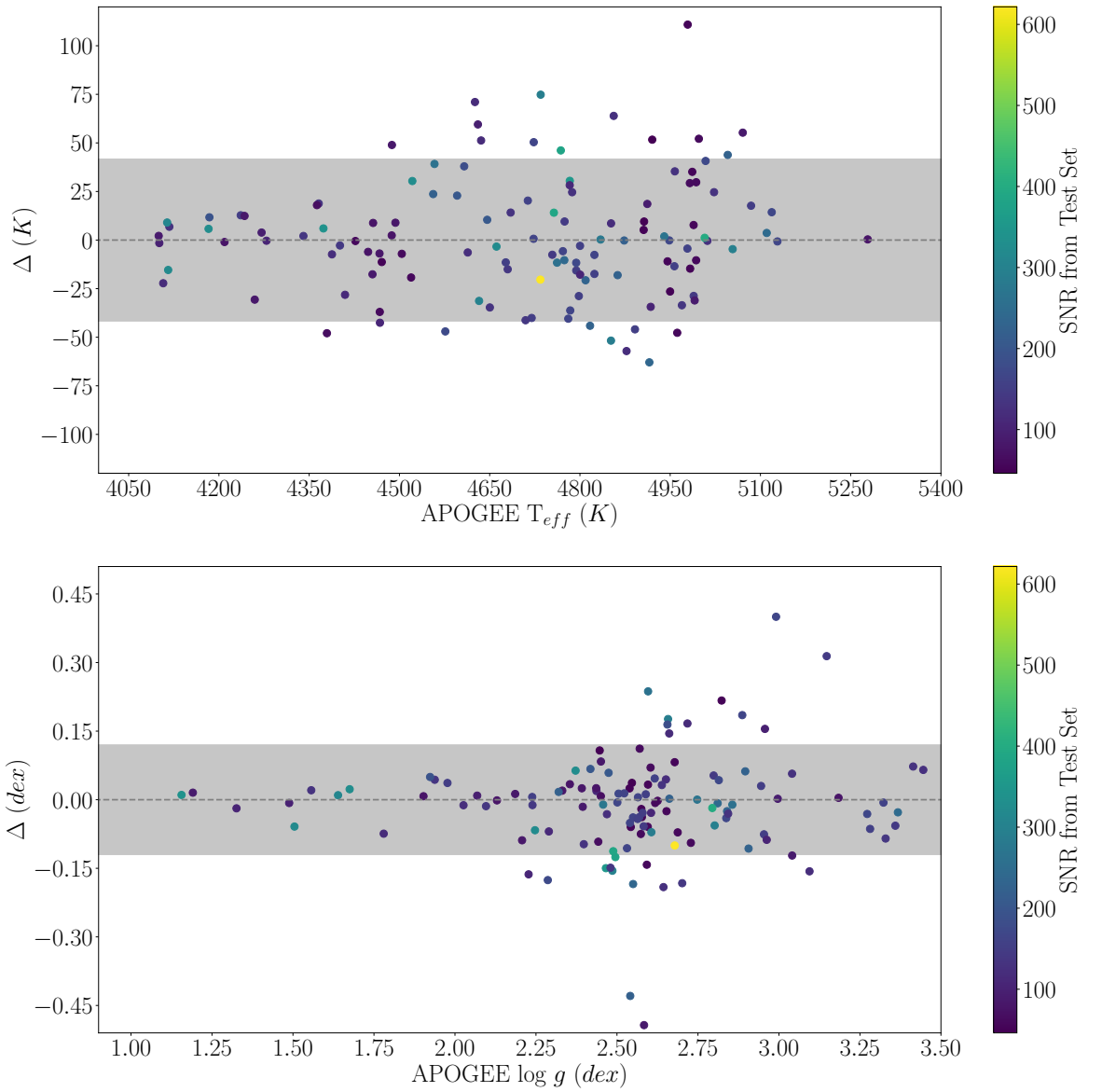

Figure 3.3: A comparison of effective temperature (T_{eff}) and surface gravity (log g) values obtained by *The Cannon* and values obtained using APOGEE DR16 data. Most of the values fall within the scatter which is illustrated by the gray shaded areas.

Chapter 4

Open Cluster Spectroscopic and Astreoseismology Calibration Results

4.1 *The Cannon* Cluster Results for MMT

After using *The Cannon* to get abundances for each star, the stars that were determined to be cluster members were used to get an average metallicity for each cluster. Table 4.1 shows the abundances from this study compared to Myers et al. (2022) as well as the number of stars used for each average and nine of the ten clusters used in this study matched. Since both of these studies used APOGEE DR17, the results from this study were expected to be relatively similar to Myers et al. (2022). The cluster NGC 2682 is a considered a calibration cluster because it has been extensively studied as evidenced by the 331 member stars considered in Myers et al. (2022). While this study only had 107 member stars, the average chemical abundances for every element determined here were well within the uncertainties. Looking at [Fe/H] for each of the other clusters, not including NGC 1758, shows that they are also in agreement. This was especially important for the clusters that have K2 asteroseismic masses because [Fe/H] has an impact on how waves propagate through the star which in turn, affects the frequencies used to determine masses.

When comparing the other elements ([Mg/Fe], [Si/Fe], [Ni/Fe], [Ca/Fe], [Na/Fe], and [V/Fe]) individually, there were some discrepancies between clusters. For [Na/Fe] and [V/Fe], these elements had larger errors in APOGEE DR17. For clusters Berkeley 29 and NGC 1746, Myers et al. (2022) had only a few stars for a cluster average of these two elements as well and NGC 1647 did not have a value for [V/Fe].

For the cluster NGC 1758, there was no data from DR17. Additionally, this cluster overlaps with the cluster NGC 1746 on the sky and there is some debate as to whether

or not these are both one cluster instead of separate clusters. When comparing the proper motions of these two clusters, they both have an average of 5.3 mas/yr and their metallicites are also very close in value. This potentially provides evidence that these two clusters are indeed one.

Table 4.1: The Cluster average abundances from Myers et al. (2022) and this work using *The Cannon* for our MMT/Hectochelle open cluster sample. The number of cluster members used in the average cluster [Fe/H] determination are given in column 2.

Cluster	Members	[Fe/H] (dex)	[Mg/Fe] (dex)	[Si/Fe] (dex)	[Ni/Fe] (dex)	[Ca/Fe] (dex)	[Na/Fe] (dex)	[V/Fe] (dex)
APOGEE OCCAM DR17 (Myers et al. 2022)								
Berkeley29	2	−0.53±0.02	+0.13±0.02	+0.03±0.02	+0.04±0.02	+0.01±0.02	+0.13±0.07	−0.18±0.10
NGC1647	1	−0.19±0.01	+0.14±0.05	−0.18±0.05	−0.09±0.03	+0.45±0.05	+0.83±0.48	...
NGC1746	1	+0.06±0.01	−0.10±0.03	+0.10±0.03	+0.02±0.03	−0.09±0.03	−0.74±0.15	−2.14±0.16
NGC1758	0	...	...	...	...	...	...	...
NGC1817	11	−0.16±0.03	−0.01±0.10	−0.03±0.09	−0.04±0.05	−0.01±0.30	+0.06±0.30	+0.28±0.42
NGC2158	61	−0.25±0.02	+0.04±0.04	+0.02±0.03	−0.04±0.02	+0.03±0.03	+0.04±0.13	−0.09±0.37
NGC2632	28	+0.14±0.06	−0.07±0.06	−0.01±0.05	+0.00±0.02	−0.01±0.04	+0.07±0.15	−0.00±0.13
NGC2682	331	−0.00±0.05	+0.00±0.06	+0.04±0.07	+0.01±0.05	−0.01±0.04	−0.06±0.35	−0.01±0.25
NGC6791	66	+0.31±0.01	+0.08±0.02	+0.01±0.03	+0.02±0.04	−0.04±0.04	+0.17±0.05	−0.20±0.20
NGC6819	46	+0.03±0.04	+0.02±0.01	+0.01±0.02	+0.00±0.02	+0.00±0.02	+0.09±0.09	−0.13±0.14
This work using *The Cannon*								
Berkeley29	45	−0.54±0.006	+0.13±0.004	+0.03±0.003	+0.01±0.003	+0.04±0.003	+0.10±0.03	−0.17±0.02
NGC1647	42	−0.17±0.006	+0.14±0.005	−0.18±0.003	−0.08±0.003	+0.38±0.003	+0.13±0.03	−0.09±0.02
NGC1746	82	+0.00±0.004	−0.05±0.003	+0.04±0.002	−0.03±0.002	−0.01±0.002	−0.13±0.02	−0.03±0.01
NGC1758	22	+0.00±0.009	−0.06±0.006	+0.05±0.004	−0.02±0.004	−0.01±0.004	−0.16±0.04	−0.05±0.03
NGC1817	38	−0.14±0.006	−0.03±0.005	+0.04±0.003	−0.01±0.003	+0.01±0.003	−0.15±0.03	+0.01±0.02
NGC2158	34	−0.26±0.007	+0.06±0.005	+0.02±0.003	−0.01±0.003	+0.02±0.003	+0.00±0.03	+0.02±0.02
NGC2632	80	+0.12±0.004	−0.04±0.003	+0.03±0.002	+0.01±0.002	+0.00±0.002	−0.15±0.02	−0.05±0.01
NGC2682	107	+0.01±0.004	−0.01±0.003	+0.05±0.002	+0.02±0.002	−0.01±0.002	−0.13±0.02	−0.03±0.01
NGC6791	37	+0.29±0.007	+0.06±0.005	+0.01±0.003	+0.03±0.003	−0.02±0.003	+0.14±0.03	−0.18±0.02
NGC6819	43	+0.06±0.006	−0.02±0.005	+0.01±0.003	+0.01±0.003	+0.00±0.003	−0.13±0.03	−0.08±0.02

4.2 Asteroseismic Mass Calibration

In total, there were 6 clusters (NGC 1746, NGC 1817, NGC 2632, NGC 2682, NGC 6791, and NGC 6819) that had asteroseismic members that could be used in the age-mass-metallicity calibration, see Tables 4.1 and 4.2. Of these clusters, two are considered calibration clusters and they are NGC 6791 and NGC 6819, with data from the original *Kepler mission*. Both of them have asteroseismic ages determined in Zinn et al. (2022) that could be compared to after determining the calibration. A three-parameter orthogonal linear regression was done to determine how age, mass, and metallicity were related to each other. A linear fit was chosen because of how metals build up in stars from one generation to the next linearly in log space. Mass also decreases linearly with age. The equation for the fit is

$$y_{\log(\text{ages})} = \beta_0 x1_{[Fe/H]} + \beta_1 x2_{mass} + \beta_2 \tag{4.1}$$

where the ages we initially fit to were the Cantat-Gaudin et al. (2020) ages, [Fe/H] values were from *The Cannon* , and the masses were from asteroseismic data described in Section 3.6. The coefficients were found to be $\beta_0 = 3.49 \pm 0.37$ $log(\text{yrs})/\text{dex}$, $\beta_1 = 0.10 \pm 0.08$ $log(\text{yrs})/M_\odot$, and $\beta_2 = 8.73 \pm 0.19$ $log(\text{yrs})$. Figure 4.1 shows the two dimensional views of the three dimensional fit to the data. Once the coefficients were known, a new age could be determined for each star.

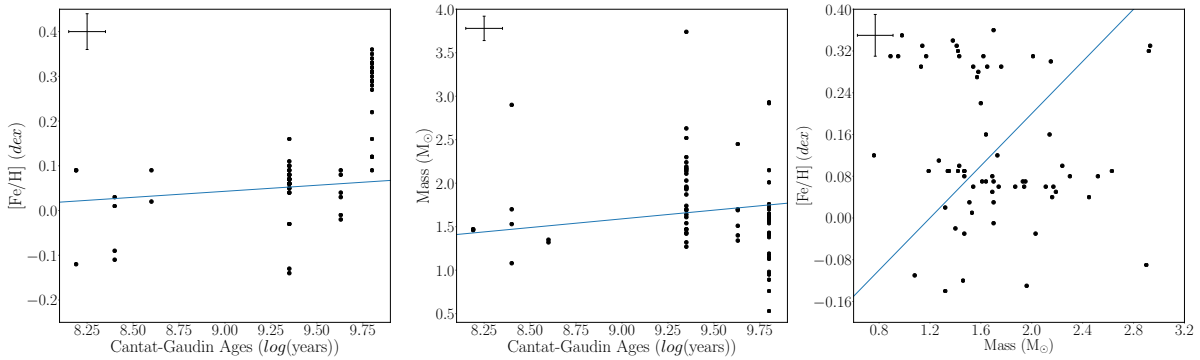

Figure 4.1: Two dimensional projections of the three dimension fit for age, mass, and chemical abundance [Fe/H]. The average errors for each parameter are shown in the upper left hand corners

4.3 Age Comparison to Pinsonneault et al. (2018) and Cantat-Gaudin et al. (2020)

After performing an orthogonal linear fit to the ages, masses, and chemical abundances, the next step was to compare the ages of stars determined from the fit to the ages of the calibration clusters in Pinsonneault et al. (2018) and the ages of all of the clusters used for the fit which were from Cantat-Gaudin et al. (2020).

Looking at the comparison to the ages of stars determined from the fit to the ages of the clusters from Cantat-Gaudin et al. (2020) in 4.2, most of the individual stellar ages were within the error. The two calibration clusters, NGC 6791 and NGC 6819, fit the best which was expected since they made up the majority of stars in the sample. The cluster NGC 2682 did not fit as well, however, the calibration cluster NGC 6791 was part of the reason why. This cluster does not follow the typical trend seen with other clusters in chemical abundance with age. While young clusters typically have more metals and older clusters have less metals, NGC 6791 is an old cluster that has a high

chemical abundance. It is thought to have formed in the inner part of the Milky Way disk where star formation has been occurring for a longer period of time as opposed to the outer parts of the galaxy. Over time, NGC 6791 eventually migrated farther out in the disk where star formation has not been going on as long (Martinez-Medina et al. (2018),Villanova et al. (2018)).

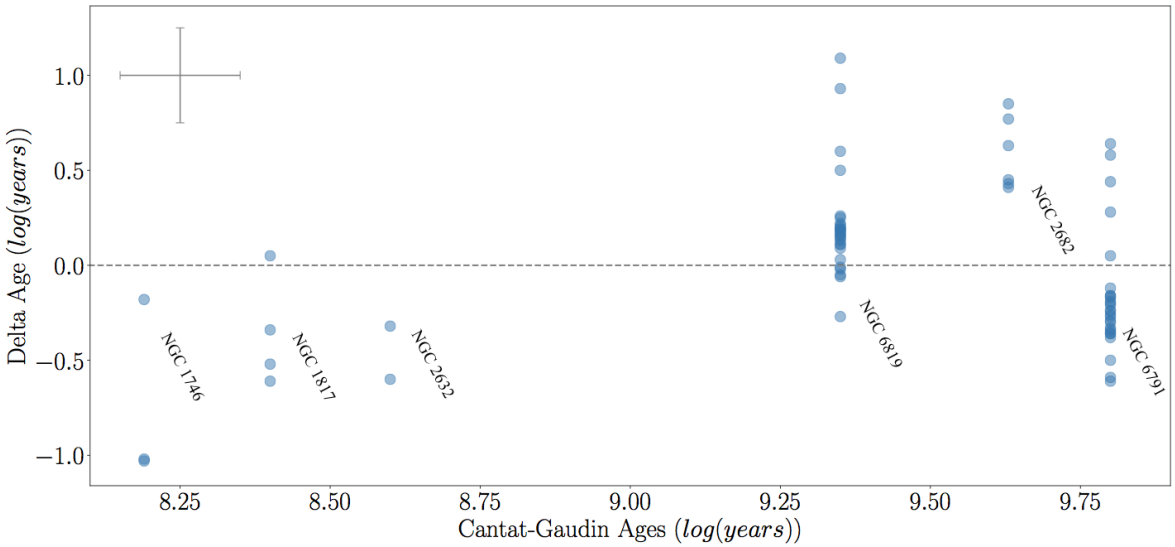

Figure 4.2: The age comparison between the ages determined with asteroseismic masses and metallicites from this study and the ages determined in Cantat-Gaudin et al. (2020).

An age comparison was also done for the two calibration clusters with ages determined in Pinsonneault et al. (2018). Figure 4.3 shows that ages for the majority of stars that matched in both clusters, blue circle for NGC 6791 and red triangles for NGC 6819, were within the error here as well. Stars for the cluster NGC 6819 fit the best and cluster NGC 6791 had a few more members that were scattered. Part of the reason for the scatter with NGC 6791 is the same as before. Since it is an outlier, some of the stars in this cluster are getting ages that are younger than expected. The age-mass-chemical abundance relation was also applied to all of the stars in Pinsonneault et al. (2018) which

included not only members of NGC 6791 and NGC 6819 but also field stars. These are shown as the grey bins in 4.3. There was a much larger spread in age values for the stars determined in this study that what was determined in Pinsonneault et al. (2018). This is also due to a large portion of the sample from Pinsonneault et al. (2018) being members of NGC 6791.

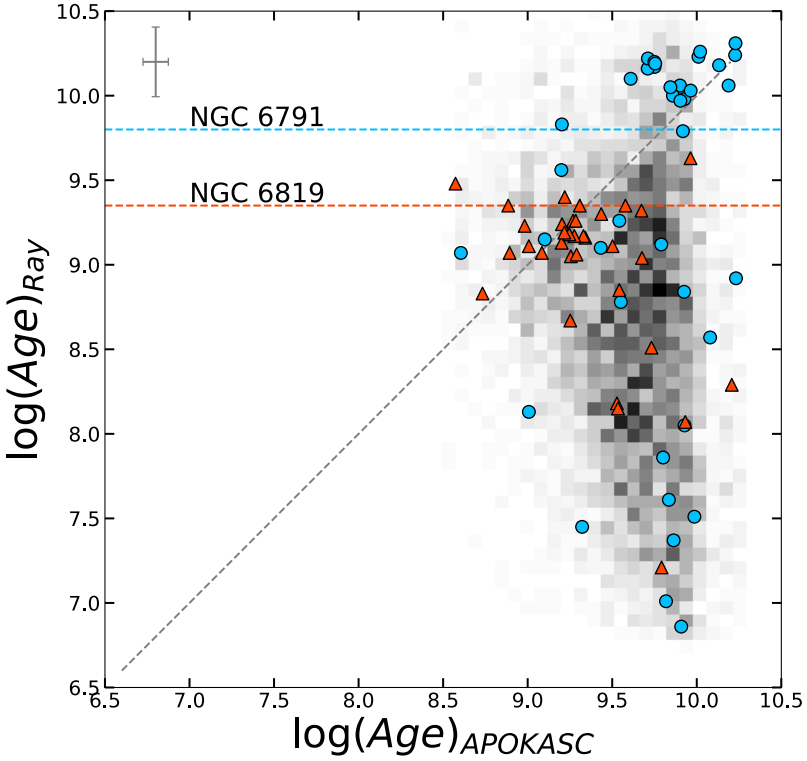

Figure 4.3: The age comparison for stars that matched to Pinsonneault et al. (2018) for the two calibration clusters NGC 6791 and NGC 6819. Blue circles represent stars that are members of NGC 6791 and red triangles are stars that are members of NGC 6819. The grey dashed line is the one-to-one line for stellar ages and the blue and red dotted lines represent the ages determined in Cantat-Gaudin et al. (2020) for the clusters NGC 6791 and 6819, respectively. Finally, the grey bins are ages of field stars after the age-mass-metallicity calibration from this study had been applied. This figure was provided by courtesy of Taylor Spoo.

Table 4.2: The output from *The Cannon* for every star in the MMT/Hectochelle open cluster sample. Cluster members used in the average Fe/H cluster determination are indicated by a "Y" in the last column.

Gaia ID	Cluster	T_{eff} (K)	log g (dex)	[Fe/H] (dex)	[Mg/Fe] (dex)	[Si/Fe] (dex)	[Ni/Fe] (dex)	[Ca/Fe] (dex)	[Na/Fe] (dex)	[V/Fe] (dex)	Member	Mass
2051081084121236736	NGC 6791	6355	5.44	+0.33	−0.04	+0.06	+0.00	+0.00	+0.15	−0.10	N	N
2051083420583645056	NGC 6791	4799	2.40	−0.14	+0.12	+0.08	+0.02	−0.02	−0.05	+0.49	N	Y
2051084107778569856	NGC 6791	4510	2.23	+0.14	+0.05	−0.05	+0.03	−0.10	−0.01	−0.25	N	Y
2051084245217489664	NGC 6791	4038	1.19	−0.38	+0.22	+0.12	+0.03	−0.01	−0.04	−0.06	N	Y
2051084691894259328	NGC 6791	4373	2.21	−0.21	+0.27	+0.13	+0.06	+0.04	+0.09	−0.32	N	Y
2051086031924019328	NGC 6791	4744	2.97	−0.09	+0.12	+0.07	+0.01	+0.04	+0.17	−0.22	N	Y
2051087028356217728	NGC 6791	4932	3.02	−0.18	+0.08	+0.07	−0.02	+0.03	+0.13	−0.11	N	Y
2051087298931991936	NGC 6791	4662	2.90	+0.12	+0.08	+0.04	+0.03	−0.01	+0.22	−0.28	N	Y
2051094072102338944	NGC 6791	4857	2.73	−0.33	+0.17	+0.09	+0.05	+0.06	+0.08	−0.01	N	Y
2051094514478219776	NGC 6791	4887	2.44	−0.12	+0.06	+0.08	+0.01	+0.00	−0.11	+0.10	N	Y

Full Table can be found in §B Table B.1

Table 4.3: Asteroseismic results for MMT/Hectochelle open cluster stars using the frequencies (ν_{max}, $\Delta\nu$) from Zinn et al. (2022) and our derived Age-relation in Equation 4.1.

ID	**Cluster**	ν_{max} (μHz)	$\Delta\nu$ (μHz)	$\mathbf{T}_{eff}$ **(K)**	**Mass** ($M_\odot$)
ID 247734180	NGC 1746	10.68±0.80	1.79±0.11	4933±43	1.20±0.49
ID 247685147	NGC 1746	40.99±0.89	4.64±0.13	4820±43	1.47±0.21
ID 247688569	NGC 1746	31.49±0.61	4.03±0.08	4933±43	1.19±0.17
ID 247719695	NGC 1746	35.94±0.48	4.26±0.10	5176±43	1.46±0.16
ID 247696469	NGC 1746	41.70±1.02	4.68±0.04	4710±43	1.47±0.14
ID 246897900	NGC 1817	9.38±0.14	1.48±0.08	4789±43	1.70±0.28
ID 246907540	NGC 1817	83.19±1.57	7.02±0.25	5153±43	2.45±0.23
ID 246899904	NGC 1817	24.06±1.23	3.43±0.02	4976±43	1.01±0.21
ID 246907932	NGC 1817	31.25±0.75	4.13±0.11	5150±43	1.08±0.20
ID 246933528	NGC 1817	65.45±1.07	5.67±0.14	5434±43	2.90±0.18
ID 246893133	NGC 1817	36.31±0.89	4.48±0.07	4903±43	1.19±0.17
ID 246909519	NGC 1817	79.15±1.03	6.69±0.16	5150±43	2.56±0.16
ID 246915802	NGC 1817	67.62±1.02	5.93±0.07	5121±43	2.58±0.12
ID 246931251	NGC 1817	29.37±0.22	3.58±0.06	4865±43	1.53±0.12
ID 246889908	NGC 1817	71.05±0.62	6.24±0.09	5083±43	2.42±0.11
ID 246871689	NGC 1817	57.00±0.37	5.24±0.04	5083±43	2.51±0.08
ID 211930807	NGC 2632	13.33±0.46	2.05±0.06	4897±43	1.35±0.25
ID 211942812	NGC 2632	32.12±0.53	3.53±0.12	5156±43	2.21±0.22
ID 211956503	NGC 2632	24.83±0.51	3.45±0.10	5115±43	1.11±0.21
ID 211971510	NGC 2632	28.95±0.57	3.55±0.01	4367±43	1.41±0.10
ID 211967060	NGC 2632	165.80±0.79	13.64±0.10	4897±43	1.32±0.08
ID 08521856+1144263	NGC 2682	33.84±1.04	3.53±0.12	4763±43	2.45±0.26
ID 211421577	NGC 2682	48.35±0.68	5.39±0.13	4873±43	1.33±0.17
ID 211418744	NGC 2682	26.35±0.44	3.38±0.05	4894±43	1.40±0.14
ID 211395962	NGC 2682	109.57±1.39	10.23±0.13	5151±43	1.24±0.12
ID 211402742	NGC 2682	41.81±0.42	4.79±0.07	4699±43	1.35±0.12
ID 08521097+1131491	NGC 2682	46.53±0.42	4.90±0.07	4652±43	1.69±0.11
ID 211379264	NGC 2682	23.41±0.42	3.59±0.01	4812±43	0.76±0.10
ID 08504964+1135089	NGC 2682	76.56±0.75	7.15±0.06	4794±43	1.70±0.10
ID 211413430	NGC 2682	72.14±0.76	7.33±0.05	5103±43	1.34±0.09
ID 211436513	NGC 2682	100.17±1.24	9.22±0.01	4886±43	1.39±0.07
ID 211417995	NGC 2682	136.34±0.38	11.74±0.09	4915±43	1.34±0.07
ID 08492491+1144057	NGC 2682	190.06±0.14	14.66±0.02	4996±43	1.51±0.04
ID 19203303+3755558	NGC 6791	0.79±0.14	0.24±0.11	4453±43	1.35±2.31
ID 19223206+3729277	NGC 6791	5.45±0.04	0.99±0.12	4038±43	1.49±0.52
ID 19210245+3812541	NGC 6791	2.06±0.02	0.48±0.04	4575±43	1.58±0.37
ID 19232489+3738534	NGC 6791	11.23±0.30	2.20±0.09	4313±43	0.56±0.28
ID 19225665+3732517	NGC 6791	4.53±0.03	0.85±0.05	4373±43	1.64±0.28

Continued on next page

Table 4.3 – Continued

ID	Cluster	ν_{max} (μHz)	$\Delta\nu$ (μHz)	T_{eff} (K)	Mass ($M_\odot$)
ID 19215905+3817308	NGC 6791	4.07±0.01	0.78±0.02	4801±43	1.75±0.14
ID 19225059+3755438	NGC 6791	7.25±0.02	1.30±0.02	4390±43	1.24±0.12
ID 19220320+3732313	NGC 6791	5.71±0.02	0.98±0.02	4932±43	2.03±0.10
ID 19204517+3744339	NGC 6791	8.24±0.02	1.52±0.02	4350±43	0.98±0.09
ID 19210483+3741036	NGC 6791	54.79±0.14	4.79±0.05	4441±43	2.92±0.08
ID 19211041+3734464	NGC 6791	16.86±0.01	2.47±0.02	4887±43	1.29±0.07
ID 19202870+3743169	NGC 6791	14.02±0.03	1.99±0.02	4484±43	1.65±0.07
ID 19205530+3743152	NGC 6791	15.92±0.03	2.18±0.01	4214±43	1.62±0.07
ID 19213974+3814517	NGC 6791	30.16±0.03	4.32±0.03	4644±43	0.76±0.06
ID 19214847+3757485	NGC 6791	17.87±0.01	2.35±0.02	4937±43	1.88±0.06
ID 19212463+3816104	NGC 6791	34.87±0.02	4.25±0.02	4452±43	1.22±0.06
ID 19210629+3744596	NGC 6791	11.97±0.02	1.68±0.01	4486±43	2.01±0.05
ID 19221596+3744553	NGC 6791	27.22±0.01	3.44±0.02	4398±43	1.34±0.05
ID 19202430+3809412	NGC 6791	31.28±0.01	3.81±0.02	5087±43	1.49±0.05
ID 19203953+3810181	NGC 6791	35.07±0.01	4.15±0.02	5404±43	1.55±0.05
ID 19210426+3747187	NGC 6791	29.26±0.02	3.74±0.01	4114±43	1.14±0.05
ID 19223049+3800110	NGC 6791	32.19±0.01	3.84±0.02	4903±43	1.53±0.05
ID 19203005+3750191	NGC 6791	27.24±0.04	3.77±0.01	4507±43	0.95±0.05
ID 19224052+3802014	NGC 6791	30.75±0.02	3.69±0.01	4564±43	1.49±0.05
ID 19212261+3802019	NGC 6791	33.44±0.02	4.16±0.01	4263±43	1.14±0.05
ID 19215971+3756169	NGC 6791	20.58±0.01	2.60±0.01	4992±43	1.93±0.05
ID 19201973+3746549	NGC 6791	15.42±0.02	2.17±0.01	4426±43	1.54±0.05
ID 19211300+3743005	NGC 6791	29.04±0.01	3.78±0.01	4498±43	1.13±0.05
ID 19210326+3741190	NGC 6791	30.67±0.02	3.78±0.01	4124±43	1.26±0.05
ID 19205003+3747282	NGC 6791	17.44±0.02	2.24±0.01	4793±43	2.08±0.05
ID 19203485+3746298	NGC 6791	32.68±0.01	3.92±0.01	4460±43	1.38±0.05
ID 19225922+3809386	NGC 6791	30.79±0.01	3.78±0.01	4724±43	1.39±0.05
ID 19205510+3747162	NGC 6791	43.61±0.02	4.27±0.01	3923±43	2.15±0.05
ID 19210604+3752049	NGC 6791	23.49±0.02	3.04±0.01	4513±43	1.43±0.04
ID 19214745+3730572	NGC 6791	21.52±0.00	2.73±0.01	4662±43	1.73±0.04
ID 19204102+3743025	NGC 6791	240.15±0.02	22.30±0.06	4455±43	0.53±0.04
ID 19210286+3737297	NGC 6791	30.71±0.01	3.73±0.01	5038±43	1.52±0.04
ID 19205368+3750236	NGC 6791	32.72±0.01	3.91±0.01	4488±43	1.41±0.04
ID 19202786+3800415	NGC 6791	24.02±0.02	3.48±0.01	4779±43	0.93±0.04
ID 19203784+3745249	NGC 6791	28.91±0.02	4.00±0.01	4479±43	0.89±0.04
ID 19235064+3753231	NGC 6791	35.86±0.00	4.04±0.01	4163±43	1.56±0.04
ID 19203934+3748048	NGC 6791	39.50±0.01	4.23±0.01	4277±43	1.76±0.04
ID 19210112+3742134	NGC 6791	41.31±0.01	4.48±0.01	4173±43	1.57±0.04
ID 19204624+3749105	NGC 6791	31.68±0.01	3.99±0.01	4439±43	1.17±0.04
ID 19202244+3751414	NGC 6791	37.05±0.02	4.12±0.01	4403±43	1.64±0.04
ID 19205629+3744334	NGC 6791	66.96±0.01	5.57±0.01	4477±43	2.93±0.04
ID 19204158+3811339	NGC 6791	23.73±0.00	2.99±0.00	4710±43	1.62±0.04

Continued on next page

Table 4.3 – Continued

ID	Cluster	ν_{max} (μHz)	$\Delta\nu$ (μHz)	T_{eff} (K)	Mass ($M_\odot$)
ID 19205338+3748282	NGC 6791	44.31±0.00	4.60±0.00	4002±43	1.70±0.04
ID 19214019+3802394	NGC 6791	48.07±0.01	4.67±0.01	4848±43	2.32±0.04
ID 19212903+3821053	NGC 6791	92.62±0.02	8.12±0.01	4842±43	1.81±0.04
ID 19213238+3817538	NGC 6791	112.47±0.01	9.28±0.01	3914±43	1.65±0.04
ID 19223563+3736262	NGC 6791	54.90±0.01	5.21±0.01	4744±43	2.20±0.04
ID 19220306+3747033	NGC 6791	38.17±0.01	4.19±0.01	5732±43	1.99±0.04
ID 19203519+3748579	NGC 6791	123.29±0.00	10.35±0.01	3976±43	1.42±0.04
ID 19222821+3752242	NGC 6791	75.52±0.01	7.22±0.01	4918±43	1.59±0.04
ID 19222484+3803157	NGC 6791	61.15±0.00	6.09±0.01	4633±43	1.60±0.04
ID 19231591+3801262	NGC 6791	57.58±0.00	5.74±0.00	4627±43	1.69±0.04
ID 19203353+3817329	NGC 6791	96.22±0.01	8.89±0.01	4983±43	1.44±0.04
ID 19230332+3738009	NGC 6791	57.93±0.01	5.81±0.00	4824±43	1.68±0.04
ID 19224166+3729115	NGC 6791	132.89±0.01	11.10±0.01	4510±43	1.46±0.04
ID 19221553+3727116	NGC 6791	56.51±0.01	5.66±0.00	4799±43	1.73±0.04
ID 19210539+3732430	NGC 6791	100.16±0.00	9.34±0.01	4857±43	1.31±0.03
ID 19200622+3753403	NGC 6791	210.81±0.01	15.49±0.01	4711±43	1.58±0.03
ID 19194601+3756520	NGC 6791	236.82±0.02	18.19±0.01	4745±43	1.19±0.03
ID 19421008+3953561	NGC 6819	0.85±0.03	0.23±0.15	5035±43	2.17±2.73
ID 19405020+4013109	NGC 6819	0.48±0.04	0.17±0.07	4778±43	1.27±1.80
ID 19425827+3956354	NGC 6819	6.47±0.08	1.16±0.27	4753±43	1.49±1.00
ID 19404617+4033082	NGC 6819	4.60±0.03	0.82±0.07	4520±43	2.02±0.39
ID 19412386+4021444	NGC 6819	2.43±0.02	0.55±0.04	4853±43	1.54±0.36
ID 19412953+4012210	NGC 6819	3.55±0.04	0.69±0.02	4805±43	1.95±0.19
ID 19395519+4012573	NGC 6819	4.09±0.01	0.75±0.02	4707±43	2.11±0.16
ID 19411253+4035286	NGC 6819	3.10±0.04	0.60±0.01	3866±43	1.96±0.14
ID 19403213+4031387	NGC 6819	4.75±0.02	0.89±0.02	4828±43	1.70±0.14
ID 19414409+4041463	NGC 6819	7.80±0.03	1.36±0.02	4681±43	1.35±0.10
ID 19404131+4025262	NGC 6819	26.42±0.02	2.85±0.04	4306±43	2.58±0.09
ID 19410991+4015495	NGC 6819	18.01±0.01	1.98±0.03	4809±43	3.74±0.09
ID 19401427+4035120	NGC 6819	62.14±0.68	6.15±0.02	4742±43	1.64±0.08
ID 19405797+4008174	NGC 6819	22.47±0.03	2.88±0.03	4815±43	1.64±0.08
ID 19412794+4037568	NGC 6819	48.59±0.02	4.57±0.04	4817±43	2.60±0.07
ID 19403444+4025068	NGC 6819	28.10±0.02	3.70±0.03	4772±43	1.16±0.06
ID 19410994+4009056	NGC 6819	33.54±0.01	3.71±0.03	5029±43	2.03±0.06
ID 19403569+4005038	NGC 6819	21.99±0.01	2.99±0.01	4776±43	1.32±0.05
ID 19412222+4016442	NGC 6819	41.66±0.02	4.36±0.02	4697±43	1.94±0.05
ID 19425416+4015349	NGC 6819	36.60±0.01	4.05±0.01	4057±43	1.61±0.05
ID 19412047+3944357	NGC 6819	14.38±0.00	2.03±0.01	4991±43	1.77±0.05
ID 19421683+4008114	NGC 6819	45.53±0.01	4.69±0.01	4815±43	1.93±0.05
ID 19412491+4007440	NGC 6819	22.04±0.00	2.88±0.01	3842±43	1.33±0.04
ID 19394143+4017052	NGC 6819	149.38±0.02	11.96±0.03	4651±43	1.57±0.04
ID 19430343+4033513	NGC 6819	62.06±0.01	6.14±0.01	4080±43	1.49±0.04

Continued on next page

Table 4.3 – Continued

ID	**Cluster**	ν_{max} (μHz)	$\Delta\nu$ (μHz)	$\mathbf{T}_{eff}$ **(K)**	**Mass** ($M_\odot$)
ID 19413439+4017482	NGC 6819	44.10±0.01	4.62±0.01	4179±43	1.69±0.04
ID 19412942+4014199	NGC 6819	47.42±0.01	4.85±0.01	4662±43	1.87±0.04
ID 19405420+4018159	NGC 6819	51.49±0.01	5.57±0.01	4527±43	1.34±0.04
ID 19421561+4032169	NGC 6819	45.24±0.01	4.70±0.01	4151±43	1.70±0.04
ID 19404440+4031310	NGC 6819	40.29±0.01	4.32±0.01	4497±43	1.78±0.04
ID 19410926+4014436	NGC 6819	47.12±0.01	4.81±0.01	4791±43	1.93±0.04
ID 19421779+4034210	NGC 6819	47.27±0.02	4.77±0.01	4606±43	1.96±0.04
ID 19422043+4028395	NGC 6819	51.79±0.00	5.17±0.01	3843±43	1.65±0.04
ID 19422325+4009213	NGC 6819	28.39±0.01	3.55±0.01	4675±43	1.40±0.04
ID 19410858+4013299	NGC 6819	26.92±0.01	3.38±0.01	4789±43	1.47±0.04
ID 19411500+4025590	NGC 6819	31.76±0.01	3.88±0.01	5163±43	1.47±0.04
ID 19404803+4008085	NGC 6819	35.16±0.01	4.14±0.01	4625±43	1.42±0.04
ID 19413027+4015218	NGC 6819	27.33±0.00	3.11±0.01	4837±43	2.16±0.04
ID 19403684+4015172	NGC 6819	48.92±0.01	4.75±0.01	4882±43	2.30±0.04
ID 19411115+4011422	NGC 6819	53.00±0.01	5.09±0.01	4638±43	2.14±0.04
ID 19414006+4023060	NGC 6819	60.88±0.01	5.42±0.01	4427±43	2.44±0.04
ID 19405601+4013395	NGC 6819	63.18±0.02	5.83±0.01	4933±43	2.19±0.04
ID 19411215+4018560	NGC 6819	42.48±0.01	4.30±0.00	4507±43	2.12±0.04
ID 19411564+4010105	NGC 6819	56.25±0.00	5.63±0.01	4756±43	1.74±0.04
ID 19424454+4015559	NGC 6819	44.14±0.01	4.42±0.00	4627±43	2.17±0.04
ID 19412707+4012283	NGC 6819	100.74±0.03	7.89±0.01	4564±43	2.52±0.04
ID 19410524+4014042	NGC 6819	66.25±0.01	5.75±0.01	4794±43	2.63±0.04
ID 19413031+4009005	NGC 6819	153.06±0.00	12.21±0.00	4107±43	1.43±0.04
ID 19432856+4017456	NGC 6819	261.00±0.02	21.62±0.02	4969±43	0.82±0.04
ID 19394311+4011067	NGC 6819	91.63±0.01	7.65±0.01	4904±43	2.24±0.04
ID 19414807+4019455	NGC 6819	133.87±0.01	10.54±0.01	4797±43	1.92±0.04
ID 19422693+4038597	NGC 6819	125.59±0.00	10.03±0.01	4537±43	1.86±0.03
ID 19411776+4009158	NGC 6819	72.31±0.01	6.98±0.01	4982±43	1.61±0.03
ID 19401611+4035471	NGC 6819	131.45±0.01	10.25±0.01	4888±43	2.06±0.03

Chapter 5

Future Work

By tripling the number of stars used in the previous asteroseismic age calibration, it was shown in Section 4.3 that it can be applied to a large number of stars, including field stars. There are several different ways this research can continue and be improved, however.

The first logical step is to get more observations for clusters that match in Kepler 2 fields. If more clusters can be added, then that would mean a larger star cluster age range could be covered. With this better age range, the calibration itself would also be much better at determining ages of field stars than it currently does. Another proposal can be submitted to the MMT after extra clusters are confirmed to have asteroseismic targets that are members. Table 5.1 shows all of the clusters that were matched to K2 fields.

Another option is to match clusters to asteroseismic targets in the Transiting Exoplanet Survey Satellite or TESS mission. Similar to Kepler, TESS is also collecting light curves and asteroseismology has also been done for a large number of stars Campante et al. (2016). One of the main advantages to using TESS is that this mission is still active today and plans on remaining active for the foreseeable future whereas Kepler was decommissioned in 2018. A disadvantage to using data from this mission is that the lightcurves are not as high resolution as Kepler was Campante et al. (2016). However, if TESS is able to observe a larger number of clusters than what currently matches to K2, then the fit for the calibration might improve.

Table 5.1: Potential K2 Cluster Targets

Cluster name	# K2 stars	RA (°)	Dec (°)	Radius (')	Age (Gyr)	Distance (kpc)
CALIBRATION SAMPLE						
NGC 2682	1070	08:51:18	+11:48:00	12.5	9.450	0.808
Melotte 22	1854	03:47:00	+24:07:00	60.0	8.131	0.133
PRIMARY SAMPLE						
NGC 2129	10	06:01:07	+23:19:20	2.5	7.000	2.200
IC 2157	11	06:04:50	+24:03:21	2.5	7.800	2.040
NGC 2168	70	06:08:54	+24:20:00	20.0	8.250	0.912
NGC 2175	64	06:09:39	+20:29:12	11.0	6.953	1.627
Collinder 89	383	06:18:00	+23:38:00	30.0	7.500	0.800
Koposov 62	28	06:18:02	+24:42:38	3.0	9.400	2.800
Berkeley 23	84	06:33:30	+20:33:00	2.0	8.900	6.918
NGC 2266	109	06:43:19	+26:58:12	2.5	8.800	3.000
Berkeley 29	16	06:53:18	+16:55:00	3.0	9.025	14.871
Collinder 302	13253	16:26:08	-26:15:00	250.0	*N/A*	*N/A*
NGC 2632	2328	08:40:24	+19:40:00	35.0	8.863	0.187
NGC 2678	57	08:50:02	+11:20:18	6.5	9.360	0.900
NGC 6698	57	18:48:04	-25:52:42	5.5	9.280	1.150
Ruprecht 145	152	18:50:36	-18:15:00	17.5	7.500	0.320
NGC 6716	12	18:54:34	-19:54:06	5.0	7.961	0.789
Ruprecht 147	202	19:16:42	-16:17:00	12.5	9.400	0.295
NGC 6531	14	18:04:13	-22:29:24	7.0	7.070	1.205
NGC 6530	202	18:04:31	-24:21:30	7.0	6.867	1.330
NGC 1647	165	04:45:55	+19:06:54	20.0	8.158	0.540
NGC 1746	488	05:03:50	+23:46:12	21.0	8.645	0.800
NGC 1750	252	05:03:55	+23:39:30	10.0	8.300	0.630
NGC 1758	125	05:04:35	+23:47:54	4.5	8.600	0.760
Platais 4	4780	05:07:22	+22:16:42	102.0	8.000	0.276
NGC 1817	467	05:12:15	+16:41:24	8.0	8.612	1.972
SECONDARY SAMPLE						
IC 2156	1	06:04:51	+24:09:30	2.0	8.400	2.100
NGC 2234	4	06:29:20	+16:45:27	4.0	7.700	4.800
NGC 6737	4	19:02:20	-18:32:59	4.4	8.700	2.120
Czernik 37	2	17:53:17	-27:22:10	2.5	8.400	1.440
Bochum 14	4	18:02:00	-23:41:00	1.0	6.996	0.578
Teutsch 14a	2	18:03:29	-22:07:50	3.5	8.000	1.720
Collinder 468	4	18:06:35	-27:27:36	0.5	9.500	7.376
NGC 6596	2	18:17:33	-16:39:00	5.0	8.600	1.100
NGC 6603	2	18:18:26	-18:24:24	3.0	8.300	3.600
NGC 6613	6	18:19:58	-17:06:06	2.5	7.223	1.296

Appendix A

The Full CTIO/Hydra Open Cluster Sample

Table A.1: The output from *The Cannon* for every star in the CTIO/Hydra open cluster sample. Cluster members used in the average Fe/H cluster determination are indicated by a "Y" in the last column.

ID	Cluster	T_{eff} (K)	log g (dex)	[Fe/H] (dex)	Member
09001428-4901040	Collinder 205	4787.27	2.48	0.08	Y
12291805-6031347	Collinder 258	3838.40	0.42	-0.53	N
12265230-6047561	Collinder 258	4772.74	2.43	0.08	Y
17245416-4953075	IC 4651	4760.83	2.77	0.02	Y
17261801-4952535	IC 4651	4738.81	2.40	0.07	N
17245259-4956313	IC 4651	4738.65	2.41	0.06	N
17252437-4958525	IC 4651	4780.07	2.82	0.03	Y
17243568-4956273	IC 4651	4773.25	2.81	0.03	Y
17250895-4953571	IC 4651	4731.56	2.71	0.03	Y
17252354-4955470	IC 4651	4770.66	2.80	0.03	Y
17234787-4947221	IC 4651	4741.17	2.40	0.06	N
17245776-5001327	IC 4651	4764.54	2.78	0.03	Y
17260141-4954283	IC 4651	4764.79	2.79	0.03	Y
17251321-4959293	IC 4651	4766.37	2.79	0.03	Y
18385292+0520165	IC 4756	4629.50	2.16	0.07	Y
18380662+0519502	IC 4756	4775.57	2.46	0.06	N
18382656+0509501	IC 4756	4771.75	2.46	0.06	N
18384377+0514200	IC 4756	4637.44	2.17	0.07	Y
18382075+0526024	IC 4756	4688.73	2.26	0.07	Y
18373582+0515379	IC 4756	3788.00	0.40	-0.43	Y
18380515+0524337	IC 4756	4658.91	2.21	0.08	Y
18380876+0520554	IC 4756	4771.74	2.45	0.07	Y
04482950+1055482	NGC 1662	4665.30	2.28	0.06	Y
04474415+1106572	NGC 1662	4749.58	2.41	0.06	N
04480658+1048553	NGC 1662	4770.54	2.45	0.07	N
04482517+1047057	NGC 1662	4758.87	2.43	0.07	N
04483208+1057589	NGC 1662	4672.08	2.32	0.07	Y
04482904+1100117	NGC 1662	4760.41	2.44	0.07	N
06210343-0719085	NGC 2215	4788.76	2.48	0.08	N
06204686-0717029	NGC 2215	4801.98	2.46	0.09	Y
07142988-2552101	NGC 2354	4804.25	2.50	0.08	N
07135193-2544242	NGC 2354	4831.83	2.55	0.11	Y
07133035-2543342	NGC 2354	4818.69	2.53	0.08	N
07140636-2536449	NGC 2354	4821.40	2.53	0.08	N
07132188-2527005	NGC 2354	4815.74	2.54	0.07	N
07132374-2533462	NGC 2354	4819.30	2.52	0.10	Y
07372858-1355585	NGC 2423	4829.17	2.54	0.08	Y
07380534-1404073	NGC 2423	4833.78	2.54	0.08	Y
07371259-1344553	NGC 2423	4832.77	2.55	0.08	Y

Continued on next page

Table A.1 – Continued

ID	Cluster	T_{eff} (K)	log g (dex)	[Fe/H] (dex)	Member
07374842-1335074	NGC 2423	4835.09	2.56	0.09	Y
07364647-1350306	NGC 2423	4836.32	2.54	0.09	Y
07370026-1345381	NGC 2423	4824.86	2.53	0.09	Y
07361592-1403461	NGC 2423	4834.41	2.54	0.09	Y
07373533-1357296	NGC 2423	4820.19	2.53	0.07	N
07421614-1449443	NGC 2437	4778.37	2.44	0.08	N
07414072-1454283	NGC 2437	4784.13	2.46	0.08	N
07413760-1443129	NGC 2437	4819.43	2.55	0.12	Y
07405803-1451026	NGC 2437	4781.65	2.46	0.08	N
07413200-1451484	NGC 2437	4778.97	2.46	0.08	N
07411127-1452280	NGC 2437	4803.82	2.49	0.08	N
07421014-1438511	NGC 2437	4815.49	2.52	0.07	N
07414194-1447158	NGC 2437	4806.49	2.50	0.08	N
07420012-1451449	NGC 2437	4809.32	2.51	0.07	N
07415842-1449247	NGC 2437	4773.80	2.44	0.09	N
07422015-1438296	NGC 2437	4793.59	2.48	0.09	N
07422286-1442555	NGC 2437	4823.00	2.55	0.11	Y
07415256-1452141	NGC 2437	4788.20	2.47	0.08	N
07410541-1445518	NGC 2437	4795.06	2.50	0.08	N
07414693-1440371	NGC 2437	4808.69	2.52	0.07	N
07414286-1457022	NGC 2437	4797.97	2.49	0.09	N
07410834-1451274	NGC 2437	4797.53	2.49	0.08	N
07413811-1452433	NGC 2437	4816.49	2.53	0.07	N
07420592-1444335	NGC 2437	4798.63	2.49	0.08	N
07410253-1447474	NGC 2437	4784.07	2.47	0.08	N
07412289-1449109	NGC 2437	4773.84	2.44	0.09	N
07424124-1459514	NGC 2437	4807.95	2.51	0.11	Y
07413129-1438220	NGC 2437	4791.33	2.49	0.06	N
07443507-2351416	NGC 2447	4775.98	2.45	0.09	N
07442573-2349529	NGC 2447	4825.81	2.52	0.10	Y
07445380-2353151	NGC 2447	4812.84	2.50	0.10	Y
07444196-2350167	NGC 2447	4789.91	2.47	0.09	N
07450246-2351137	NGC 2447	4784.88	2.47	0.09	N
07444142-2351037	NGC 2447	4786.01	2.46	0.09	N
07443281-2357504	NGC 2447	4790.09	2.46	0.10	Y
07441844-2353236	NGC 2447	4811.86	2.49	0.11	Y
07441545-2350327	NGC 2447	4778.51	2.46	0.08	N
07450947-2349325	NGC 2447	4805.01	2.48	0.10	Y
07442803-2342458	NGC 2447	4764.14	2.42	0.10	N
07444418-2347222	NGC 2447	4822.71	2.51	0.09	Y
07435090-2341436	NGC 2447	4815.99	2.50	0.10	Y
07443373-2348488	NGC 2447	4794.46	2.49	0.08	N
07442457-2350440	NGC 2447	4792.19	2.46	0.09	Y

Continued on next page

Table A.1 – Continued

ID	Cluster	T_{eff} (K)	log g (dex)	[Fe/H] (dex)	Member
07574523-6055353	NGC 2516	4764.43	2.42	0.09	N
07561863-6031352	NGC 2516	4735.68	2.31	0.09	Y
07595779-6044484	NGC 2516	4793.95	2.49	0.08	N
07573787-6054321	NGC 2516	4789.77	2.47	0.08	N
07580963-6049007	NGC 2516	4648.56	2.16	0.09	Y
08104884-1250289	NGC 2539	4804.93	2.51	0.08	N
08104286-1240117	NGC 2539	4834.55	2.55	0.11	Y
08102302-1250433	NGC 2539	4824.28	2.53	0.10	Y
08101609-1254061	NGC 2539	4798.90	2.49	0.08	N
08100631-1255197	NGC 2539	4791.31	2.49	0.08	N
08102909-1243329	NGC 2539	4805.44	2.51	0.08	N
08103495-1251577	NGC 2539	4779.92	2.45	0.07	N
08111558-3739567	NGC 2546	4796.49	2.44	0.08	Y
08121540-3731450	NGC 2546	4801.62	2.52	0.06	N
08141471-3738428	NGC 2546	4844.87	2.95	0.02	N
08112772-3740402	NGC 2546	4807.90	2.55	0.05	N
08111698-3736417	NGC 2546	4808.27	2.53	0.05	N
08135440-0558476	NGC 2548	4805.47	2.52	0.06	N
08142812-0542161	NGC 2548	4825.16	2.51	0.08	Y
08134483-0548008	NGC 2548	4817.36	2.50	0.08	Y
08133964-0547148	NGC 2548	4794.72	2.48	0.07	N
08134771-5372590	NGC 2548	4797.03	2.50	0.07	N
08141703-0554007	NGC 2548	4837.39	2.52	0.08	Y
08134291-0535471	NGC 2548	4806.27	2.53	0.06	N
08123723-0540509	NGC 2548	4823.41	2.51	0.08	Y
08204217-3613125	NGC 2579	4667.75	2.20	0.10	Y
08210039-3617163	NGC 2579	4729.18	2.31	0.09	Y
08463129-5252414	NGC 2669	4718.10	2.29	0.09	Y
08511710+1148160	NGC 2682	4852.30	2.60	0.11	Y
08512898+1150330	NGC 2682	4847.91	2.59	0.10	Y
08511747+1145226	NGC 2682	4859.56	2.62	0.11	Y
08514235+1151230	NGC 2682	4847.76	2.59	0.10	Y
08511704+1150464	NGC 2682	4848.58	2.58	0.10	Y
08512280+1148016	NGC 2682	4847.55	2.59	0.11	Y
08504964+1135089	NGC 2682	4836.58	2.58	0.09	Y
08512377+1149493	NGC 2682	4841.68	2.58	0.08	Y
08512990+1147168	NGC 2682	4826.25	2.56	0.09	Y
08511269+1152423	NGC 2682	4851.35	2.59	0.11	Y
11252623-4311239	NGC 3680	3792.87	0.35	-0.43	Y
11252924-4315477	NGC 3680	3798.49	0.35	-0.46	Y
11253582-4311211	NGC 3680	4725.16	2.35	0.08	N
11253865-4313587	NGC 3680	4557.96	2.04	0.10	Y
11253807-4316064	NGC 3680	3785.80	0.34	-0.44	Y

Continued on next page

Table A.1 – Continued

ID	Cluster	T_{eff} (K)	log g (dex)	[Fe/H] (dex)	Member
11250152-4310231	NGC 3680	4729.66	2.36	0.09	N
11261027-4321592	NGC 3680	4722.45	2.35	0.09	N
11254853-4309524	NGC 3680	3792.71	0.33	-0.45	Y
11254991-4312157	NGC 3680	3783.29	0.34	-0.38	Y
11254329-4315563	NGC 3680	4674.15	2.25	0.09	N
13462566-6255556	NGC 5281	3853.97	0.43	-0.56	Y
13460048-6255149	NGC 5281	4797.12	2.49	0.07	N
14294260-6039313	NGC 5617	4767.91	2.44	0.08	N
14295016-6041121	NGC 5617	4645.96	2.23	0.07	Y
14292873-6042188	NGC 5617	4618.83	2.19	0.08	Y
15035344-5414055	NGC 5822	4710.26	2.32	0.09	N
15034041-5428128	NGC 5822	4703.20	2.32	0.09	N
15030047-5428176	NGC 5822	4669.98	2.27	0.09	Y
15045198-5419086	NGC 5822	4731.67	2.37	0.09	N
15053113-5426201	NGC 5822	4683.56	2.28	0.08	Y
15042824-5417416	NGC 5822	4747.35	2.39	0.08	N
15042202-5424032	NGC 5822	4728.79	2.36	0.09	N
15042125-5423056	NGC 5822	4673.80	2.27	0.09	Y
15052349-5421348	NGC 5822	4678.25	2.28	0.08	Y
15040342-5405419	NGC 5822	4703.10	2.33	0.08	Y
15041417-5425473	NGC 5822	4694.47	2.31	0.08	Y
15035000-5414304	NGC 5822	4659.06	2.25	0.09	Y
15031585-5416391	NGC 5822	4632.48	2.20	0.09	Y
15041709-5423386	NGC 5822	4695.83	2.30	0.09	N
15031209-5414065	NGC 5822	4697.29	2.30	0.09	N
15034941-5420105	NGC 5822	4625.32	2.17	0.09	Y
16131847-5414040	NGC 6067	4714.63	2.33	0.09	Y
16130280-5421369	NGC 6067	4670.69	2.25	0.10	Y
16130403-5412187	NGC 6067	4657.75	2.27	0.08	Y
16133568-5407364	NGC 6067	4630.93	2.21	0.08	Y
16123981-5417410	NGC 6067	4736.69	2.41	0.07	Y
16132470-5420055	NGC 6067	4758.74	2.77	0.03	Y
16253239-4043477	NGC 6124	4784.62	2.49	0.07	N
16255169-4044280	NGC 6124	4772.21	2.44	0.07	N
16243712-4029170	NGC 6124	4788.87	2.49	0.06	N
16271625-4037254	NGC 6124	4789.93	2.48	0.06	N
16242387-4043492	NGC 6124	4787.63	2.49	0.06	N
16255980-4033307	NGC 6124	4748.34	2.74	0.03	Y
16243609-4037027	NGC 6124	4787.79	2.51	0.06	N
16260042-4051026	NGC 6124	4742.16	2.72	0.03	Y
16270442-4033171	NGC 6124	4794.07	2.51	0.06	N
16242637-4045386	NGC 6124	4744.73	2.73	0.03	Y
16244606-4039576	NGC 6124	4782.51	2.49	0.06	N

Continued on next page

Table A.1 – Continued

ID	Cluster	T_{eff} (K)	log g (dex)	[Fe/H] (dex)	Member
16234611-4046305	NGC 6124	4780.97	2.47	0.06	N
16262353-4039538	NGC 6124	4790.38	2.50	0.06	N
16260855-4036035	NGC 6124	4782.92	2.48	0.06	N
16250138-4028260	NGC 6124	4778.58	2.46	0.07	N
16275628-4910297	NGC 6134	4658.73	2.24	0.08	Y
16275584-4908108	NGC 6134	4703.64	2.35	0.07	Y
16280018-4909063	NGC 6134	4693.53	2.31	0.08	Y
16280553-4912399	NGC 6134	4671.56	2.28	0.09	Y
16275101-4906559	NGC 6134	4735.52	2.40	0.07	Y
16273219-4906459	NGC 6134	4675.52	2.28	0.08	Y
16281579-4907195	NGC 6134	4629.12	2.19	0.08	Y
16343259-4931418	NGC 6167	4651.69	2.25	0.07	Y
16350391-4940290	NGC 6167	4783.95	2.49	0.06	N
16351464-4938348	NGC 6167	4800.28	2.52	0.05	N
16354597-4931130	NGC 6167	4731.07	2.68	0.02	Y
16570817-4556281	NGC 6250	4798.96	2.45	0.07	Y
17042880-3754355	NGC 6281	4738.73	2.37	0.08	N
17043597-3759311	NGC 6281	4573.56	2.09	0.10	Y
17044867-3806261	NGC 6281	4778.17	2.44	0.08	N
17044753-3753147	NGC 6281	4618.51	2.17	0.09	Y
17043637-3754271	NGC 6281	4762.71	2.42	0.09	N
17043881-3758442	NGC 6281	4737.59	2.38	0.09	N
17044830-3757244	NGC 6281	4744.81	2.38	0.08	N
17394124-3217576	NGC 6405	4765.60	2.43	0.08	N
17401652-3217511	NGC 6405	4803.61	2.50	0.07	N
17405971-3209342	NGC 6405	4800.66	2.49	0.07	N
17405855-3212520	NGC 6405	4577.10	2.10	0.08	Y
17401109-3215237	NGC 6405	4783.62	2.46	0.08	Y
17400226-3209367	NGC 6405	4775.60	2.46	0.08	N
18513150-0622062	NGC 6705	4803.16	2.50	0.06	N
18505407-0616503	NGC 6705	4801.24	2.52	0.06	Y
18505981-0617243	NGC 6705	4797.14	2.49	0.07	N
18510975-0610486	NGC 6705	4807.86	2.52	0.07	N
20113141+2632535	NGC 6885	3792.03	0.34	-0.42	Y
20114389+2635071	NGC 6885	3758.72	0.35	-0.34	Y
16284223-5131496	Ruprecht 119	4781.56	2.47	0.06	Y

Appendix B

The Full MMT/Hectochelle Open Cluster Sample

Table B.1: The output from *The Cannon* for every star in the MMT/Hectochelle open cluster sample. Cluster members used in the average Fe/H cluster determination are indicated by a "Y" in the last column.

Gaia ID	Cluster	T_{eff} (K)	log g (dex)	[Fe/H] (dex)	[Mg/Fe] (dex)	[Si/Fe] (dex)	[Ni/Fe] (dex)	[Ca/Fe] (dex)	[Na/Fe] (dex)	[V/Fe] (dex)	Member	Mass
2051081084121236736	NGC6791	6355	5.44	+0.33	−0.04	+0.06	+0.00	+0.00	+0.15	−0.10	N	N
2051083420583645056	NGC6791	4799	2.40	−0.14	+0.12	+0.08	+0.02	−0.02	−0.05	+0.49	N	Y
2051084107778569856	NGC6791	4510	2.23	+0.14	+0.05	−0.05	+0.03	−0.10	−0.01	−0.25	N	Y
2051084245217489664	NGC6791	4038	1.19	−0.38	+0.22	+0.12	+0.03	−0.01	−0.04	−0.06	N	Y
2051084691894259328	NGC6791	4373	2.21	−0.21	+0.27	+0.13	+0.06	+0.04	+0.09	−0.32	N	Y
2051086031924019328	NGC6791	4744	2.97	−0.09	+0.12	+0.07	+0.01	+0.04	+0.17	−0.22	N	Y
2051087028356217728	NGC6791	4932	3.02	−0.18	+0.08	+0.07	−0.02	+0.03	+0.13	−0.11	N	Y
2051087298931991936	NGC6791	4662	2.90	+0.12	+0.08	+0.04	+0.03	−0.01	+0.22	−0.28	N	Y
2051094072102338944	NGC6791	4857	2.73	−0.33	+0.17	+0.09	+0.05	+0.06	+0.08	−0.01	N	Y
2051094514478219776	NGC6791	4887	2.44	−0.12	+0.06	+0.08	+0.01	+0.00	−0.11	+0.10	N	Y
2051097813013102208	NGC6791	5038	2.86	−0.18	+0.08	+0.04	+0.03	+0.00	−0.01	+0.08	N	Y
2051098809449283840	NGC6791	4087	1.36	−0.38	+0.27	+0.13	+0.06	+0.08	−0.06	−0.40	N	N
2051098985545026304	NGC6791	4495	2.37	+0.22	+0.13	+0.00	+0.05	−0.01	+0.05	−0.01	Y	N
2051099260422933632	NGC6791	4504	2.58	+0.31	+0.08	+0.04	+0.04	+0.00	+0.12	−0.03	Y	N
2051103383591935232	NGC6791	5732	3.91	−0.06	−0.05	−0.02	+0.03	−0.03	−0.38	−0.10	N	Y
2051104105146054784	NGC6791	4124	1.51	−0.27	+0.15	+0.06	+0.04	+0.02	−0.51	−0.09	N	Y
2051104105146057728	NGC6791	4441	2.28	+0.32	+0.08	+0.00	+0.02	−0.07	+0.10	−0.37	Y	Y
2051104276944822912	NGC6791	4498	2.59	+0.29	+0.16	+0.01	+0.00	−0.01	+0.15	−0.19	Y	Y
2051104861060304640	NGC6791	4173	2.06	+0.27	+0.06	+0.02	+0.02	−0.06	+0.16	−0.15	Y	Y
2051105101578548480	NGC6791	4486	2.42	+0.31	+0.05	+0.00	+0.00	−0.04	+0.11	−0.37	Y	Y
2051105135938204160	NGC6791	4214	2.12	+0.31	+0.06	−0.01	+0.01	−0.05	+0.10	−0.33	Y	Y
2051105239017444992	NGC6791	4477	2.30	+0.33	+0.05	−0.02	+0.01	−0.06	+0.07	−0.41	Y	Y
2051105651334466688	NGC6791	4515	2.42	+0.23	+0.12	+0.01	+0.03	+0.00	+0.05	−0.06	Y	N
2051105754413616000	NGC6791	4114	1.75	+0.33	+0.02	−0.02	+0.03	−0.08	+0.05	−0.30	Y	Y

Continued on next page

Table B.1 – Continued

Gaia ID	Cluster	T_{eff} (K)	log g (dex)	[Fe/H] (dex)	[Mg/Fe] (dex)	[Si/Fe] (dex)	[Ni/Fe] (dex)	[Ca/Fe] (dex)	[Na/Fe] (dex)	[V/Fe] (dex)	Member	Mass
2051286795872609920	NGC6791	4484	2.58	+0.29	+0.10	+0.07	+0.07	+0.01	+0.10	+0.00	N	Y
2051286933311576192	NGC6791	4455	2.80	+0.31	+0.06	−0.08	+0.05	+0.09	+0.22	−0.88	Y	Y
2051287002031070208	NGC6791	6354	5.29	+0.32	−0.04	+0.05	+0.01	−0.01	+0.25	−0.20	Y	N
2051287070750544128	NGC6791	4350	2.45	+0.35	+0.06	−0.03	−0.02	−0.05	+0.14	−0.35	Y	Y
2051287311268706432	NGC6791	4479	2.60	+0.31	+0.09	−0.03	+0.00	+0.06	+0.11	−0.08	Y	Y
2051288067183227008	NGC6791	4460	2.38	+0.34	+0.06	+0.01	+0.01	−0.05	+0.14	−0.53	Y	Y
2051288204622141568	NGC6791	4443	2.45	+0.31	+0.10	+0.04	+0.04	+0.01	+0.08	−0.08	Y	N
2051291228279110912	NGC6791	4426	2.54	+0.29	+0.06	+0.00	+0.04	−0.01	+0.10	−0.14	Y	Y
2051291674955780992	NGC6791	4403	2.43	+0.16	+0.13	+0.04	+0.05	+0.02	+0.03	−0.12	N	Y
2051292808827117952	NGC6791	4711	2.68	+0.24	+0.02	−0.01	+0.09	−0.04	+0.15	−0.14	N	Y
2051293118064539520	NGC6791	3923	1.49	+0.30	+0.03	−0.02	+0.05	−0.08	+0.27	+0.05	Y	Y
2051293289863222272	NGC6791	4793	3.02	+0.07	+0.08	+0.03	+0.04	+0.04	−0.03	−0.26	N	Y
2051293319920668160	NGC6791	4002	1.65	+0.36	+0.02	−0.02	+0.04	−0.09	+0.16	−0.12	Y	Y
2051293977058270592	NGC6791	4557	2.61	+0.35	+0.07	+0.04	+0.03	−0.01	+0.14	−0.10	Y	N
2051294045777739520	NGC6791	4277	2.23	+0.29	+0.07	−0.01	+0.01	−0.05	+0.10	−0.31	Y	Y
2051294114497261952	NGC6791	4439	2.65	+0.31	+0.01	+0.04	−0.07	+0.06	+0.13	+0.00	Y	Y
2051294213273828224	NGC6791	3910	1.49	+0.27	+0.02	−0.04	+0.05	−0.07	+0.35	+0.13	Y	N
2051294251936167424	NGC6791	3976	1.62	+0.32	+0.02	−0.03	+0.04	−0.07	+0.23	+0.06	Y	Y
2051294423734922112	NGC6791	4579	2.79	+0.30	+0.09	+0.01	+0.01	+0.01	+0.12	−0.18	Y	N
2051294522512945536	NGC6791	4488	2.36	+0.33	+0.06	+0.01	−0.01	+0.00	+0.13	−0.36	Y	Y
2051295351447969152	NGC6791	4513	2.69	+0.31	+0.13	+0.01	+0.06	+0.02	+0.12	−0.11	Y	Y
2051297275593144192	NGC6791	4507	2.51	+0.31	+0.07	+0.00	+0.01	−0.03	+0.15	−0.42	Y	Y
2051298168946719488	NGC6791	4453	2.15	−0.41	+0.33	+0.15	+0.09	+0.11	−0.13	−0.29	Y	Y
2051305590649763072	NGC6791	4745	2.86	+0.09	+0.03	+0.00	+0.01	+0.02	−0.03	+0.00	N	Y
2051311191287335168	NGC6791	4779	2.85	−0.34	+0.30	+0.18	+0.08	+0.14	−0.07	+0.06	N	Y
2051314661621040896	NGC6791	5087	2.90	+0.04	+0.00	+0.01	+0.00	−0.01	+0.05	+0.26	N	Y

Continued on next page

Table B.1 – Continued

Gaia ID	Cluster	T_{eff} (K)	log g (dex)	[Fe/H] (dex)	[Mg/Fe] (dex)	[Si/Fe] (dex)	[Ni/Fe] (dex)	[Ca/Fe] (dex)	[Na/Fe] (dex)	[V/Fe] (dex)	Member	Mass
2051357267698768512	NGC6791	5049	3.03	+0.04	+0.02	+0.01	−0.01	+0.02	+0.03	+0.11	N	N
2052541201201097728	NGC6791	4313	2.10	+0.01	+0.11	+0.04	+0.04	−0.10	+0.14	−0.36	N	Y
2052586723554691712	NGC6791	4824	2.82	−0.13	+0.14	+0.08	+0.02	+0.02	+0.09	−0.19	N	Y
2052591916176088960	NGC6791	6250	5.62	+0.37	−0.03	+0.04	+0.04	+0.00	+0.49	−0.12	N	N
2052597993548864896	NGC6791	4163	1.81	+0.12	+0.07	+0.01	+0.02	−0.03	+0.02	−0.39	N	Y
2052603495407853440	NGC6791	4398	2.36	−0.13	+0.23	+0.10	+0.03	+0.04	+0.11	−0.26	N	Y
2052606038028635008	NGC6791	4918	2.59	+0.07	+0.03	+0.01	+0.03	−0.02	+0.00	+0.07	N	Y
2052606450345583232	NGC6791	4390	2.02	+0.03	+0.07	−0.01	+0.04	−0.05	−0.18	−0.21	Y	Y
2052608821167401216	NGC6791	4992	3.56	−0.06	+0.05	+0.03	+0.04	+0.05	+0.04	−0.01	N	Y
2052609817600144768	NGC6791	4937	2.46	−0.51	+0.31	+0.23	+0.07	+0.14	+0.15	+0.03	N	Y
2052610779672610432	NGC6791	4903	2.95	−0.27	+0.13	+0.06	+0.04	+0.06	+0.12	−0.05	Y	Y
2052611157629959424	NGC6791	4633	2.52	+0.22	+0.02	+0.00	+0.05	−0.04	+0.13	−0.37	N	Y
2052613013055715328	NGC6791	4627	2.17	−0.37	+0.18	+0.12	+0.05	+0.06	+0.14	−0.07	N	Y
2052614421804974464	NGC6791	6039	3.88	+0.28	−0.06	+0.09	+0.05	−0.03	+0.13	+0.06	N	N
2052616723907385984	NGC6791	4564	2.51	+0.02	+0.08	+0.02	+0.06	−0.03	+0.15	−0.32	N	Y
2052619090428215552	NGC6791	4724	2.54	+0.10	+0.06	+0.05	+0.07	−0.03	+0.01	−0.10	N	Y
2052798035944728320	NGC6791	4848	2.51	−0.47	+0.35	+0.25	+0.08	+0.15	−0.04	+0.17	N	Y
2052798521280766208	NGC6791	4263	2.07	+0.20	+0.00	−0.04	+0.01	−0.05	−0.07	−0.21	N	Y
2052801785455888000	NGC6791	6352	4.85	+0.08	−0.05	+0.08	−0.09	+0.02	−0.40	−0.12	Y	N
2052805049633748480	NGC6791	4905	2.53	−0.12	+0.12	+0.09	+0.04	+0.05	−0.13	+0.01	N	N
2052805393228584448	NGC6791	4644	2.61	+0.12	+0.04	+0.04	+0.08	−0.05	+0.04	+0.10	N	Y
2052806144842981376	NGC6791	4834	2.65	−0.51	+0.39	+0.25	+0.09	+0.18	+0.00	+0.04	N	N
2052811023925825024	NGC6791	4801	2.34	−0.19	+0.07	+0.05	+0.04	+0.02	−0.10	−0.02	N	Y
2052815563711057408	NGC6791	4575	2.79	+0.28	+0.06	+0.03	+0.06	−0.02	+0.14	−0.05	N	Y
2052815696850247168	NGC6791	5404	4.02	+0.06	+0.01	+0.03	+0.03	+0.03	−0.36	+0.01	N	Y
2052815804229152000	NGC6791	4710	2.72	−0.05	+0.10	+0.05	+0.05	+0.04	−0.16	−0.04	N	Y

Continued on next page

Table B.1 – Continued

Gaia ID	Cluster	T_{eff} (K)	log g (dex)	[Fe/H] (dex)	[Mg/Fe] (dex)	[Si/Fe] (dex)	[Ni/Fe] (dex)	[Ca/Fe] (dex)	[Na/Fe] (dex)	[V/Fe] (dex)	Member	Mass
2052817350417520128	NGC6791	4452	2.36	−0.08	+0.19	+0.09	+0.05	+0.06	−0.09	−0.38	N	Y
2052817449196899968	NGC6791	6017	4.02	+0.07	−0.03	+0.10	+0.02	−0.01	−0.17	−0.02	N	N
2052817522216235264	NGC6791	3914	1.00	−0.46	+0.14	+0.03	+0.05	+0.00	−0.14	−0.03	N	Y
2052819893038589568	NGC6791	4983	3.37	−0.32	+0.13	+0.06	+0.05	+0.07	−0.04	+0.18	N	Y
2052823775688633856	NGC6791	4842	2.42	−0.54	+0.34	+0.24	+0.05	+0.14	−0.21	+0.16	N	Y
2076272510428578304	NGC6819	4991	2.86	−0.06	+0.06	+0.00	+0.02	−0.01	−0.05	+0.22	N	Y
2076280924256937600	NGC6819	5035	2.96	+0.06	−0.01	−0.02	−0.01	−0.02	+0.07	+0.07	N	Y
2076295600172704512	NGC6819	5028	3.11	+0.01	+0.01	−0.02	+0.02	+0.03	+0.22	−0.09	Y	N
2076298761268676352	NGC6819	4107	1.67	+0.10	+0.00	−0.03	+0.02	−0.05	−0.04	−0.27	Y	Y
2076298829988110976	NGC6819	3842	1.10	−0.07	+0.10	−0.01	+0.03	−0.02	+0.41	+0.29	N	Y
2076298864347818624	NGC6819	6250	4.22	+0.07	−0.10	+0.06	−0.04	−0.01	−0.32	−0.06	Y	N
2076298898707580416	NGC6819	6085	4.25	+0.05	−0.07	+0.07	+0.01	−0.03	−0.80	−0.17	Y	N
2076299311024414592	NGC6819	5029	3.12	−0.03	−0.01	+0.00	+0.02	+0.04	−0.05	+0.17	Y	Y
2076299448463334144	NGC6819	4815	2.59	+0.07	−0.01	−0.01	−0.01	+0.01	+0.14	−0.10	Y	Y
2076299482823088000	NGC6819	6309	4.23	+0.07	−0.09	+0.07	−0.06	+0.00	−0.20	+0.00	Y	N
2076299654621826176	NGC6819	4982	2.84	+0.07	−0.03	−0.01	+0.00	−0.01	+0.15	+0.08	Y	Y
2076299719033591424	NGC6819	4756	2.58	+0.06	−0.03	−0.02	+0.02	+0.00	+0.02	−0.13	Y	Y
2076299998219216256	NGC6819	4638	2.31	+0.16	−0.04	−0.04	+0.00	−0.03	+0.15	−0.26	Y	Y
2076300135658216192	NGC6819	6097	4.33	+0.05	−0.06	+0.06	+0.01	−0.02	−0.78	−0.04	Y	N
2076371260315683200	NGC6819	4753	2.82	−0.30	+0.25	+0.12	+0.08	+0.11	−0.13	+0.05	N	Y
2076385657045853568	NGC6819	4057	1.51	−0.12	+0.14	+0.03	+0.01	−0.04	−0.03	−0.31	N	Y
2076386546088447744	NGC6819	4969	3.61	−0.12	+0.18	+0.04	+0.10	+0.09	+0.06	−0.02	N	Y
2076388440186586880	NGC6819	4601	2.63	+0.11	+0.06	−0.02	+0.09	−0.02	+0.02	−0.07	N	N
2076388852501354624	NGC6819	4815	2.91	−0.05	+0.13	+0.07	+0.03	+0.00	+0.11	−0.21	N	Y
2076390364329873536	NGC6819	4675	2.49	−0.15	+0.13	+0.09	+0.03	+0.01	+0.12	−0.11	N	Y
2076393658554297600	NGC6819	4564	2.31	+0.08	−0.01	−0.02	+0.00	−0.03	+0.10	−0.32	Y	Y

Continued on next page

Table B.1 – Continued

Gaia ID	Cluster	T_{eff} (K)	log g (dex)	[Fe/H] (dex)	[Mg/Fe] (dex)	[Si/Fe] (dex)	[Ni/Fe] (dex)	[Ca/Fe] (dex)	[Na/Fe] (dex)	[V/Fe] (dex)	Member	Mass
2076393662864626176	NGC6819	4805	2.54	+0.07	+0.00	+0.01	+0.01	+0.01	+0.02	−0.09	Y	Y
2076393869023076608	NGC6819	4662	2.45	+0.06	+0.01	−0.03	+0.01	−0.03	+0.04	−0.31	Y	Y
2076394040821761152	NGC6819	6278	4.37	+0.08	−0.11	+0.05	−0.01	−0.02	−0.58	+0.00	Y	N
2076394178262903296	NGC6819	6060	4.31	+0.02	−0.08	+0.06	+0.04	−0.09	-1.16	−0.71	Y	N
2076394281339968256	NGC6819	6209	4.34	+0.09	−0.10	+0.05	+0.00	−0.02	−0.61	−0.01	Y	N
2076394315699729536	NGC6819	5888	4.21	+0.14	−0.09	+0.03	+0.05	+0.00	−0.20	+0.02	Y	N
2076394448828275584	NGC6819	4837	2.53	+0.04	+0.02	+0.05	+0.01	+0.01	−0.06	−0.04	Y	Y
2076394659297111552	NGC6819	4179	1.64	+0.05	+0.02	+0.00	+0.00	−0.05	−0.03	−0.38	Y	Y
2076394831095848448	NGC6819	4811	2.70	−0.15	+0.10	−0.01	+0.04	−0.02	−0.10	−0.04	N	N
2076396033686708480	NGC6819	4797	2.58	−0.08	+0.09	+0.09	+0.04	+0.03	+0.08	+0.16	N	Y
2076397064478968320	NGC6819	4627	2.37	−0.10	+0.09	+0.08	+0.00	−0.03	+0.04	−0.26	N	Y
2076403180512455424	NGC6819	3843	1.30	+0.27	+0.06	+0.00	+0.07	−0.07	+0.37	+0.14	Y	Y
2076427919524661248	NGC6819	4080	1.52	−0.20	+0.07	+0.02	+0.04	−0.02	−0.15	−0.24	N	Y
2076484681808279296	NGC6819	4904	2.66	+0.10	−0.03	−0.01	+0.00	+0.00	+0.12	+0.01	N	Y
2076485094125237376	NGC6819	4776	2.72	−0.14	+0.05	+0.02	+0.04	+0.03	−0.13	+0.14	N	Y
2076485678240859136	NGC6819	4625	2.44	+0.09	−0.01	−0.02	+0.01	+0.00	+0.04	−0.21	Y	Y
2076487499307051008	NGC6819	6020	4.23	+0.06	−0.06	+0.06	+0.01	−0.02	−0.70	−0.05	Y	N
2076487838597288320	NGC6819	4789	2.62	+0.08	−0.01	−0.02	+0.00	+0.01	+0.06	−0.11	Y	Y
2076487872957025408	NGC6819	4791	2.53	+0.07	+0.01	+0.00	+0.00	+0.02	+0.02	−0.12	Y	Y
2076487976036241536	NGC6819	4933	2.93	+0.05	+0.01	−0.01	−0.01	+0.04	+0.03	+0.05	Y	Y
2076488049062931328	NGC6819	4794	2.60	+0.09	−0.01	+0.00	+0.03	+0.02	+0.05	−0.02	Y	Y
2076488323940775680	NGC6819	4778	2.54	+0.11	+0.00	−0.01	+0.00	+0.03	+0.03	−0.06	Y	Y
2076488736257663872	NGC6819	6179	4.15	+0.00	−0.05	+0.07	−0.07	+0.00	−0.34	+0.08	Y	N
2076488942416130688	NGC6819	6244	4.23	+0.09	−0.09	+0.05	−0.03	−0.01	−0.31	−0.05	Y	N
2076489251653787904	NGC6819	4527	2.37	+0.16	+0.04	−0.01	+0.04	−0.02	−0.05	−0.20	N	Y
2076490660402814336	NGC6819	4707	2.60	+0.06	+0.05	+0.01	+0.01	+0.04	−0.04	−0.12	N	Y

Continued on next page

Table B.1 – Continued

Gaia ID	Cluster	T_{eff} (K)	log g (dex)	[Fe/H] (dex)	[Mg/Fe] (dex)	[Si/Fe] (dex)	[Ni/Fe] (dex)	[Ca/Fe] (dex)	[Na/Fe] (dex)	[V/Fe] (dex)	Member	Mass
2076491515089601408	NGC6819	4882	2.90	+0.08	+0.00	+0.00	+0.01	+0.03	+0.07	+0.11	Y	Y
2076495161528280192	NGC6819	6222	4.20	+0.14	−0.08	+0.08	−0.02	+0.01	−0.16	+0.00	N	N
2076503575359113728	NGC6819	4651	2.67	+0.21	+0.07	+0.04	+0.06	−0.01	+0.07	−0.09	N	Y
2076581679348332544	NGC6819	6143	4.27	+0.07	−0.08	+0.06	+0.00	−0.03	−0.64	−0.09	Y	N
2076581816787312896	NGC6819	4697	2.59	+0.06	+0.01	−0.01	+0.03	+0.02	+0.13	−0.22	Y	Y
2076581919866484224	NGC6819	4809	2.53	+0.04	+0.02	+0.02	+0.01	+0.04	−0.05	−0.06	Y	Y
2076582710140560000	NGC6819	4853	2.58	+0.06	+0.02	+0.02	+0.02	+0.02	+0.01	−0.07	Y	Y
2076582916298933888	NGC6819	4507	2.36	+0.21	+0.04	−0.01	+0.08	−0.05	+0.10	−0.39	N	Y
2076582950658667264	NGC6819	6044	5.81	+0.42	−0.04	+0.04	+0.02	+0.00	+0.26	−0.01	Y	N
2076583534763920896	NGC6819	4128	1.62	+0.06	+0.02	−0.01	+0.02	−0.04	−0.07	−0.28	Y	N
2076584084530142208	NGC6819	4427	1.47	−0.38	+0.06	+0.06	+0.01	+0.03	+0.10	−0.37	N	Y
2076587451784377856	NGC6819	4306	1.35	−0.59	+0.17	+0.09	+0.05	+0.08	−0.03	−0.35	N	Y
2076587486144092416	NGC6819	4772	2.98	+0.09	+0.03	+0.00	+0.07	+0.03	+0.08	−0.31	N	Y
2076588237752668416	NGC6819	5163	3.23	−0.03	+0.04	+0.00	+0.02	+0.01	−0.03	+0.07	N	Y
2076590372362296576	NGC6819	3866	1.03	−0.13	+0.08	+0.00	+0.02	−0.01	+0.21	+0.18	N	Y
2076592708824592768	NGC6819	4151	1.86	+0.19	+0.07	+0.01	+0.05	−0.02	−0.08	−0.17	N	Y
2076592949342776192	NGC6819	4606	2.28	−0.45	+0.17	+0.13	+0.05	+0.09	−0.88	−0.04	N	Y
2076593670897318400	NGC6819	4537	2.48	−0.02	+0.12	+0.04	+0.07	+0.00	+0.11	−0.28	N	Y
2076596350956816640	NGC6819	4817	2.69	−0.18	+0.05	+0.04	+0.02	+0.04	+0.38	+0.00	N	Y
2076598206382734976	NGC6819	4681	2.38	−0.11	+0.06	+0.05	+0.00	+0.00	+0.00	−0.14	N	Y
2076599993088947584	NGC6819	4497	2.50	+0.05	+0.06	−0.02	+0.07	+0.01	+0.03	−0.27	N	Y
2076600233607135872	NGC6819	4520	2.43	+0.09	+0.07	+0.02	+0.06	+0.00	+0.05	−0.31	N	Y
2076600886442113280	NGC6819	4828	2.54	+0.07	−0.01	+0.00	+0.02	+0.01	−0.04	+0.00	Y	Y
2076604077595370752	NGC6819	4888	2.49	−0.22	+0.10	+0.06	+0.03	+0.08	−0.21	+0.03	N	Y
2076604077595371008	NGC6819	4742	2.48	−0.22	+0.07	+0.04	+0.05	+0.03	−0.15	−0.01	N	Y
3358114433438409728	Berkely29	4754	2.87	+0.19	+0.10	−0.01	−0.01	+0.11	−0.07	−0.03	N	N

Continued on next page

Table B.1 – Continued

Gaia ID	Cluster	T_{eff} (K)	log g (dex)	[Fe/H] (dex)	[Mg/Fe] (dex)	[Si/Fe] (dex)	[Ni/Fe] (dex)	[Ca/Fe] (dex)	[Na/Fe] (dex)	[V/Fe] (dex)	Member	Mass
3358130990534142208	Berkely29	5947	4.39	+0.16	−0.04	+0.06	+0.03	+0.00	−0.23	−0.06	N	N
3358132094343932032	Berkely29	4964	3.07	+0.08	+0.09	+0.00	+0.00	+0.10	−0.07	+0.01	N	N
3358159955793287296	Berkely29	5209	4.32	+0.21	+0.05	+0.04	+0.05	+0.04	−0.17	−0.13	N	N
3358170096214972288	Berkely29	6261	4.23	+0.06	−0.09	+0.08	−0.03	+0.00	−0.23	−0.01	N	N
3358170852129166464	Berkely29	5186	3.36	+0.05	+0.06	+0.00	+0.00	+0.08	−0.03	+0.04	N	N
3358171191428998144	Berkely29	6200	5.16	+0.12	−0.02	+0.08	+0.02	+0.03	−0.54	+0.14	N	N
3358172054720004352	Berkely29	6210	5.33	+0.21	−0.05	+0.07	+0.01	+0.02	−0.31	+0.07	N	N
3358191433612425984	Berkely29	6197	4.32	+0.08	−0.09	+0.03	+0.00	+0.02	−0.23	−0.03	N	N
3358208162506903552	Berkely29	5540	4.35	+0.17	−0.02	+0.03	+0.03	+0.03	−0.35	−0.04	N	N
3358208372963666304	Berkely29	6278	4.27	+0.09	−0.09	+0.05	−0.04	+0.00	−0.22	−0.03	N	N
3358209055859413376	Berkely29	6430	4.28	+0.11	−0.11	+0.08	−0.04	+0.01	−0.08	+0.03	N	N
3358209438115018240	Berkely29	4682	2.71	+0.18	+0.09	−0.01	−0.02	+0.11	−0.08	+0.02	N	N
3358212427412279424	Berkely29	6156	4.24	+0.10	−0.06	+0.07	−0.01	+0.02	−0.24	−0.01	N	N
3358213355125243136	Berkely29	5647	4.37	+0.20	−0.04	+0.02	+0.02	+0.02	−0.28	−0.05	N	N
3358218298629048064	Berkely29	5582	4.52	+0.21	−0.03	+0.03	+0.03	+0.02	−0.40	−0.06	N	N
3358219123264074112	Berkely29	5609	4.42	+0.19	−0.02	+0.04	+0.03	+0.04	−0.32	+0.06	N	N
3358219402439487488	Berkely29	6324	4.34	+0.10	−0.11	+0.05	−0.03	+0.01	−0.18	−0.06	N	N
3358219677316904064	Berkely29	5022	3.20	+0.13	+0.07	−0.01	+0.00	+0.09	−0.04	+0.01	N	N
3358220330151880320	Berkely29	6273	4.19	+0.02	−0.10	+0.07	−0.05	+0.00	−0.16	−0.03	N	N
3358223319449164288	Berkely29	6017	4.09	+0.05	−0.02	+0.07	−0.03	+0.02	−0.32	+0.03	N	N
3358223731766513152	Berkely29	4940	3.06	+0.12	+0.07	−0.01	+0.00	+0.10	−0.06	+0.01	N	N
3358227786215272576	Berkely29	6357	4.29	+0.07	−0.11	+0.07	−0.03	+0.01	−0.14	+0.00	N	N
3358229366763222016	Berkely29	6328	4.30	+0.08	−0.11	+0.05	−0.02	+0.00	−0.22	−0.09	N	N
3358233077615635712	Berkely29	5908	4.34	+0.15	−0.07	+0.02	+0.03	+0.00	−0.05	−0.01	N	N
3358240052641779968	Berkely29	5608	3.86	+0.00	−0.03	−0.03	+0.02	+0.01	−0.19	+0.15	N	N
3358242419166519296	Berkely29	4358	1.59	+0.05	+0.18	+0.08	+0.03	+0.01	−0.16	+0.10	N	N

Continued on next page

Table B.1 – Continued

Gaia ID	Cluster	T_{eff} (K)	log g (dex)	[Fe/H] (dex)	[Mg/Fe] (dex)	[Si/Fe] (dex)	[Ni/Fe] (dex)	[Ca/Fe] (dex)	[Na/Fe] (dex)	[V/Fe] (dex)	Member	Mass
3358244278889473664	Berkely29	5217	3.43	+0.10	+0.02	−0.02	+0.01	+0.07	−0.05	+0.04	N	N
3358247165107518464	Berkely29	6319	4.26	+0.15	−0.10	+0.07	−0.02	+0.00	−0.04	+0.05	N	N
3358247263890116480	Berkely29	5180	3.11	+0.00	+0.03	−0.02	+0.01	+0.05	−0.10	+0.13	N	N
3358248367698351232	Berkely29	5775	4.21	+0.16	−0.06	−0.01	+0.04	+0.03	−0.24	+0.04	N	N
3358261012082036992	Berkely29	6248	4.84	+0.28	−0.05	+0.02	−0.01	+0.01	−0.03	−0.11	N	N
3358262077233937792	Berkely29	5454	3.65	−0.10	+0.07	+0.05	+0.04	−0.03	+0.01	−0.17	N	N
3358264649917239296	Berkely29	5418	3.81	+0.10	+0.04	−0.01	+0.05	+0.05	−0.06	−0.12	N	N
3358265994244132864	Berkely29	5980	5.30	+0.34	+0.01	+0.03	+0.05	+0.02	+0.38	−0.13	N	N
3358419960232790144	Berkely29	5100	3.23	+0.08	+0.04	−0.02	+0.00	+0.08	−0.07	+0.04	N	N
3358421850018277376	Berkely29	5898	4.32	+0.14	−0.06	+0.03	+0.03	−0.01	+0.00	−0.07	N	N
3358422021817028480	Berkely29	5657	4.35	+0.17	−0.01	+0.04	+0.03	+0.03	−0.22	−0.01	N	N
3358427652515682816	Berkely29	4575	1.80	+0.03	+0.16	+0.07	+0.03	+0.01	−0.17	+0.11	N	N
3358432398457904512	Berkely29	5188	3.34	+0.02	+0.08	+0.00	+0.03	+0.08	−0.11	−0.02	N	N
3358434494401853952	Berkely29	6059	4.61	+0.28	−0.02	+0.01	+0.02	+0.01	−0.01	−0.23	N	N
3358455007165570304	Berkely29	5090	3.26	+0.12	+0.06	−0.02	+0.01	+0.08	−0.07	−0.06	N	N
3358458821096492800	Berkely29	5274	3.41	+0.03	+0.05	−0.01	+0.01	+0.06	−0.11	−0.01	N	N
3393882955436718080	NGC1817	4696	2.33	+0.08	+0.09	+0.07	+0.02	+0.04	−0.08	+0.00	N	N
3393884295466504832	NGC1817	5306	3.49	−0.24	+0.10	+0.07	+0.05	+0.07	+0.04	+0.14	Y	N
3393976654443500416	NGC1817	6112	4.05	−0.06	−0.06	+0.05	−0.02	−0.04	−0.21	−0.23	N	N
3393977891394098688	NGC1817	6048	4.18	+0.08	−0.08	+0.07	+0.02	+0.00	−0.41	−0.05	N	N
3393977994473340672	NGC1817	3966	1.01	−0.30	+0.10	+0.06	+0.04	−0.07	+0.09	+0.26	Y	N
3393978853466780160	NGC1817	6251	4.31	+0.06	−0.11	+0.00	−0.01	−0.03	−0.16	−0.11	Y	N
3393982903620015616	NGC1817	6115	4.20	+0.04	−0.08	+0.03	+0.01	−0.03	−0.24	−0.07	N	N
3393983010995083904	NGC1817	6151	4.18	+0.04	−0.09	+0.03	−0.01	−0.01	−0.07	−0.08	N	N
3393985519255968640	NGC1817	6046	4.20	+0.00	−0.04	+0.01	+0.03	−0.05	−0.04	−0.20	N	N
3393986064716591744	NGC1817	6158	4.12	−0.03	−0.06	+0.01	−0.01	−0.04	−0.06	−0.19	N	N

Continued on next page

Table B.1 – Continued

Gaia ID	Cluster	T_{eff} (K)	log g (dex)	[Fe/H] (dex)	[Mg/Fe] (dex)	[Si/Fe] (dex)	[Ni/Fe] (dex)	[Ca/Fe] (dex)	[Na/Fe] (dex)	[V/Fe] (dex)	Member	Mass
3394008574640397696	NGC1817	6111	4.37	+0.06	−0.08	+0.03	+0.06	+0.04	−0.31	+0.11	N	N
3394013556802465920	NGC1817	5152	3.18	−0.16	+0.04	+0.05	−0.04	+0.01	+0.03	−0.13	Y	N
3394635188893039872	NGC1817	5957	4.30	+0.20	−0.07	−0.01	+0.02	−0.01	+0.04	−0.14	N	N
3394635296268445568	NGC1817	6206	4.22	+0.04	−0.13	+0.02	−0.04	−0.01	−0.07	−0.04	Y	N
3394635846024024192	NGC1817	5980	4.08	+0.01	−0.08	+0.02	−0.03	−0.02	−0.03	+0.04	N	N
3394637460931745664	NGC1817	5098	2.98	−0.23	+0.04	+0.04	−0.01	+0.05	+0.20	+0.13	N	N
3394651960741320064	NGC1817	5083	2.93	−0.11	+0.01	−0.02	+0.01	+0.02	−0.15	+0.18	Y	Y
3394651960741320832	NGC1817	6593	4.38	+0.09	−0.07	+0.12	−0.11	+0.04	−0.21	+0.08	N	N
3394653468273900928	NGC1817	5480	4.13	+0.07	−0.04	+0.00	+0.03	+0.02	−0.04	+0.10	N	N
3394656839824146944	NGC1817	4956	4.31	+0.13	+0.03	+0.02	+0.02	+0.04	−0.12	−0.10	N	N
3394657149061773440	NGC1817	5808	3.94	−0.01	+0.00	+0.07	−0.04	+0.01	−0.28	+0.10	N	N
3394657419643723648	NGC1817	6318	4.25	+0.00	−0.10	+0.07	−0.07	+0.00	−0.22	+0.05	Y	N
3394657664457867264	NGC1817	5061	2.83	−0.09	+0.02	+0.00	+0.00	+0.00	+0.03	+0.23	N	N
3394705287055983488	NGC1817	5970	4.02	+0.02	−0.03	+0.08	−0.04	+0.02	−0.37	−0.01	N	N
3394735798503688704	NGC1817	6188	4.25	+0.02	−0.11	+0.02	−0.04	−0.02	−0.05	−0.08	Y	N
3394740608867014784	NGC1817	5809	4.01	−0.03	−0.01	+0.00	+0.05	−0.03	−0.17	−0.02	N	N
3394741463563658752	NGC1817	5083	3.16	−0.11	+0.04	+0.04	−0.02	−0.01	+0.14	−0.20	Y	Y
3394742429933179648	NGC1817	5172	3.23	−0.11	−0.01	−0.05	+0.02	−0.01	−0.36	+0.21	Y	N
3394744285358806144	NGC1817	5820	4.00	+0.02	+0.00	+0.02	+0.02	−0.04	+0.06	−0.17	N	N
3394749164441742720	NGC1817	4873	2.85	+0.03	+0.08	+0.00	+0.00	+0.07	−0.03	−0.03	N	N
3394754314105787008	NGC1817	6194	4.16	+0.03	−0.07	+0.07	−0.05	+0.00	−0.29	+0.02	Y	N
3394755143036198656	NGC1817	6291	4.21	+0.08	−0.09	+0.08	−0.07	+0.00	−0.28	+0.06	N	N
3394756311267231488	NGC1817	4789	2.73	+0.03	+0.09	+0.02	−0.01	+0.09	−0.11	+0.01	Y	Y
3394756414346436736	NGC1817	4976	2.79	−0.07	+0.05	+0.02	+0.01	+0.06	−0.07	+0.08	N	Y
3394757754376213248	NGC1817	6244	4.27	+0.02	−0.11	+0.02	−0.02	−0.01	−0.14	−0.15	Y	N
3394757960534898304	NGC1817	4777	2.25	−0.04	+0.06	+0.02	+0.02	+0.03	−0.16	+0.08	Y	N

Continued on next page

Table B.1 – Continued

Gaia ID	Cluster	T_{eff} (K)	log g (dex)	[Fe/H] (dex)	[Mg/Fe] (dex)	[Si/Fe] (dex)	[Ni/Fe] (dex)	[Ca/Fe] (dex)	[Na/Fe] (dex)	[V/Fe] (dex)	Member	Mass
3394758780871784704	NGC1817	6177	4.12	+0.05	−0.08	+0.08	−0.01	+0.00	−0.16	+0.04	N	N
3394759781601050240	NGC1817	5258	4.20	+0.00	+0.00	+0.02	+0.03	+0.04	−0.07	+0.08	N	N
3394760262637163776	NGC1817	6197	4.18	+0.07	−0.07	+0.07	−0.02	+0.00	−0.29	−0.04	N	N
3394761804528747008	NGC1817	5150	3.13	−0.09	+0.00	−0.02	+0.01	+0.01	−0.15	+0.22	Y	Y
3394762083703243904	NGC1817	5150	3.08	−0.11	+0.02	−0.01	+0.01	+0.03	−0.08	+0.12	N	Y
3394762255501947776	NGC1817	5111	3.15	−0.08	+0.12	+0.07	+0.03	+0.08	−0.17	+0.02	N	N
3394762972759919360	NGC1817	5121	3.05	−0.09	+0.01	−0.02	+0.01	+0.02	−0.16	+0.19	Y	Y
3394764278431922560	NGC1817	5732	3.72	−0.09	−0.01	+0.05	−0.06	−0.02	−0.11	−0.12	N	N
3394764523244911104	NGC1817	4903	2.69	−0.25	+0.08	+0.04	−0.02	+0.01	−0.01	−0.22	Y	Y
3394764999986360064	NGC1817	5017	3.02	−0.16	+0.07	+0.07	−0.04	+0.01	+0.03	−0.26	Y	N
3394765760195485312	NGC1817	5868	4.00	−0.02	−0.04	+0.01	+0.02	−0.03	−0.16	+0.00	N	N
3394766035073385344	NGC1817	6064	4.22	+0.00	−0.10	−0.01	−0.01	−0.02	−0.35	+0.14	Y	N
3394767168944744320	NGC1817	6357	4.35	+0.09	−0.13	+0.03	−0.01	+0.01	−0.24	−0.02	N	N
3394768062297941376	NGC1817	5339	3.30	−0.10	+0.04	+0.03	−0.04	+0.02	−0.14	+0.16	N	N
3394769814644614144	NGC1817	5523	3.69	+0.01	+0.01	−0.01	+0.02	−0.01	−0.01	+0.01	N	N
3394781836256227328	NGC1817	5153	3.10	−0.10	+0.02	−0.03	+0.02	+0.00	−0.20	+0.10	Y	Y
3394781840552762624	NGC1817	4876	2.57	−0.30	+0.07	+0.04	−0.01	+0.02	+0.04	−0.10	Y	N
3394783283661760896	NGC1817	6261	4.68	+0.18	−0.01	+0.06	+0.00	+0.00	+0.02	−0.20	N	N
3394783902137028096	NGC1817	5430	3.63	−0.03	+0.02	+0.00	+0.02	−0.01	−0.01	+0.09	N	N
3394785448325237376	NGC1817	5090	3.00	−0.07	+0.05	−0.01	+0.01	−0.01	+0.03	+0.10	N	N
3394785551404444416	NGC1817	6257	4.18	+0.07	−0.11	+0.08	−0.04	−0.02	−0.22	+0.01	N	N
3394787333814420736	NGC1817	6124	4.12	+0.06	−0.07	+0.08	−0.01	+0.00	−0.33	−0.10	Y	N
3394788880002644224	NGC1817	6065	4.09	+0.10	−0.09	+0.09	+0.00	−0.03	−0.12	+0.02	N	N
3394789640213316224	NGC1817	6010	3.96	+0.12	−0.04	+0.10	+0.03	−0.01	−0.08	+0.01	N	N
3394790018170420864	NGC1817	4865	2.79	+0.01	+0.04	−0.01	+0.01	+0.07	−0.07	+0.06	N	Y
3394795240850626432	NGC1817	6160	4.15	+0.07	−0.09	+0.08	−0.01	−0.03	−0.09	+0.01	N	N

Continued on next page

Table B.1 – Continued

Gaia ID	Cluster	T_{eff} (K)	log g (dex)	[Fe/H] (dex)	[Mg/Fe] (dex)	[Si/Fe] (dex)	[Ni/Fe] (dex)	[Ca/Fe] (dex)	[Na/Fe] (dex)	[V/Fe] (dex)	Member	Mass
3394796306002521728	NGC1817	6306	4.18	+0.07	−0.10	+0.07	−0.02	+0.00	−0.16	−0.04	N	N
3394799772039648000	NGC1817	5611	4.18	+0.03	−0.06	+0.01	+0.02	+0.02	+0.04	+0.15	N	N
3394800802833941248	NGC1817	6266	4.21	+0.10	−0.10	+0.06	−0.03	+0.00	−0.14	−0.04	N	N
3394801872280405888	NGC1817	5952	4.00	+0.05	−0.04	+0.07	−0.02	+0.00	−0.40	−0.05	N	N
3394802555183937024	NGC1817	5854	4.72	+0.22	−0.08	+0.02	+0.02	+0.00	−0.48	+0.06	N	N
3394807747795611904	NGC1817	5005	3.62	−0.37	+0.18	+0.08	+0.07	+0.13	−0.03	+0.26	N	N
3394810698436488832	NGC1817	5243	3.37	−0.14	+0.11	+0.08	+0.02	+0.07	−0.30	+0.10	N	N
3394810977610919168	NGC1817	4600	2.38	+0.05	+0.10	+0.02	+0.00	+0.08	−0.16	−0.01	N	N
3394811115049862016	NGC1817	6258	4.15	+0.04	−0.11	+0.05	−0.02	−0.01	−0.14	−0.05	N	N
3394812317641074816	NGC1817	5923	4.11	+0.10	−0.04	+0.07	+0.03	+0.00	−0.23	−0.10	N	N
3394813417152408448	NGC1817	4995	4.34	+0.10	+0.03	+0.02	+0.03	+0.04	−0.09	−0.07	N	N
3394813863829010816	NGC1817	6302	4.17	−0.01	−0.07	+0.07	−0.05	+0.00	−0.33	−0.02	N	N
3394825988520813184	NGC1817	6173	4.62	+0.29	−0.03	+0.03	−0.02	+0.01	−0.07	−0.13	N	N
3394836609975682944	NGC1817	6195	4.21	+0.10	−0.09	+0.06	−0.01	+0.00	−0.09	−0.02	N	N
3394840011589821312	NGC1817	5434	3.53	−0.09	+0.00	+0.00	+0.00	+0.00	−0.09	+0.23	Y	Y
3394840080309298304	NGC1817	4892	4.29	+0.12	+0.03	+0.02	+0.01	+0.04	−0.06	−0.11	N	N
3394840149028758144	NGC1817	5081	2.91	−0.13	+0.06	+0.02	−0.02	+0.05	−0.09	+0.12	Y	N
3394841660857191552	NGC1817	5031	3.12	−0.31	+0.10	+0.05	+0.05	+0.05	−0.04	+0.14	N	N
3394843481923279872	NGC1817	6191	4.18	+0.00	−0.08	+0.04	−0.03	+0.01	+0.13	+0.01	N	N
3394844478355710720	NGC1817	6315	4.25	+0.07	−0.11	+0.06	−0.03	+0.01	−0.22	−0.07	N	N
3394844680217745920	NGC1817	6068	4.07	+0.04	−0.06	+0.07	−0.03	−0.02	−0.34	−0.08	N	N
3409822884742934400	NGC1647	6050	4.15	+0.05	−0.05	+0.06	−0.06	+0.01	−0.37	+0.03	N	N
3409868617554732544	NGC1647	5860	4.64	+0.15	−0.06	+0.04	+0.02	+0.01	−0.82	+0.00	N	N
3409871194535078784	NGC1647	5607	4.11	+0.08	−0.03	+0.06	+0.03	−0.06	-1.39	−0.59	N	N
3409872603284384896	NGC1647	6168	4.22	+0.08	−0.08	+0.06	−0.05	−0.01	−0.30	−0.01	N	N
3409875317703681024	NGC1647	6004	4.51	+0.10	−0.06	+0.05	+0.01	+0.00	−0.86	−0.02	N	N

Continued on next page

Table B.1 – Continued

Gaia ID	Cluster	T_{eff} (K)	log g (dex)	[Fe/H] (dex)	[Mg/Fe] (dex)	[Si/Fe] (dex)	[Ni/Fe] (dex)	[Ca/Fe] (dex)	[Na/Fe] (dex)	[V/Fe] (dex)	Member	Mass
3409878375720453120	NGC1647	5954	4.11	+0.04	−0.09	+0.02	−0.03	−0.01	+0.23	+0.04	N	N
3409880024987880320	NGC1647	6008	4.19	+0.06	−0.10	+0.02	−0.03	−0.02	+0.07	+0.08	N	N
3409882670687736320	NGC1647	5977	4.04	+0.01	−0.04	+0.06	−0.07	+0.02	−0.30	−0.01	N	N
3409884904070719360	NGC1647	6268	4.23	+0.00	−0.11	+0.03	−0.06	+0.01	−0.03	−0.01	N	N
3409887515410798080	NGC1647	6144	4.16	+0.04	−0.07	+0.06	−0.07	+0.01	−0.36	+0.02	N	N
3409888202605581056	NGC1647	6117	4.13	+0.00	−0.07	+0.05	−0.05	+0.00	−0.38	+0.06	N	N
3409889405196442368	NGC1647	6112	4.22	+0.04	−0.06	+0.06	−0.07	+0.00	−0.25	−0.02	N	N
3409889576995124992	NGC1647	5894	4.13	+0.04	−0.09	+0.02	−0.02	−0.01	+0.18	+0.07	N	N
3409896448942728960	NGC1647	6085	4.20	+0.10	−0.11	+0.01	−0.02	−0.01	+0.16	+0.02	N	N
3409897819035991040	NGC1647	5759	4.68	+0.18	−0.05	+0.03	+0.02	+0.02	−0.70	+0.03	N	N
3409898235649158656	NGC1647	5873	4.62	+0.14	−0.05	+0.04	+0.01	+0.01	−0.76	+0.02	N	N
3409898712388889856	NGC1647	5949	4.25	+0.05	−0.07	+0.06	+0.05	−0.09	-1.18	−0.77	N	N
3409899781837372032	NGC1647	5907	4.65	+0.16	−0.06	+0.04	+0.02	+0.00	−0.78	−0.01	N	N
3409900159794476416	NGC1647	5931	4.60	+0.17	−0.07	+0.04	+0.01	+0.00	−0.72	−0.02	N	N
3409900434672383616	NGC1647	5952	4.41	+0.11	−0.06	+0.05	+0.00	−0.01	−0.74	−0.05	N	N
3409900778269752064	NGC1647	5755	4.02	+0.01	−0.07	+0.02	−0.01	+0.00	+0.15	+0.11	N	N
3409900950068449408	NGC1647	5802	4.15	+0.05	−0.08	+0.02	+0.00	+0.00	+0.15	+0.10	N	N
3409901121865631744	NGC1647	5833	4.13	+0.05	−0.09	+0.02	−0.01	+0.00	+0.21	+0.12	N	N
3409902564976142080	NGC1647	6190	4.21	+0.07	−0.09	+0.06	−0.05	−0.01	−0.30	−0.03	N	N
3409907164885022464	NGC1647	5646	4.16	+0.02	−0.05	+0.02	+0.02	+0.02	+0.10	+0.11	N	N
3409907615857666048	NGC1647	6222	4.14	+0.00	−0.07	+0.05	−0.02	+0.01	−0.06	−0.05	N	N
3409908577930343040	NGC1647	5088	2.87	−0.32	+0.05	+0.04	+0.00	+0.04	+0.10	+0.12	N	N
3409909265125096320	NGC1647	6157	4.17	+0.02	−0.11	+0.03	−0.04	−0.01	−0.02	+0.02	N	N
3409914075488503168	NGC1647	6120	4.15	+0.04	−0.08	+0.07	−0.04	−0.01	−0.37	−0.05	N	N
3409914247287190784	NGC1647	6018	4.08	−0.02	−0.08	+0.05	−0.04	+0.01	+0.09	+0.14	N	N
3409914384726162432	NGC1647	5871	4.67	+0.15	−0.05	+0.04	+0.02	+0.01	−0.79	+0.03	N	N

Continued on next page

Table B.1 – Continued

Gaia ID	Cluster	T_{eff} (K)	log g (dex)	[Fe/H] (dex)	[Mg/Fe] (dex)	[Si/Fe] (dex)	[Ni/Fe] (dex)	[Ca/Fe] (dex)	[Na/Fe] (dex)	[V/Fe] (dex)	Member	Mass
3409914487805370368	NGC1647	5958	4.51	+0.12	−0.06	+0.05	+0.01	+0.00	−0.72	−0.01	N	N
3409914590884594176	NGC1647	5986	4.44	+0.09	−0.05	+0.06	+0.00	+0.00	−0.71	+0.00	N	N
3409914865762488704	NGC1647	5999	4.13	+0.05	−0.10	+0.03	−0.03	−0.01	+0.12	+0.08	N	N
3409916137072825088	NGC1647	5860	4.70	+0.17	−0.05	+0.04	+0.02	+0.01	−0.82	+0.01	N	N
3409918851492142976	NGC1647	5752	4.05	+0.01	−0.07	+0.02	−0.01	+0.00	+0.26	+0.09	N	N
3409919401247942912	NGC1647	5832	4.12	+0.06	−0.08	+0.01	+0.00	+0.00	+0.18	+0.05	N	N
3409921153594589696	NGC1647	6164	4.14	+0.01	−0.08	+0.06	−0.05	−0.01	−0.14	+0.01	N	N
3409922871581483520	NGC1647	6269	4.28	+0.05	−0.12	+0.03	−0.03	−0.01	−0.22	−0.14	N	N
3409923009020434304	NGC1647	5214	3.16	−0.15	+0.05	+0.00	+0.01	+0.02	−0.02	+0.10	N	N
3409923455695476864	NGC1647	6026	4.23	+0.10	−0.08	+0.02	+0.00	−0.04	−0.04	−0.14	N	N
3409924417769734912	NGC1647	5867	4.12	+0.07	−0.08	+0.02	+0.00	−0.01	+0.12	+0.02	N	N
3409924589568428160	NGC1647	5238	3.24	−0.25	+0.04	+0.05	+0.00	+0.06	+0.24	+0.10	N	N
3409925723440125568	NGC1647	5884	3.91	+0.00	−0.05	+0.05	−0.05	−0.01	−0.18	−0.01	N	N
3409927505850313984	NGC1647	5938	3.97	−0.01	−0.04	+0.04	+0.00	+0.00	+0.28	−0.08	N	N
3409928334779883008	NGC1647	5755	4.05	+0.02	−0.05	+0.02	+0.00	−0.01	+0.15	+0.00	N	N
3410076597051009152	NGC1647	4947	2.99	+0.06	+0.07	+0.00	+0.00	+0.10	−0.02	+0.04	N	N
3410078143239306880	NGC1647	5958	4.07	+0.01	−0.09	+0.03	−0.03	−0.01	+0.04	+0.08	N	N
3410079861226264448	NGC1647	5744	3.80	−0.07	−0.07	+0.00	−0.03	+0.00	+0.13	+0.02	N	N
3410098209326420480	NGC1647	4932	2.94	+0.04	+0.05	−0.02	+0.00	+0.09	−0.01	+0.09	N	N
3410099652435421568	NGC1647	5701	3.87	−0.04	−0.05	−0.02	+0.00	+0.00	−0.22	+0.13	N	N
3410103088409251968	NGC1647	6107	4.11	−0.02	−0.09	+0.05	−0.07	−0.03	−0.29	+0.00	N	N
3410104600236685056	NGC1647	6320	5.10	+0.21	−0.11	+0.05	+0.00	−0.01	−0.75	−0.04	N	N
3410104703317052672	NGC1647	5971	4.25	+0.09	−0.09	+0.02	+0.01	−0.01	−0.05	+0.03	N	N
3410105253072863104	NGC1647	6108	4.22	+0.08	−0.10	+0.02	−0.02	−0.02	+0.10	−0.02	N	N
3410107005419517184	NGC1647	6150	4.21	−0.03	−0.07	+0.03	−0.02	−0.02	−0.07	−0.26	N	N
3410107314657156096	NGC1647	6037	4.47	+0.13	−0.10	+0.01	+0.03	−0.01	−0.16	+0.04	N	N

Continued on next page

Table B.1 – Continued

Gaia ID	Cluster	T_{eff} (K)	log g (dex)	[Fe/H] (dex)	[Mg/Fe] (dex)	[Si/Fe] (dex)	[Ni/Fe] (dex)	[Ca/Fe] (dex)	[Na/Fe] (dex)	[V/Fe] (dex)	Member	Mass
3410107349016895616	NGC1647	5919	4.23	+0.05	−0.04	+0.00	+0.04	−0.03	−0.12	−0.08	N	N
3410107555175327488	NGC1647	4461	1.87	−0.53	+0.16	+0.05	+0.04	+0.00	+0.03	−0.15	N	N
3410107658254539264	NGC1647	6063	4.40	+0.02	−0.10	+0.05	+0.04	−0.13	-1.34	−0.92	N	N
3410107726974013824	NGC1647	6031	4.31	+0.02	−0.09	+0.05	+0.04	−0.11	-1.15	−0.80	N	N
3410108203715054336	NGC1647	5490	4.20	+0.17	−0.03	+0.03	+0.03	−0.01	−0.03	−0.20	N	N
3410109376241364096	NGC1647	6093	4.14	+0.03	−0.09	+0.02	−0.04	−0.03	−0.13	−0.07	N	N
3410110677614867840	NGC1647	6061	4.16	+0.01	−0.04	+0.05	+0.02	−0.02	+0.14	−0.18	N	N
3410114495842471552	NGC1647	6026	4.44	+0.06	−0.09	+0.05	+0.06	−0.12	-1.39	−0.93	N	N
3410116007670950912	NGC1647	6229	4.25	−0.01	−0.10	+0.01	−0.04	−0.02	−0.03	−0.18	N	N
3410116523067021952	NGC1647	5673	3.64	−0.07	−0.01	+0.00	−0.04	+0.00	+0.04	−0.12	N	N
3410117313342257664	NGC1647	6470	4.52	+0.16	−0.13	+0.01	+0.02	−0.04	−0.64	−0.02	N	N
3410118412852640128	NGC1647	6184	4.40	+0.11	−0.11	+0.01	+0.01	−0.02	−0.23	−0.06	N	N
3410123154496440192	NGC1647	5957	4.12	+0.03	−0.06	+0.01	−0.01	−0.02	+0.03	−0.08	N	N
3410125284800199296	NGC1647	6127	4.65	+0.21	−0.11	+0.02	+0.04	+0.02	−0.44	+0.08	N	N
3410131950589556352	NGC1647	4654	1.85	−0.07	+0.11	+0.05	+0.00	+0.01	−0.24	+0.16	N	N
3410132088028391040	NGC1647	6021	4.01	−0.12	−0.06	+0.09	−0.09	−0.01	−0.18	−0.16	N	N
3418477999759734656	NGC1746	6179	4.17	+0.03	−0.07	+0.07	−0.06	+0.01	−0.29	+0.00	N	N
3418501811058420480	NGC1746	6047	4.07	−0.03	−0.10	+0.04	−0.05	−0.02	+0.01	+0.11	N	N
3418501944199642752	NGC1746	5925	4.01	+0.00	−0.08	+0.02	−0.06	−0.04	−0.13	+0.09	N	N
3418582350284420352	NGC1746	5192	3.15	−0.09	+0.03	+0.00	+0.00	+0.06	−0.03	+0.17	N	N
3418582827023754368	NGC1746	5288	3.41	−0.10	−0.01	−0.01	+0.00	+0.03	−0.20	+0.24	N	N
3418583926535380736	NGC1746	5679	3.86	−0.02	−0.05	+0.01	+0.00	+0.00	+0.02	+0.12	N	N
3418661996158743296	NGC1746	6040	4.11	+0.01	−0.04	+0.08	−0.04	−0.01	−0.39	−0.01	N	N
3418663645426173696	NGC1746	5914	4.20	+0.04	−0.06	+0.06	+0.05	−0.08	-1.15	−0.67	N	N
3418663954663816064	NGC1746	5740	4.24	+0.09	−0.09	+0.00	+0.02	+0.01	+0.02	+0.14	Y	N
3418665741370188288	NGC1746	6173	4.16	+0.00	−0.07	+0.08	−0.09	+0.01	−0.30	+0.05	N	N

Continued on next page

Table B.1 – Continued

Gaia ID	Cluster	T_{eff} (K)	log g (dex)	[Fe/H] (dex)	[Mg/Fe] (dex)	[Si/Fe] (dex)	[Ni/Fe] (dex)	[Ca/Fe] (dex)	[Na/Fe] (dex)	[V/Fe] (dex)	Member	Mass
3418666046311446272	NGC1746	6324	4.28	+0.01	−0.10	+0.04	−0.01	−0.01	−0.23	−0.07	N	N
3418666497284439808	NGC1746	5933	4.33	+0.10	−0.06	+0.05	+0.03	−0.02	−0.93	−0.14	N	N
3418666806522080640	NGC1746	6254	4.45	+0.14	−0.09	+0.06	−0.08	+0.01	−0.35	+0.05	N	N
3418668692011302912	NGC1746	6306	4.17	−0.01	−0.09	+0.06	−0.03	+0.00	−0.19	−0.08	N	N
3418668833746665344	NGC1758	6342	4.29	+0.01	−0.10	+0.05	−0.03	+0.02	−0.14	−0.09	N	N
3418668932529469312	NGC1746	4674	2.69	+0.15	+0.08	−0.01	−0.02	+0.11	−0.05	+0.02	N	N
3418669005545360512	NGC1746	6083	4.11	+0.09	−0.05	+0.07	−0.03	+0.02	−0.25	+0.01	N	N
3418669108624573696	NGC1758	5904	4.29	+0.06	−0.04	+0.05	+0.01	+0.01	−0.69	+0.00	N	N
3418669280423257728	NGC1746	6278	4.21	+0.04	−0.10	+0.05	−0.04	+0.01	−0.24	−0.02	N	N
3418669280423257728	NGC1758	6272	4.19	+0.05	−0.09	+0.05	−0.04	+0.01	−0.18	+0.01	N	N
3418669486581686912	NGC1746	5490	3.48	−0.15	−0.04	+0.02	−0.03	+0.03	+0.11	+0.13	N	N
3418669619724227584	NGC1746	6247	4.19	+0.00	−0.11	+0.04	−0.04	+0.00	−0.11	−0.06	N	N
3418669692740110208	NGC1746	6160	4.09	−0.03	−0.04	+0.08	−0.07	+0.02	−0.36	+0.05	N	N
3418670105056961280	NGC1746	5956	3.94	−0.06	+0.02	+0.09	+0.03	−0.01	−0.02	−0.17	Y	N
3418670105056961280	NGC1758	5922	3.98	−0.02	+0.00	+0.08	−0.02	+0.01	−0.36	+0.02	N	N
3418670139416699136	NGC1746	6257	4.16	−0.01	−0.07	+0.08	−0.08	+0.01	−0.29	+0.04	N	N
3418670311215382528	NGC1746	6271	4.18	−0.04	−0.08	+0.08	−0.10	+0.01	−0.24	+0.04	N	N
3418670822315071360	NGC1746	6282	4.16	+0.05	−0.10	+0.06	−0.05	+0.01	−0.11	−0.01	N	N
3418670822315071360	NGC1758	6291	4.17	+0.05	−0.10	+0.06	−0.05	+0.01	−0.14	+0.00	N	N
3418670895330947712	NGC1758	6325	4.26	+0.04	−0.10	+0.05	−0.05	+0.01	−0.26	+0.01	N	N
3418671067129633152	NGC1746	5143	3.03	−0.28	+0.06	+0.05	+0.00	+0.06	+0.20	+0.15	N	N
3418671101489379328	NGC1758	6052	4.08	+0.01	−0.09	+0.03	−0.04	−0.01	+0.02	+0.10	N	N
3418671582525694720	NGC1746	5121	3.32	+0.05	+0.03	−0.01	+0.01	+0.08	+0.05	+0.09	N	N
3418671582525694720	NGC1758	4940	2.98	+0.05	+0.05	+0.00	+0.00	+0.09	−0.04	+0.07	N	N
3418671823043859456	NGC1746	6006	4.06	−0.03	−0.09	+0.04	−0.05	−0.01	+0.13	+0.09	N	N
3418672922555564416	NGC1746	6064	4.14	+0.08	−0.05	+0.06	−0.06	+0.01	−0.31	−0.06	N	N

Continued on next page

Table B.1 – Continued

Gaia ID	Cluster	T_{eff} (K)	log g (dex)	[Fe/H] (dex)	[Mg/Fe] (dex)	[Si/Fe] (dex)	[Ni/Fe] (dex)	[Ca/Fe] (dex)	[Na/Fe] (dex)	[V/Fe] (dex)	Member	Mass
3418673261856511744	NGC1746	5859	5.56	+0.29	−0.04	+0.03	+0.02	+0.02	−0.01	+0.03	N	N
3418674537463329536	NGC1746	5949	4.22	+0.01	−0.06	+0.07	+0.05	−0.10	-1.29	−0.83	N	N
3418674606182736384	NGC1758	6137	4.14	+0.01	−0.06	+0.07	−0.07	+0.01	−0.29	+0.09	N	N
3418675705694132864	NGC1746	6123	4.16	+0.08	−0.07	+0.05	−0.06	+0.00	−0.30	−0.01	N	N
3418676083652258944	NGC1758	5230	3.26	−0.08	+0.02	+0.00	+0.00	+0.06	−0.09	+0.18	N	N
3418676324169472128	NGC1746	5088	4.42	+0.11	+0.04	+0.02	+0.04	+0.04	−0.17	−0.05	N	N
3418676392888948608	NGC1746	5057	4.61	+0.16	+0.00	+0.02	+0.01	+0.03	+0.01	−0.11	N	N
3418676392888948608	NGC1758	4998	4.61	+0.15	+0.03	+0.02	+0.03	+0.04	−0.04	−0.10	N	N
3418676427248683904	NGC1746	6161	4.11	+0.03	−0.06	+0.08	−0.05	+0.00	−0.30	+0.01	N	N
3418676495968155008	NGC1746	6056	4.14	+0.02	−0.12	+0.01	−0.05	−0.01	+0.04	+0.04	N	N
3418676495968155008	NGC1758	6062	4.11	+0.01	−0.07	+0.04	−0.07	+0.01	−0.20	+0.09	N	N
3418676663470606208	NGC1746	4820	2.73	+0.09	+0.06	+0.02	−0.02	+0.08	−0.05	−0.01	N	Y
3418676667766855168	NGC1746	5941	4.33	+0.08	−0.05	+0.05	+0.01	+0.01	−0.66	−0.04	N	N
3418677148803178880	NGC1746	4933	2.93	+0.11	+0.07	+0.02	−0.01	+0.09	−0.09	−0.03	Y	Y
3418677148803178880	NGC1758	4918	2.89	+0.11	+0.07	+0.03	−0.01	+0.09	−0.09	−0.01	N	N
3418678763710843136	NGC1746	5069	3.50	−0.40	+0.16	+0.08	+0.07	+0.11	+0.14	+0.20	N	N
3418678763710843136	NGC1758	5378	4.46	+0.16	−0.02	+0.02	+0.03	+0.03	−0.38	−0.04	N	N
3418678798070595840	NGC1758	6120	4.17	+0.00	−0.05	+0.06	−0.06	+0.02	−0.43	+0.10	N	N
3418678901150033024	NGC1746	6241	4.16	+0.01	−0.08	+0.07	−0.05	−0.01	−0.25	−0.02	N	N
3418679480969489024	NGC1746	6255	4.24	+0.06	−0.10	+0.06	−0.05	−0.02	−0.33	−0.01	N	N
3418679480969489024	NGC1758	6204	4.19	+0.03	−0.08	+0.05	−0.07	+0.00	−0.35	+0.04	N	N
3418680717919727104	NGC1746	5239	4.48	+0.16	+0.01	+0.02	+0.04	+0.04	−0.25	−0.06	N	N
3418680717919727104	NGC1758	5074	4.52	+0.15	+0.00	+0.01	+0.03	+0.03	−0.04	−0.07	N	N
3418681203252478720	NGC1746	5794	4.36	+0.08	−0.02	+0.05	+0.01	+0.03	−0.47	+0.06	N	N
3418681753008279552	NGC1746	6258	4.24	+0.04	−0.09	+0.05	−0.05	+0.00	−0.30	+0.00	N	N
3418682268404109568	NGC1758	5722	3.63	−0.16	−0.04	+0.04	−0.06	+0.02	+0.08	+0.21	N	N

Continued on next page

Table B.1 – Continued

Gaia ID	Cluster	T_{eff} (K)	log g (dex)	[Fe/H] (dex)	[Mg/Fe] (dex)	[Si/Fe] (dex)	[Ni/Fe] (dex)	[Ca/Fe] (dex)	[Na/Fe] (dex)	[V/Fe] (dex)	Member	Mass
3418682642065479808	NGC1758	6162	4.12	−0.04	−0.06	+0.07	−0.09	+0.01	−0.37	+0.07	N	N
3418683157461575936	NGC1746	6271	4.20	+0.03	−0.08	+0.08	−0.04	+0.00	−0.45	−0.04	N	N
3418683367915964160	NGC1746	6183	4.41	+0.03	−0.06	+0.05	−0.03	+0.02	−0.68	+0.15	N	N
3418683367915967104	NGC1746	6079	4.03	−0.03	−0.07	+0.06	−0.08	+0.01	−0.23	+0.11	N	N
3418683677153600768	NGC1758	5831	3.83	−0.07	−0.04	+0.03	−0.01	+0.01	+0.09	+0.10	N	N
3418683780232817024	NGC1758	5992	4.06	+0.02	−0.08	+0.05	−0.01	−0.01	−0.01	+0.06	N	N
3418683952031503616	NGC1746	6021	4.05	+0.03	−0.08	+0.03	−0.03	−0.01	+0.13	+0.00	N	N
3418684261269161216	NGC1746	5747	3.89	+0.01	+0.08	+0.09	+0.05	+0.04	+0.04	−0.22	N	N
3418684329988644096	NGC1758	5275	3.23	−0.27	+0.03	+0.05	−0.02	+0.06	+0.17	+0.14	N	N
3418684948463641984	NGC1746	6204	4.21	−0.01	−0.08	+0.05	−0.06	−0.04	−0.15	−0.01	N	N
3418684948463643008	NGC1746	4919	2.81	−0.08	+0.06	+0.00	−0.03	+0.07	−0.02	+0.11	N	N
3418684948463643008	NGC1758	5188	4.56	+0.17	−0.01	+0.02	+0.02	+0.03	−0.14	−0.08	N	N
3418685051542849664	NGC1746	6126	4.06	−0.04	−0.08	+0.05	−0.05	+0.01	+0.18	−0.01	N	N
3418685257701351040	NGC1758	5943	4.06	+0.03	−0.03	+0.07	−0.06	+0.02	−0.40	+0.01	N	N
3418685395140315392	NGC1746	5238	4.64	+0.17	−0.01	+0.02	+0.02	+0.03	−0.04	−0.07	N	N
3418685807457141888	NGC1746	5094	2.80	−0.21	+0.05	+0.03	+0.00	+0.04	−0.09	+0.16	N	N
3418687246269977216	NGC1746	5861	4.14	+0.13	−0.06	+0.07	+0.02	−0.01	−0.41	−0.22	N	N
3418687903401141376	NGC1746	6161	4.09	−0.05	−0.09	+0.04	−0.05	−0.01	+0.08	+0.01	N	N
3418688281358258560	NGC1746	6028	4.08	+0.00	−0.07	+0.06	−0.06	−0.04	−0.24	−0.04	N	N
3418688350077734784	NGC1746	5899	3.92	−0.05	−0.10	+0.02	−0.06	−0.03	−0.12	+0.14	N	N
3418688350077734784	NGC1758	5970	4.02	−0.06	−0.09	+0.03	−0.04	−0.01	+0.10	+0.08	N	N
3418688521876453248	NGC1746	5849	4.41	+0.13	−0.10	+0.01	+0.02	+0.00	+0.14	+0.08	N	N
3418688655022016640	NGC1746	4874	2.74	+0.01	+0.04	+0.00	−0.02	+0.08	−0.03	+0.06	N	N
3418688964257605504	NGC1746	5673	3.85	+0.02	−0.07	−0.01	−0.02	+0.01	+0.25	+0.00	N	N
3418688964257605504	NGC1758	5337	4.51	+0.24	−0.03	+0.01	+0.02	+0.01	−0.26	−0.12	N	N
3418689209071183360	NGC1746	4976	3.22	+0.09	+0.08	+0.00	+0.03	+0.08	−0.03	−0.20	N	N

Continued on next page

Table B.1 – Continued

Gaia ID	Cluster	T_{eff} (K)	log g (dex)	[Fe/H] (dex)	[Mg/Fe] (dex)	[Si/Fe] (dex)	[Ni/Fe] (dex)	[Ca/Fe] (dex)	[Na/Fe] (dex)	[V/Fe] (dex)	Member	Mass
3418690823979167872	NGC1746	6231	4.20	+0.02	−0.10	+0.05	−0.06	−0.01	−0.21	+0.01	N	N
3418690823979167872	NGC1758	6212	4.30	+0.08	−0.10	+0.01	+0.01	−0.03	−0.19	−0.19	N	N
3418690858338903296	NGC1746	5379	4.41	+0.17	−0.03	+0.01	+0.04	+0.02	−0.04	−0.07	N	N
3418691098857074688	NGC1758	6168	4.24	+0.10	−0.10	+0.04	+0.00	+0.00	−0.34	−0.03	N	N
3418691167576546048	NGC1746	6057	4.16	+0.02	−0.05	+0.07	−0.01	−0.07	−0.17	−0.17	N	N
3418691231999652480	NGC1746	6150	4.15	+0.03	−0.10	+0.03	−0.02	+0.00	−0.03	−0.04	N	N
3418691231999652480	NGC1758	6160	4.23	+0.06	−0.10	+0.01	−0.01	−0.03	−0.12	−0.11	N	N
3418691545533660032	NGC1746	5781	3.77	−0.05	−0.05	+0.03	−0.05	−0.02	−0.13	−0.05	N	N
3418691545533660032	NGC1758	5928	4.11	+0.05	−0.06	+0.03	+0.03	−0.04	−0.02	−0.10	N	N
3418691648612870656	NGC1758	5845	4.43	+0.17	−0.09	+0.01	+0.04	+0.01	−0.13	+0.03	N	N
3418691923490764288	NGC1746	5869	4.05	−0.01	−0.07	+0.03	−0.01	+0.00	+0.20	+0.07	N	N
3418693985075105920	NGC1758	5983	4.28	+0.03	−0.07	+0.06	+0.05	−0.09	-1.20	−0.77	N	N
3418694294312745984	NGC1758	6006	3.96	−0.05	−0.06	+0.02	−0.04	−0.02	−0.15	−0.07	N	N
3418694672269849088	NGC1746	5983	4.13	+0.08	−0.05	+0.04	+0.02	−0.06	+0.07	−0.15	N	N
3418694805412941696	NGC1746	6108	4.09	−0.02	−0.09	+0.04	−0.06	−0.02	−0.08	+0.07	N	N
3418694878428279936	NGC1746	5965	4.07	+0.00	−0.08	+0.02	−0.04	+0.00	+0.20	+0.03	N	N
3418695256385613440	NGC1758	6192	4.18	−0.04	−0.10	+0.03	−0.03	−0.03	−0.32	−0.33	N	N
3418695359464637696	NGC1746	6045	4.16	+0.04	−0.02	+0.03	+0.04	−0.04	−0.03	−0.12	N	N
3418695462543841408	NGC1758	6138	4.16	+0.01	−0.10	+0.02	−0.02	−0.03	−0.13	−0.11	N	N
3418695703061997696	NGC1746	6075	4.11	−0.01	−0.06	+0.07	−0.08	+0.00	−0.30	+0.03	N	N
3418696836933330688	NGC1746	6430	4.30	+0.08	−0.12	+0.07	−0.02	+0.03	−0.31	+0.01	N	N
3418697249250212096	NGC1746	6284	4.26	+0.00	−0.11	+0.05	−0.04	−0.01	−0.08	−0.03	N	N
3418697695926807168	NGC1746	5739	4.00	+0.03	−0.01	+0.04	+0.01	−0.07	+0.06	−0.17	N	N
3418697764646275840	NGC1746	6084	4.17	+0.03	−0.08	+0.06	−0.05	−0.03	−0.30	−0.05	N	N
3418697970804700672	NGC1746	6128	4.11	−0.05	−0.09	+0.05	−0.08	−0.02	−0.13	+0.06	N	N
3418702987326494976	NGC1746	6111	4.13	−0.04	−0.09	+0.04	−0.06	−0.02	+0.02	+0.05	N	N

Continued on next page

Table B.1 – Continued

Gaia ID	Cluster	T_{eff} (K)	log g (dex)	[Fe/H] (dex)	[Mg/Fe] (dex)	[Si/Fe] (dex)	[Ni/Fe] (dex)	[Ca/Fe] (dex)	[Na/Fe] (dex)	[V/Fe] (dex)	Member	Mass
3418703056045970432	NGC1746	6101	4.13	+0.00	−0.07	+0.06	−0.09	+0.00	−0.26	+0.02	N	N
3418703124765439232	NGC1746	5966	4.07	+0.01	−0.02	+0.00	+0.02	−0.05	−0.03	−0.10	Y	N
3418707243637713664	NGC1746	6042	4.11	+0.00	−0.03	+0.02	+0.01	−0.04	−0.01	−0.13	N	N
3418707316653581824	NGC1746	6171	4.42	+0.14	−0.12	+0.03	+0.02	+0.01	−0.40	+0.01	N	N
3418707557171744000	NGC1746	5939	4.03	−0.05	−0.07	−0.03	+0.02	−0.03	−0.34	+0.11	N	N
3418707625891221248	NGC1746	5991	4.07	−0.01	−0.07	+0.04	−0.04	−0.02	−0.03	+0.05	N	N
3418707625891221248	NGC1758	5883	4.03	+0.00	−0.06	+0.05	−0.02	−0.03	−0.13	−0.03	N	N
3418707728970432256	NGC1746	5923	3.97	−0.05	−0.04	+0.04	−0.01	+0.01	+0.23	−0.01	N	N
3418707728970432256	NGC1758	5574	4.05	+0.03	+0.05	+0.04	+0.07	+0.06	+0.08	−0.01	N	N
3418708416165206016	NGC1746	5780	4.13	+0.15	−0.06	+0.05	+0.05	−0.10	−0.76	−0.74	N	N
3418708965921004160	NGC1746	4802	2.56	−0.30	+0.10	+0.04	+0.03	+0.01	+0.08	−0.06	N	N
3418709099062283392	NGC1746	5705	3.78	−0.07	−0.02	+0.02	+0.01	+0.00	−0.06	+0.12	N	N
3418709103359676288	NGC1746	5217	2.91	−0.18	+0.02	+0.04	−0.03	+0.00	−0.06	+0.30	N	N
3418709103359676288	NGC1758	5483	4.05	+0.15	+0.01	+0.01	+0.05	+0.02	+0.18	−0.19	N	N
3418709412597592576	NGC1746	6100	4.27	+0.12	−0.10	+0.00	−0.02	−0.01	+0.16	−0.14	N	N
3418709927993658240	NGC1746	6327	4.16	−0.02	−0.03	+0.09	−0.11	+0.05	−0.04	+0.11	N	N
3418709996713128704	NGC1746	6136	4.13	−0.07	−0.08	+0.07	−0.10	−0.01	−0.26	+0.00	N	N
3418710099792339456	NGC1746	6143	4.15	−0.02	−0.08	+0.03	−0.04	−0.01	+0.10	−0.05	Y	N
3418710409030006528	NGC1746	6109	4.51	+0.18	−0.12	+0.02	+0.04	+0.03	−0.55	+0.13	N	N
3418710576531027840	NGC1746	5846	3.99	+0.00	+0.00	+0.02	+0.01	−0.05	+0.00	−0.16	N	N
3418710890066335744	NGC1746	5191	3.06	−0.15	+0.09	+0.04	+0.01	+0.02	−0.12	+0.14	N	N
3418711783419291392	NGC1758	6242	4.07	+0.00	−0.07	+0.09	−0.04	+0.00	−0.32	+0.00	N	N
3418712127016652032	NGC1746	6058	4.07	+0.04	−0.09	+0.03	−0.02	−0.02	−0.10	−0.06	N	N
3418712230095847040	NGC1746	5902	3.96	+0.01	−0.04	+0.04	+0.00	−0.03	+0.06	−0.05	N	N
3418712298815323904	NGC1746	6081	4.09	−0.01	−0.09	+0.03	−0.03	−0.01	+0.10	−0.05	N	N
3418712397597159680	NGC1746	6167	4.13	−0.06	−0.08	+0.02	−0.06	+0.01	−0.08	−0.20	N	N

Continued on next page

Table B.1 – Continued

Gaia ID	Cluster	T_{eff} (K)	log g (dex)	[Fe/H] (dex)	[Mg/Fe] (dex)	[Si/Fe] (dex)	[Ni/Fe] (dex)	[Ca/Fe] (dex)	[Na/Fe] (dex)	[V/Fe] (dex)	Member	Mass
3418712642412742016	NGC1746	5868	4.04	+0.12	−0.08	+0.00	−0.02	−0.01	+0.27	−0.01	N	N
3418712672475070080	NGC1746	5771	3.89	−0.06	−0.02	+0.01	+0.02	−0.01	−0.15	−0.01	N	N
3418712672475070080	NGC1758	6016	3.97	+0.07	−0.04	+0.10	+0.01	+0.00	−0.14	+0.01	N	N
3418712848571159040	NGC1746	5735	3.71	−0.13	−0.01	+0.07	−0.07	−0.01	−0.17	−0.12	N	N
3418713192168533504	NGC1746	5773	4.02	−0.01	−0.02	−0.01	+0.03	−0.03	−0.12	−0.06	N	N
3418713192168533504	NGC1758	5641	3.82	−0.04	−0.04	−0.02	+0.00	−0.01	−0.20	+0.16	N	N
3418713875066151296	NGC1746	6116	4.03	−0.07	−0.09	+0.08	−0.08	−0.02	−0.29	−0.05	N	N
3418713875066151296	NGC1758	6128	4.02	−0.06	−0.07	+0.07	−0.08	−0.01	−0.20	+0.00	N	N
3418713943785378944	NGC1746	5360	3.46	−0.13	+0.09	+0.02	+0.05	−0.02	−0.02	−0.08	N	N
3418714910155427456	NGC1746	6076	4.02	−0.08	−0.07	+0.06	−0.06	−0.03	−0.23	−0.09	N	N
3418715047594373376	NGC1746	5842	3.79	−0.06	−0.02	+0.03	−0.01	+0.01	+0.13	−0.05	Y	N
3418715734789432960	NGC1746	6281	4.30	+0.06	−0.12	+0.02	−0.01	+0.00	−0.22	−0.04	Y	N
3418717109178958336	NGC1746	6154	4.09	−0.06	−0.09	+0.02	−0.05	−0.02	−0.10	−0.14	N	N
3418720304634627840	NGC1746	6195	4.15	−0.01	−0.10	+0.01	−0.04	−0.01	−0.04	−0.14	N	N
3418720304634627840	NGC1758	6241	4.24	+0.02	−0.11	+0.03	−0.03	−0.01	−0.07	−0.17	N	N
3418724771400569088	NGC1746	4832	2.88	+0.07	+0.09	+0.00	+0.00	+0.11	−0.06	+0.04	N	N
3418724908839513472	NGC1746	6270	4.16	+0.05	−0.09	+0.08	−0.03	+0.00	−0.31	−0.01	N	N
3418725041982217216	NGC1746	4710	2.59	+0.09	+0.09	+0.02	−0.01	+0.09	−0.10	−0.01	Y	Y
3418725149357679488	NGC1746	5180	3.31	−0.41	+0.12	+0.09	+0.05	+0.10	+0.05	+0.22	N	N
3418725939631664256	NGC1746	6289	4.44	+0.10	−0.11	+0.04	−0.06	+0.00	−0.47	+0.08	N	N
3418726244573050496	NGC1746	5128	2.95	−0.11	+0.04	+0.01	−0.01	+0.05	−0.14	+0.16	N	N
3418726455027722112	NGC1746	5435	3.57	−0.08	+0.00	+0.05	−0.01	+0.06	−0.03	+0.31	N	N
3418726661186150528	NGC1746	5074	2.91	−0.27	+0.06	+0.02	+0.01	+0.02	−0.01	+0.12	N	N
3418726759969117952	NGC1746	5368	3.51	−0.16	+0.04	+0.03	+0.03	+0.03	−0.02	+0.15	N	N
3418726798625094656	NGC1746	6165	4.13	+0.01	−0.04	+0.08	−0.07	+0.01	−0.33	+0.08	N	N
3418727073502982528	NGC1746	6293	4.25	+0.03	−0.10	+0.06	−0.06	−0.01	−0.24	−0.03	N	N

Continued on next page

Table B.1 – Continued

Gaia ID	Cluster	T_{eff} (K)	log g (dex)	[Fe/H] (dex)	[Mg/Fe] (dex)	[Si/Fe] (dex)	[Ni/Fe] (dex)	[Ca/Fe] (dex)	[Na/Fe] (dex)	[V/Fe] (dex)	Member	Mass
3418730921793692928	NGC1746	5205	3.15	−0.15	+0.00	+0.00	−0.02	+0.05	−0.24	+0.28	N	N
3418731162311870208	NGC1746	5176	3.03	−0.12	+0.03	+0.00	+0.01	+0.06	−0.08	+0.17	Y	Y
3418731192375351040	NGC1746	6057	4.28	+0.05	−0.05	+0.06	+0.00	+0.00	−0.58	+0.01	N	N
3418732811579288320	NGC1746	6168	4.15	−0.04	−0.11	+0.04	−0.07	−0.01	+0.16	+0.06	N	N
3418734147312849280	NGC1746	5122	2.85	−0.14	+0.01	−0.01	+0.00	+0.04	−0.13	+0.22	N	N
3418734147312849280	NGC1758	5091	2.77	−0.13	+0.02	+0.00	+0.00	+0.04	−0.11	+0.21	N	N
3418735349902397184	NGC1746	4982	2.95	−0.34	+0.10	+0.06	+0.04	+0.05	−0.07	+0.14	N	N
3418735972675145216	NGC1746	6079	4.14	+0.03	−0.09	+0.05	−0.05	−0.04	−0.21	−0.07	N	N
3418736007034872320	NGC1746	5083	4.31	+0.11	−0.01	+0.01	+0.02	+0.02	+0.10	−0.06	N	N
3418736384991970944	NGC1746	5984	4.06	−0.01	−0.07	+0.06	−0.05	−0.04	−0.15	−0.12	N	N
3418736797308859264	NGC1746	5998	4.06	−0.03	−0.08	+0.05	−0.04	−0.03	−0.10	−0.01	N	N
3418737136608785792	NGC1746	5107	3.14	+0.01	+0.05	+0.00	+0.00	+0.08	−0.08	+0.01	N	N
3418737793741228800	NGC1746	6000	4.06	+0.04	−0.04	+0.06	−0.06	+0.02	−0.34	−0.07	N	N
3418737965540006144	NGC1746	4998	2.88	−0.05	+0.04	−0.01	+0.00	+0.08	−0.08	+0.11	N	N
3418738206058516352	NGC1758	5148	3.03	−0.11	+0.02	−0.01	+0.01	+0.02	−0.06	+0.18	N	N
3418738309137383808	NGC1746	5083	3.08	−0.23	+0.05	+0.05	+0.00	+0.05	+0.26	+0.15	N	N
3418738996332158464	NGC1746	6155	4.30	+0.06	−0.09	+0.04	−0.07	−0.02	−0.25	+0.03	N	N
3418740061484004352	NGC1746	6229	4.26	+0.00	−0.10	+0.01	−0.02	−0.02	−0.25	−0.32	N	N
3418741023556649344	NGC1758	4885	4.45	+0.14	+0.02	+0.01	+0.02	+0.04	+0.00	−0.13	N	N
3418741500302452992	NGC1746	5987	3.96	−0.05	−0.08	+0.04	−0.05	+0.01	+0.31	+0.05	N	N
3418741500302452992	NGC1758	6071	4.10	+0.01	−0.10	+0.03	−0.05	−0.01	+0.04	+0.07	N	N
3418741607672217216	NGC1746	5497	4.46	+0.11	+0.09	+0.04	+0.09	+0.08	+0.07	+0.02	N	N
3418745073708351360	NGC1746	4933	2.71	−0.12	+0.06	+0.02	+0.01	+0.07	−0.10	+0.09	N	Y
3418751778154795776	NGC1746	6175	4.10	+0.00	−0.08	+0.08	−0.06	−0.01	−0.58	+0.00	N	N
3418753324343004288	NGC1746	5112	3.00	−0.42	+0.12	+0.08	+0.03	+0.07	+0.10	+0.05	N	N
3418755042330994176	NGC1746	5964	4.08	+0.01	−0.06	+0.01	−0.01	−0.03	+0.15	−0.15	N	N

Continued on next page

Table B.1 – Continued

Gaia ID	Cluster	T_{eff} (K)	log g (dex)	[Fe/H] (dex)	[Mg/Fe] (dex)	[Si/Fe] (dex)	[Ni/Fe] (dex)	[Ca/Fe] (dex)	[Na/Fe] (dex)	[V/Fe] (dex)	Member	Mass
3418761261442532480	NGC1746	6046	4.04	−0.04	−0.08	+0.04	−0.06	−0.02	+0.06	+0.02	N	N
3418761261442532480	NGC1758	5967	4.03	−0.01	−0.08	+0.04	−0.04	−0.01	+0.08	+0.08	N	N
3418761605040186624	NGC1746	5775	3.73	−0.11	−0.03	+0.03	−0.02	+0.02	+0.21	+0.02	N	N
3418761605040186624	NGC1758	5823	3.83	−0.09	−0.04	+0.03	−0.02	+0.01	+0.18	+0.06	N	N
3418762670191735424	NGC1746	6002	4.06	−0.04	−0.07	+0.06	−0.03	−0.03	−0.09	−0.13	N	N
3418762670191735424	NGC1758	5916	4.00	−0.03	−0.06	+0.02	−0.02	−0.03	−0.10	−0.08	N	N
3418763254307314688	NGC1746	4977	2.86	−0.28	+0.09	+0.05	+0.01	+0.05	+0.20	+0.03	N	N
3418763868485207808	NGC1746	5884	4.08	−0.01	−0.07	−0.02	+0.02	−0.03	−0.24	−0.07	N	N
3418764216379954432	NGC1746	6031	4.02	−0.02	−0.09	+0.05	−0.05	−0.03	−0.13	−0.03	N	N
3418764216379954432	NGC1758	6050	4.06	−0.01	−0.09	+0.04	−0.03	−0.02	+0.02	+0.04	N	N
3418764663056621056	NGC1746	6044	4.07	−0.01	−0.08	+0.01	−0.03	−0.02	−0.02	−0.06	N	N
3418765212812413056	NGC1746	4980	2.79	−0.34	+0.09	+0.06	+0.03	+0.06	+0.01	+0.13	N	N
3418765212812413056	NGC1758	4988	2.74	−0.37	+0.10	+0.07	+0.03	+0.05	+0.03	+0.13	N	N
3418766003086402944	NGC1746	4826	2.20	+0.04	+0.11	+0.07	+0.02	+0.03	−0.13	+0.08	N	N
3418766003086402944	NGC1758	4833	2.46	+0.14	+0.10	+0.09	+0.02	+0.04	−0.09	+0.01	N	N
3418766445465581056	NGC1746	4726	2.40	+0.18	+0.10	+0.08	+0.02	+0.05	−0.04	+0.08	N	N
3418766789062968704	NGC1746	4741	2.10	−0.30	+0.13	+0.13	+0.02	−0.04	+0.07	+0.10	N	N
3418767033878510080	NGC1746	4752	2.44	−0.44	+0.11	+0.04	+0.02	+0.02	+0.04	−0.14	N	N
3418767033878510080	NGC1758	4998	2.77	−0.12	+0.04	−0.01	+0.01	+0.06	−0.16	+0.19	N	N
3418767132660349696	NGC1746	4734	4.25	+0.13	+0.04	+0.01	+0.02	+0.03	+0.07	−0.16	N	N
3418767205677185408	NGC1746	5753	4.49	+0.20	−0.01	−0.01	+0.07	+0.02	+0.23	−0.10	N	N
3418767721073288192	NGC1746	5987	4.03	−0.04	+0.02	+0.08	+0.05	−0.05	+0.10	−0.28	N	N
3418767721073288192	NGC1758	6030	4.11	−0.02	−0.01	+0.07	+0.03	−0.04	+0.11	−0.21	N	N
3418769576499111680	NGC1746	5578	4.09	+0.07	−0.03	+0.01	+0.04	+0.03	−0.08	−0.06	N	N
3418769576499111680	NGC1758	5517	3.94	+0.05	−0.01	+0.02	+0.04	+0.02	−0.02	−0.01	N	N
3418773459149555968	NGC1746	5464	3.54	−0.07	+0.07	+0.06	+0.05	+0.00	+0.17	−0.22	N	N

Continued on next page

Table B.1 – Continued

Gaia ID	Cluster	T_{eff} (K)	log g (dex)	[Fe/H] (dex)	[Mg/Fe] (dex)	[Si/Fe] (dex)	[Ni/Fe] (dex)	[Ca/Fe] (dex)	[Na/Fe] (dex)	[V/Fe] (dex)	Member	Mass
3418775177136447360	NGC1746	6086	4.83	+0.22	−0.09	+0.02	+0.06	+0.02	−0.08	−0.02	N	N
3418778235153243392	NGC1746	6237	4.26	+0.06	−0.11	+0.00	−0.02	−0.01	−0.10	−0.13	N	N
3418778441311673728	NGC1746	6206	4.20	+0.13	−0.09	+0.07	−0.01	−0.02	−0.18	−0.04	N	N
3418779162866184192	NGC1746	6213	4.17	+0.01	−0.09	+0.07	−0.06	−0.02	−0.33	+0.00	N	N
3425498587661491328	NGC2158	4986	3.05	−0.35	+0.14	+0.06	+0.06	+0.08	+0.12	+0.17	N	N
3426163654759089280	NGC2158	4940	2.51	−0.29	+0.04	+0.03	−0.01	−0.03	−0.20	+0.32	N	N
3426163723478576128	NGC2158	5036	2.61	−0.24	+0.03	+0.01	+0.00	−0.01	+0.16	+0.12	N	N
3426163963996725888	NGC2158	4872	2.38	−0.30	+0.07	+0.03	+0.00	+0.02	+0.04	+0.03	N	N
3426164341953838336	NGC2158	5047	2.78	−0.13	+0.02	+0.02	−0.01	+0.05	+0.08	+0.11	N	N
3426165024852665472	NGC2158	4983	2.53	−0.30	+0.05	+0.03	+0.00	+0.03	+0.04	+0.11	N	N
3426165200947293440	NGC2158	5000	2.58	−0.19	+0.04	+0.02	−0.02	+0.04	+0.00	+0.10	N	N
3426165269666731776	NGC2158	5012	2.60	−0.25	+0.04	+0.03	−0.06	+0.07	+0.20	+0.07	N	N
3426165334090122240	NGC2158	4634	2.43	+0.03	+0.10	+0.03	−0.01	+0.07	−0.10	−0.05	N	N
3426165334090305664	NGC2158	5010	2.72	−0.22	+0.04	+0.04	−0.04	+0.04	−0.13	+0.29	N	N
3426165372745992832	NGC2158	4956	2.46	−0.23	+0.05	+0.03	−0.02	+0.05	−0.10	+0.11	N	N
3426165578901208448	NGC2158	4869	2.33	−0.29	+0.05	+0.02	−0.01	+0.03	+0.02	+0.02	N	N
3426165613264124800	NGC2158	5184	2.73	−0.30	+0.04	+0.04	−0.03	+0.05	+0.13	+0.08	N	N
3426165716343310464	NGC2158	6087	3.87	−0.13	−0.08	+0.04	−0.05	+0.00	+0.00	+0.06	N	N
3426165853782251904	NGC2158	4912	2.42	−0.32	+0.06	+0.03	−0.01	+0.03	+0.05	+0.01	N	N
3426165956861468288	NGC2158	4951	2.57	−0.26	+0.02	+0.04	−0.02	−0.02	−0.11	+0.29	N	N
3426165991221223552	NGC2158	5021	2.67	−0.29	+0.06	+0.02	−0.02	+0.04	+0.07	+0.02	N	N
3426165991221226496	NGC2158	4937	2.45	−0.32	+0.06	+0.04	+0.00	+0.04	−0.03	+0.10	N	N
3426166090004630144	NGC2158	4985	2.57	−0.27	+0.06	+0.02	+0.00	+0.03	+0.00	+0.01	N	N
3426175199631200256	NGC2158	4720	2.24	−0.29	+0.03	+0.04	+0.01	+0.00	−0.13	+0.07	N	N
3426175474508496512	NGC2158	4906	2.31	−0.29	+0.05	+0.01	+0.00	−0.01	−0.01	+0.00	N	N
3426175577588305920	NGC2158	4953	2.47	−0.27	+0.08	+0.04	+0.00	+0.05	+0.02	+0.01	N	N

Continued on next page

Table B.1 – Continued

Gaia ID	Cluster	T_{eff} (K)	log g (dex)	[Fe/H] (dex)	[Mg/Fe] (dex)	[Si/Fe] (dex)	[Ni/Fe] (dex)	[Ca/Fe] (dex)	[Na/Fe] (dex)	[V/Fe] (dex)	Member	Mass
3426175680667516544	NGC2158	4978	2.56	−0.23	+0.05	+0.02	+0.00	+0.02	+0.00	+0.13	N	N
3426175989906017536	NGC2158	4659	1.99	−0.27	+0.06	+0.02	+0.02	−0.02	+0.02	−0.07	N	N
3426176299142221184	NGC2158	4960	2.51	−0.29	+0.06	+0.02	−0.03	+0.03	+0.05	+0.01	N	N
3426177055056423424	NGC2158	5711	3.54	−0.11	+0.00	+0.03	+0.01	+0.01	+0.17	−0.06	N	N
3426177261215463680	NGC2158	5026	2.66	−0.22	+0.05	+0.02	−0.01	+0.02	−0.12	+0.16	N	N
3426177329934915712	NGC2158	4817	2.18	−0.26	+0.06	+0.02	+0.01	+0.02	−0.08	+0.05	N	N
3426177364294635008	NGC2158	5227	3.01	−0.17	+0.03	+0.00	−0.02	+0.00	−0.14	+0.16	N	N
3426177394363639424	NGC2158	4905	2.45	−0.23	+0.07	+0.01	+0.00	+0.01	+0.02	−0.08	N	N
3426177433014108800	NGC2158	6087	3.93	−0.09	−0.06	+0.03	−0.02	−0.03	−0.11	−0.07	N	N
3426177433014118272	NGC2158	6173	4.27	−0.10	−0.02	+0.03	+0.07	−0.05	−0.25	−0.15	N	N
3426177570448833024	NGC2158	4455	1.85	−0.22	+0.04	−0.02	+0.00	+0.00	+0.01	−0.37	N	N
3426177604812185216	NGC2158	4901	2.58	−0.27	+0.09	+0.03	−0.02	+0.01	+0.03	−0.18	N	N
3426178085848497408	NGC2158	4982	2.66	−0.27	+0.05	+0.01	−0.04	+0.02	+0.01	−0.07	N	N
3426178120208222976	NGC2158	4938	2.56	−0.28	+0.04	+0.02	−0.03	+0.04	+0.02	−0.10	N	N
3426178257647156352	NGC2158	4818	2.39	−0.25	+0.08	+0.01	+0.00	+0.01	+0.01	−0.12	N	N
3426178463805635200	NGC2158	4869	2.49	−0.26	+0.07	+0.00	−0.05	+0.00	+0.02	−0.36	N	N
3426178498165388928	NGC2158	4571	2.06	−0.38	+0.10	+0.04	+0.00	−0.01	−0.03	−0.31	N	N
3426178979201672064	NGC2158	4936	2.63	−0.29	+0.11	+0.02	+0.02	+0.01	+0.12	−0.12	N	N
3426179219719854464	NGC2158	5098	2.67	−0.22	+0.06	−0.01	−0.03	+0.00	−0.16	+0.07	N	N
3426179936979172224	NGC2158	4985	2.69	−0.18	+0.04	−0.01	+0.00	+0.01	−0.28	+0.20	N	N
3426180044355147264	NGC2158	4956	2.80	−0.33	+0.11	+0.07	+0.03	+0.07	+0.05	+0.10	N	N
3426181590541866496	NGC2158	5858	3.84	−0.05	−0.03	+0.02	+0.00	−0.02	−0.06	−0.03	N	N
3426181624901594368	NGC2158	4955	2.49	−0.23	+0.11	−0.01	+0.00	+0.05	−0.04	−0.15	N	N
3426182174657343232	NGC2158	5126	2.84	−0.21	+0.04	+0.00	−0.04	+0.00	−0.08	−0.10	N	N
3426235741489525376	NGC2158	4853	2.26	−0.13	+0.05	+0.08	−0.02	−0.03	+0.02	−0.03	N	N
3426260102544844800	NGC2158	4565	2.21	−0.02	+0.12	+0.06	+0.01	+0.06	−0.15	−0.06	N	N

Continued on next page

Table B.1 – Continued

Gaia ID	Cluster	T_{eff} (K)	log g (dex)	[Fe/H] (dex)	[Mg/Fe] (dex)	[Si/Fe] (dex)	[Ni/Fe] (dex)	[Ca/Fe] (dex)	[Na/Fe] (dex)	[V/Fe] (dex)	Member	Mass
3426271814916387200	NGC2158	4953	2.47	−0.25	+0.05	+0.05	−0.04	+0.01	+0.00	+0.13	N	N
3426272025373784832	NGC2158	4808	2.33	−0.28	+0.08	+0.04	+0.00	+0.01	+0.09	−0.03	N	N
3426325042450057600	NGC2158	4924	2.65	−0.33	+0.09	+0.07	−0.04	+0.05	+0.12	−0.13	N	N
598696352046226560	NGC2682	5208	3.39	−0.09	+0.10	+0.06	+0.02	+0.06	−0.23	+0.10	N	N
598697142320464384	NGC2682	6146	4.05	+0.03	−0.04	+0.08	−0.04	+0.01	−0.28	+0.00	Y	N
598882547468555392	NGC2682	4812	2.64	+0.02	+0.08	+0.02	−0.02	+0.07	−0.08	+0.02	N	Y
598884952650222336	NGC2682	6087	4.16	−0.05	−0.08	+0.09	+0.10	−0.13	−0.23	−0.07	Y	N
598885979147130496	NGC2682	6042	4.11	−0.01	+0.00	+0.07	+0.01	−0.05	−0.18	+0.10	Y	N
598886052161980160	NGC2682	5282	4.43	+0.15	−0.01	+0.00	+0.03	+0.07	−0.47	+0.11	N	N
598886120881330816	NGC2682	5470	4.48	+0.12	+0.05	+0.04	+0.05	+0.06	−0.08	+0.09	N	N
598890347129151104	NGC2682	6231	4.46	+0.10	−0.09	+0.05	+0.01	+0.01	−0.85	−0.08	Y	N
598890759446010624	NGC2682	5132	4.44	+0.20	−0.01	+0.02	+0.02	+0.01	−0.05	−0.12	N	N
598898073775010816	NGC2682	6064	4.05	+0.04	−0.03	+0.06	−0.06	+0.00	−0.21	−0.17	Y	N
598900788194342528	NGC2682	5991	4.22	+0.05	+0.00	+0.06	+0.05	−0.02	−0.33	−0.39	Y	N
598901685842835584	NGC2682	5646	4.63	+0.10	−0.02	+0.03	+0.04	+0.01	−0.14	+0.06	N	N
598901754562312448	NGC2682	5824	3.75	−0.13	+0.01	+0.08	+0.01	+0.02	+0.31	−0.07	Y	N
598903094592098944	NGC2682	5347	4.24	+0.00	+0.06	+0.04	+0.05	+0.07	−0.11	+0.10	N	N
598904434621914496	NGC2682	4985	4.50	−0.06	−0.06	−0.01	+0.02	+0.06	+0.06	+0.04	N	N
598907183400955648	NGC2682	5138	4.30	+0.07	−0.01	+0.02	+0.01	+0.04	+0.02	−0.01	N	N
598952400816572160	NGC2682	6323	4.69	+0.29	−0.04	+0.09	+0.03	+0.01	+0.50	−0.01	N	N
598955115237068032	NGC2682	4529	2.15	+0.18	+0.10	+0.04	+0.02	+0.04	−0.10	−0.06	Y	N
598955149595631872	NGC2682	5978	4.05	+0.03	−0.03	+0.07	−0.02	−0.03	−0.19	+0.00	Y	N
598955561913661440	NGC2682	5044	3.34	−0.30	+0.12	+0.05	+0.06	+0.06	−0.03	+0.13	N	N
598955596272229888	NGC2682	5980	4.12	−0.06	−0.08	+0.08	+0.12	−0.13	−0.35	−0.12	N	N
598955802430663680	NGC2682	5974	4.03	+0.00	−0.04	+0.09	+0.01	−0.02	+0.03	−0.01	Y	N
598959032246073216	NGC2682	4996	3.21	+0.03	+0.05	+0.02	+0.04	+0.05	+0.00	+0.04	Y	Y

Continued on next page

Table B.1 – Continued

Gaia ID	Cluster	T_{eff} (K)	log g (dex)	[Fe/H] (dex)	[Mg/Fe] (dex)	[Si/Fe] (dex)	[Ni/Fe] (dex)	[Ca/Fe] (dex)	[Na/Fe] (dex)	[V/Fe] (dex)	Member	Mass
598959100965548416	NGC2682	4981	3.36	−0.56	+0.32	+0.19	+0.11	+0.21	−0.04	+0.14	N	N
604701953276603520	NGC2682	6074	4.12	+0.04	−0.04	+0.08	−0.03	+0.00	−0.36	+0.02	Y	N
604703052788343296	NGC2682	5086	3.63	+0.04	+0.03	+0.02	+0.03	+0.04	+0.04	+0.07	Y	N
604703941846497280	NGC2682	6028	4.04	+0.03	−0.03	+0.08	−0.05	+0.00	−0.31	+0.01	Y	N
604704770775147520	NGC2682	4652	2.70	+0.08	+0.01	−0.01	+0.05	−0.01	+0.11	−0.11	Y	Y
604713463788946176	NGC2682	4699	2.62	+0.14	+0.07	+0.01	+0.00	+0.06	−0.06	−0.03	N	Y
604890038485174912	NGC2682	6001	4.13	+0.05	+0.00	+0.07	+0.06	−0.08	−0.19	−0.26	Y	N
604891550313644672	NGC2682	6055	4.14	+0.03	−0.03	+0.08	−0.03	+0.00	−0.38	+0.08	Y	N
604891584673389312	NGC2682	5919	3.83	+0.00	+0.00	+0.07	−0.08	+0.03	−0.28	+0.07	Y	N
604893165221336064	NGC2682	6019	3.97	+0.00	+0.00	+0.11	−0.06	−0.03	−0.32	+0.13	Y	N
604893646257664256	NGC2682	5796	4.85	+0.15	−0.02	+0.03	+0.04	+0.03	−0.36	+0.16	Y	N
604893676321680128	NGC2682	5945	3.87	−0.01	−0.03	+0.06	+0.01	+0.02	+0.14	−0.02	Y	N
604894638394355584	NGC2682	6191	4.14	−0.02	−0.02	+0.06	+0.00	+0.03	−0.43	+0.17	Y	N
604894707113832704	NGC2682	6039	4.27	+0.01	−0.03	+0.03	−0.02	+0.01	−0.94	−0.18	Y	N
604895364244625920	NGC2682	5956	4.03	+0.02	−0.01	+0.07	−0.03	+0.01	−0.32	+0.04	Y	N
604895639122534656	NGC2682	5151	4.13	+0.06	+0.09	+0.05	+0.06	+0.07	−0.14	+0.03	N	Y
604896150222841088	NGC2682	5987	4.28	+0.03	−0.02	+0.07	+0.00	−0.02	−0.41	−0.01	Y	N
604896395036758528	NGC2682	6080	3.98	+0.03	−0.04	+0.08	−0.03	−0.04	−0.10	+0.16	Y	N
604897288389928832	NGC2682	6036	4.07	+0.01	−0.03	+0.08	−0.02	−0.01	−0.39	−0.02	Y	N
604899453053404160	NGC2682	6172	4.28	+0.05	−0.08	+0.06	+0.01	−0.01	−0.61	−0.08	Y	N
604901308479244672	NGC2682	6028	4.42	+0.23	−0.02	+0.01	+0.02	+0.02	+0.07	−0.38	N	N
604901823875341056	NGC2682	5086	3.59	−0.04	+0.05	+0.03	+0.04	+0.04	+0.08	+0.06	Y	N
604903232624649344	NGC2682	6170	4.15	+0.05	−0.07	+0.08	−0.02	−0.01	−0.33	−0.06	Y	N
604903468852379904	NGC2682	5983	3.99	+0.01	−0.04	+0.09	−0.01	−0.02	−0.23	+0.00	Y	N
604904297776551680	NGC2682	5977	4.10	+0.00	−0.03	+0.08	+0.01	−0.01	−0.53	−0.07	Y	N
604904332136281856	NGC2682	6154	4.17	+0.07	−0.06	+0.08	−0.03	+0.00	−0.27	+0.01	Y	N

Continued on next page

Table B.1 – Continued

Gaia ID	Cluster	T_{eff} (K)	log g (dex)	[Fe/H] (dex)	[Mg/Fe] (dex)	[Si/Fe] (dex)	[Ni/Fe] (dex)	[Ca/Fe] (dex)	[Na/Fe] (dex)	[V/Fe] (dex)	Member	Mass
604904469575229696	NGC2682	6069	4.08	+0.03	−0.04	+0.08	−0.01	−0.02	−0.27	−0.01	Y	N
604905156769963136	NGC2682	4763	2.68	+0.04	+0.03	+0.01	+0.05	−0.02	+0.12	−0.17	Y	Y
604905500367349888	NGC2682	5337	3.73	−0.08	+0.04	+0.01	+0.06	+0.03	+0.01	+0.15	Y	N
604906428080283776	NGC2682	6026	4.43	+0.06	−0.02	+0.07	−0.02	−0.02	−0.26	+0.06	Y	N
604907390153062272	NGC2682	4794	2.81	−0.01	+0.04	+0.03	+0.05	−0.01	+0.07	+0.06	Y	Y
604908146067299712	NGC2682	5992	3.99	+0.00	+0.00	+0.08	−0.02	+0.00	−0.22	−0.05	Y	N
604908347929907328	NGC2682	5915	4.09	−0.06	−0.01	+0.06	−0.03	+0.00	−0.67	+0.01	Y	N
604908863325982976	NGC2682	6040	4.23	+0.12	+0.00	+0.12	+0.03	+0.01	+0.05	+0.08	Y	N
604909000764935936	NGC2682	5939	4.04	−0.01	−0.02	+0.05	−0.03	+0.01	−0.31	+0.27	Y	N
604909657895767680	NGC2682	6034	4.24	+0.03	−0.02	+0.07	+0.00	−0.01	−0.42	+0.11	Y	N
604909726615246336	NGC2682	6022	4.12	+0.10	+0.01	+0.07	+0.02	+0.02	+0.03	−0.23	Y	N
604910001493155584	NGC2682	5671	3.88	+0.02	+0.00	+0.06	+0.00	+0.02	−0.34	+0.04	Y	N
604910546953207680	NGC2682	6090	4.10	+0.05	−0.03	+0.09	−0.03	+0.00	−0.23	−0.01	Y	N
604910860486613632	NGC2682	6138	4.47	+0.11	−0.07	+0.05	+0.01	−0.01	−0.64	−0.06	Y	N
604911375882674176	NGC2682	6057	4.07	+0.04	−0.08	+0.03	−0.02	+0.00	+0.09	−0.06	Y	N
604911749544005632	NGC2682	5968	3.92	+0.02	−0.01	+0.12	+0.00	−0.03	−0.10	−0.01	Y	N
604912406674856064	NGC2682	5946	4.22	+0.05	−0.09	+0.07	−0.02	+0.03	+0.05	+0.31	Y	N
604912647193030016	NGC2682	5006	3.38	−0.07	+0.06	+0.02	+0.05	+0.02	+0.06	+0.07	Y	N
604912715912500480	NGC2682	5130	3.30	−0.53	+0.26	+0.16	+0.09	+0.19	+0.13	+0.17	N	N
604913093869450112	NGC2682	5749	3.93	−0.02	−0.05	+0.07	−0.03	+0.03	+0.26	+0.06	N	N
604913952863074688	NGC2682	5722	4.33	−0.07	+0.02	+0.04	+0.06	+0.02	−0.16	+0.23	Y	N
604914021582551168	NGC2682	5910	4.20	+0.06	−0.05	+0.06	+0.04	−0.01	−0.17	+0.05	Y	N
604914468259140224	NGC2682	6052	3.90	+0.07	−0.03	+0.11	+0.03	+0.04	−0.24	−0.05	Y	N
604914601402325504	NGC2682	5040	3.60	+0.02	+0.05	+0.03	+0.03	+0.04	−0.19	+0.06	Y	N
604914708777297280	NGC2682	5987	4.03	−0.02	−0.04	+0.07	−0.01	−0.06	−0.10	−0.11	Y	N
604914807560715776	NGC2682	5891	4.03	+0.02	+0.00	+0.06	+0.02	+0.06	+0.58	−0.04	Y	N

Continued on next page

Table B.1 – Continued

Gaia ID	Cluster	T_{eff} (K)	log g (dex)	[Fe/H] (dex)	[Mg/Fe] (dex)	[Si/Fe] (dex)	[Ni/Fe] (dex)	[Ca/Fe] (dex)	[Na/Fe] (dex)	[V/Fe] (dex)	Member	Mass
604914983655018496	NGC2682	5825	4.04	+0.00	+0.01	+0.02	+0.04	−0.05	−0.01	−0.10	Y	N
604915189813463808	NGC2682	6018	4.26	+0.06	−0.04	+0.07	+0.02	+0.01	+0.07	+0.03	Y	N
604915705209528320	NGC2682	5870	4.03	−0.02	+0.00	+0.06	+0.04	−0.04	+0.11	−0.07	Y	N
604916701642080000	NGC2682	5955	4.21	−0.01	−0.06	+0.06	−0.05	−0.06	−0.07	+0.23	Y	N
604916873440769152	NGC2682	4841	2.99	+0.01	+0.04	+0.02	+0.04	+0.02	+0.17	−0.06	Y	N
604917217038188288	NGC2682	4792	2.89	+0.03	+0.03	+0.01	+0.05	+0.01	+0.13	−0.06	Y	N
604917281461920256	NGC2682	6036	3.96	−0.05	−0.06	+0.08	+0.03	−0.04	-1.00	-1.01	Y	N
604917320117398528	NGC2682	5429	3.83	+0.04	−0.02	−0.02	+0.03	+0.07	−0.10	+0.06	Y	N
604917388836860544	NGC2682	5922	3.88	−0.01	−0.01	+0.10	+0.02	−0.01	−0.09	−0.07	Y	N
604917560635577472	NGC2682	6057	4.05	+0.03	−0.06	+0.11	−0.04	−0.04	−0.21	−0.11	Y	N
604917831217725312	NGC2682	6003	4.05	+0.04	−0.05	+0.05	−0.07	+0.00	−0.28	+0.02	Y	N
604917831217881728	NGC2682	5987	3.94	−0.02	−0.06	+0.09	−0.04	+0.00	−0.61	−0.51	Y	N
604917934296936704	NGC2682	4835	2.75	−0.07	+0.04	+0.04	+0.02	−0.01	+0.13	−0.03	Y	N
604919239966985984	NGC2682	6017	3.97	+0.04	−0.04	+0.14	+0.02	−0.07	−0.17	+0.04	Y	N
604919450421136000	NGC2682	5820	4.01	−0.04	−0.02	+0.03	+0.02	−0.02	−0.18	+0.15	Y	N
604920584292552832	NGC2682	5910	3.94	−0.07	−0.06	+0.05	+0.02	−0.02	−0.52	−0.46	Y	N
604920957953908864	NGC2682	6089	4.09	+0.00	−0.02	+0.05	−0.03	−0.04	−0.11	−0.05	Y	N
604921374566321920	NGC2682	6142	4.36	+0.13	−0.10	+0.03	+0.04	+0.00	−0.16	+0.08	Y	N
604921679508385664	NGC2682	5953	4.51	+0.12	−0.05	+0.03	+0.08	+0.04	−0.14	+0.13	Y	N
604921988746029312	NGC2682	5877	4.05	+0.00	+0.04	+0.07	+0.04	+0.00	+0.27	−0.10	Y	N
604922164840316672	NGC2682	4713	2.56	+0.02	+0.06	+0.04	+0.01	−0.05	+0.16	−0.24	Y	N
604922302279259008	NGC2682	5754	3.96	+0.02	+0.03	+0.03	+0.02	−0.03	−0.03	−0.04	Y	N
604922886394972160	NGC2682	6120	3.96	+0.01	−0.06	+0.09	−0.05	−0.03	+0.12	+0.11	Y	N
604923367432823808	NGC2682	4760	2.66	+0.05	+0.03	+0.03	+0.00	−0.03	+0.17	−0.19	Y	N
604923470510324224	NGC2682	5088	3.65	−0.07	+0.11	+0.04	+0.08	+0.07	+0.13	+0.13	Y	N
604924290848519168	NGC2682	4919	2.99	−0.18	+0.10	+0.05	+0.04	+0.00	+0.13	−0.04	Y	N

Continued on next page

Table B.1 – Continued

Gaia ID	Cluster	T_{eff} (K)	log g (dex)	[Fe/H] (dex)	[Mg/Fe] (dex)	[Si/Fe] (dex)	[Ni/Fe] (dex)	[Ca/Fe] (dex)	[Na/Fe] (dex)	[V/Fe] (dex)	Member	Mass
604924393927734528	NGC2682	5521	3.68	−0.03	+0.04	+0.03	+0.02	−0.01	+0.05	−0.03	Y	N
604931064012660992	NGC2682	6040	4.11	+0.05	−0.06	+0.08	−0.01	−0.06	−0.09	+0.04	Y	N
604931132732290944	NGC2682	5981	4.18	+0.05	−0.03	+0.06	+0.03	−0.05	+0.09	−0.05	Y	N
604931476329520000	NGC2682	4896	4.22	+0.13	+0.04	+0.02	+0.02	+0.04	+0.01	−0.12	N	N
604933125596954240	NGC2682	5914	4.17	+0.03	−0.03	+0.07	+0.02	−0.04	−0.16	+0.06	Y	N
604942505805554176	NGC2682	5568	3.99	+0.03	−0.01	−0.02	+0.07	+0.05	−0.03	+0.15	Y	N
604943227360042240	NGC2682	6098	3.97	−0.01	−0.03	+0.11	+0.02	+0.00	+0.10	−0.08	Y	N
604946835132357120	NGC2682	6006	4.08	+0.01	−0.04	+0.06	+0.00	−0.04	−0.15	+0.02	Y	N
604946972571361152	NGC2682	6121	4.07	−0.02	−0.05	+0.08	−0.01	+0.00	−0.70	+0.04	Y	N
604948381320634880	NGC2682	6092	4.19	+0.01	−0.04	+0.02	+0.03	−0.04	−0.14	−0.03	N	N
604948724917993088	NGC2682	6056	4.17	+0.05	−0.04	+0.05	+0.03	−0.06	−0.05	−0.13	Y	N
604948965436170112	NGC2682	5957	4.07	+0.02	−0.02	+0.06	+0.03	−0.05	+0.05	−0.14	Y	N
604949034155646592	NGC2682	6062	4.27	+0.17	−0.06	+0.05	+0.07	+0.02	−0.06	+0.19	Y	N
604949171593589120	NGC2682	5868	4.91	+0.35	−0.10	−0.04	+0.06	−0.01	+0.51	−0.12	N	N
604961163143414912	NGC2682	6009	4.10	+0.01	−0.04	+0.07	+0.03	−0.04	−0.14	−0.07	Y	N
604962193935568896	NGC2682	3985	1.36	−0.06	+0.00	+0.01	+0.04	−0.10	+0.09	−0.10	Y	N
604962640612163200	NGC2682	5884	4.50	+0.06	−0.03	+0.03	+0.09	+0.05	−0.18	+0.15	Y	N
604962984209526400	NGC2682	5751	3.79	−0.06	+0.02	+0.04	+0.05	−0.04	+0.03	−0.09	Y	N
604964904059073024	NGC2682	5103	3.12	−0.11	+0.06	+0.00	+0.03	+0.00	−0.08	+0.17	Y	Y
604965664269158656	NGC2682	4476	1.92	+0.18	+0.11	+0.03	+0.03	+0.01	−0.08	+0.00	Y	N
604966076586017024	NGC2682	4636	2.11	−0.15	+0.06	+0.08	+0.02	−0.07	−0.03	+0.00	N	N
604967244817098240	NGC2682	4894	2.47	−0.02	+0.09	+0.06	+0.03	+0.03	−0.09	+0.18	Y	Y
604967996435524224	NGC2682	5977	4.16	+0.03	+0.01	+0.05	+0.06	−0.05	−0.04	−0.30	Y	N
604968413048207488	NGC2682	4873	2.91	+0.05	+0.09	+0.02	+0.02	+0.07	−0.13	−0.02	Y	Y
604969748782357888	NGC2682	5958	4.11	−0.05	−0.01	+0.01	+0.07	−0.01	−0.26	+0.06	Y	N
604969783142095744	NGC2682	5906	4.11	−0.02	+0.01	+0.01	+0.06	−0.05	−0.09	−0.09	Y	N

Continued on next page

Table B.1 – Continued

Gaia ID	Cluster	T_{eff} (K)	log g (dex)	[Fe/H] (dex)	[Mg/Fe] (dex)	[Si/Fe] (dex)	[Ni/Fe] (dex)	[Ca/Fe] (dex)	[Na/Fe] (dex)	[V/Fe] (dex)	Member	Mass
604972226979105664	NGC2682	4952	3.69	−0.10	+0.14	+0.03	+0.07	+0.05	+0.21	−0.11	N	N
604972944238043904	NGC2682	5943	4.63	+0.22	−0.06	+0.05	+0.05	+0.03	−0.03	+0.22	Y	N
604973085972551296	NGC2682	6004	4.26	+0.09	+0.00	+0.03	+0.06	−0.08	+0.26	−0.02	Y	N
604973635728426752	NGC2682	6357	4.06	+0.20	−0.04	+0.14	+0.00	+0.04	+0.06	+0.10	Y	N
604974632160829312	NGC2682	4968	3.63	−0.34	+0.24	+0.10	+0.10	+0.14	+0.07	+0.03	N	N
604977037342478592	NGC2682	3946	1.00	−0.20	+0.08	+0.06	+0.03	−0.11	+0.11	+0.09	N	N
604977071702225280	NGC2682	5873	3.93	−0.03	−0.02	+0.01	−0.01	−0.06	−0.03	−0.29	Y	N
604978102494447744	NGC2682	4915	2.99	+0.09	+0.07	−0.02	+0.01	+0.07	−0.02	−0.05	N	Y
604978858408693888	NGC2682	6064	4.65	+0.00	−0.03	+0.08	+0.02	−0.03	−0.19	+0.02	Y	N
604979987984213632	NGC2682	6078	4.11	+0.07	−0.02	+0.08	+0.05	−0.11	+0.05	−0.45	Y	N
604981607187745792	NGC2682	6040	4.15	+0.01	−0.04	+0.04	+0.03	−0.04	−0.08	−0.07	Y	N
604984871362889728	NGC2682	4996	4.21	+0.07	+0.03	+0.01	+0.04	+0.03	−0.04	−0.12	N	N
604988680998017536	NGC2682	5241	3.79	−0.59	+0.37	+0.19	+0.15	+0.18	+0.35	+0.04	N	N
604989372488540416	NGC2682	5653	3.89	−0.06	+0.03	+0.01	+0.07	−0.03	−0.10	−0.05	Y	N
604989677430427776	NGC2682	4886	3.67	+0.08	+0.06	+0.05	+0.02	+0.02	+0.18	−0.24	N	Y
604996068341455744	NGC2682	6036	4.15	+0.00	−0.02	+0.02	+0.04	−0.06	−0.05	−0.15	N	N
604997206508853632	NGC2682	6268	4.39	+0.08	−0.10	+0.03	+0.04	+0.04	−0.33	+0.14	Y	N
605000092726888192	NGC2682	6036	4.56	+0.29	−0.04	−0.01	+0.02	−0.06	+0.43	−0.14	N	N
605003185103316352	NGC2682	6061	4.15	+0.04	−0.05	+0.01	+0.01	−0.03	−0.15	−0.05	N	N
605004078456479360	NGC2682	5797	3.98	+0.09	−0.02	+0.01	+0.01	−0.04	−0.08	−0.10	N	N
661199842876628736	NGC2632A	4897	3.03	+0.09	+0.09	+0.00	+0.01	+0.09	−0.05	+0.01	Y	Y
661199842876628736	NGC2632B	4659	2.59	+0.05	+0.10	+0.04	+0.01	+0.06	−0.09	−0.08	N	N
661200083394793216	NGC2632A	6391	4.38	+0.08	−0.13	+0.04	−0.01	+0.01	−0.27	−0.02	N	N
661200083396357248	NGC2632A	6133	4.37	+0.17	−0.10	+0.04	+0.01	−0.02	−0.18	−0.01	Y	N
661200083396357248	NGC2632B	6042	4.36	+0.12	−0.06	+0.05	+0.00	−0.02	−0.42	+0.04	Y	N
661200388334061824	NGC2632B	5954	4.04	+0.07	−0.05	+0.07	+0.01	−0.02	−0.48	−0.14	N	N

Continued on next page

Table B.1 – Continued

Gaia ID	Cluster	T_{eff} (K)	log g (dex)	[Fe/H] (dex)	[Mg/Fe] (dex)	[Si/Fe] (dex)	[Ni/Fe] (dex)	[Ca/Fe] (dex)	[Na/Fe] (dex)	[V/Fe] (dex)	Member	Mass
661202003241762176	NGC2632B	6170	4.15	+0.04	−0.06	+0.08	−0.05	+0.00	−0.31	+0.05	N	N
661205306075038080	NGC2632B	6125	4.29	+0.06	−0.06	+0.06	+0.00	−0.01	−0.63	+0.02	N	N
661206577385260800	NGC2632A	6438	4.21	+0.17	−0.12	+0.09	−0.04	+0.01	−0.11	+0.07	Y	N
661209566682500736	NGC2632B	5895	5.40	+0.29	−0.04	+0.03	+0.04	+0.02	−0.14	+0.05	Y	N
661210253877269248	NGC2632B	5287	3.84	−0.10	+0.05	+0.03	+0.04	+0.05	−0.19	+0.18	N	N
661210666194127360	NGC2632B	4706	4.34	+0.13	+0.05	+0.00	+0.02	+0.04	−0.03	−0.15	Y	N
661211147230556160	NGC2632B	4707	4.04	+0.04	+0.08	+0.00	+0.04	+0.06	−0.20	−0.07	Y	N
661211727047722752	NGC2632B	4909	3.93	+0.10	+0.01	+0.00	+0.04	+0.03	−0.43	+0.00	Y	N
661212452900513536	NGC2632B	5976	4.16	+0.04	−0.05	+0.05	+0.00	−0.01	−0.57	+0.03	N	N
661212933936844416	NGC2632A	5951	4.42	+0.21	−0.10	+0.01	+0.03	+0.00	−0.12	−0.02	Y	N
661212933936844416	NGC2632B	5736	4.42	+0.15	−0.05	+0.02	+0.01	+0.00	−0.46	+0.08	Y	N
661213238876208128	NGC2632B	5614	4.16	+0.07	−0.03	+0.02	+0.02	+0.01	−0.37	+0.11	N	N
661215270399043840	NGC2632B	5323	4.01	+0.07	−0.01	+0.01	+0.04	+0.03	−0.18	+0.11	N	N
661216369910684544	NGC2632A	6224	4.44	+0.26	−0.15	+0.00	+0.00	−0.03	+0.05	−0.09	Y	N
661216743570426240	NGC2632A	6261	4.36	+0.19	−0.13	+0.04	+0.00	−0.01	−0.08	−0.02	Y	N
661216816587286912	NGC2632B	5171	3.56	−0.30	+0.11	+0.06	+0.06	+0.09	−0.06	+0.24	N	N
661217258966500480	NGC2632B	5181	3.96	+0.06	+0.01	+0.02	+0.03	+0.03	−0.25	+0.02	N	N
661224577591160448	NGC2632A	6221	4.27	+0.19	−0.10	+0.07	+0.00	−0.01	−0.11	+0.02	Y	N
661224577591160448	NGC2632B	6183	4.16	+0.14	−0.09	+0.08	−0.01	−0.01	−0.22	−0.10	Y	N
661225234723252224	NGC2632B	4356	1.95	−0.13	+0.20	+0.10	+0.05	+0.07	−0.26	−0.06	N	N
661227639904931200	NGC2632B	5156	3.30	−0.24	+0.08	+0.04	+0.05	+0.06	−0.04	+0.20	Y	Y
661227674266243456	NGC2632B	6132	4.13	+0.04	−0.07	+0.07	−0.02	−0.02	−0.43	−0.11	N	N
661228189660736768	NGC2632B	6059	4.10	+0.05	−0.07	+0.07	+0.00	−0.02	−0.46	−0.11	N	N
661234473194513664	NGC2632B	4745	4.26	+0.14	+0.04	+0.01	+0.02	+0.03	+0.06	−0.11	Y	N
661237737369661952	NGC2632B	6105	4.16	+0.12	−0.07	+0.07	−0.02	−0.02	−0.29	−0.09	N	N
661238635021126656	NGC2632B	6225	5.34	+0.31	−0.10	+0.03	+0.00	−0.02	−0.13	+0.04	Y	N

Continued on next page

Table B.1 – Continued

Gaia ID	Cluster	T_{eff} (K)	log g (dex)	[Fe/H] (dex)	[Mg/Fe] (dex)	[Si/Fe] (dex)	[Ni/Fe] (dex)	[Ca/Fe] (dex)	[Na/Fe] (dex)	[V/Fe] (dex)	Member	Mass
661239390935360512	NGC2632B	5059	4.35	+0.17	+0.00	+0.01	+0.02	+0.02	+0.02	−0.06	Y	N
661241486881063680	NGC2632B	4993	3.38	−0.31	+0.16	+0.08	+0.06	+0.10	+0.01	+0.19	N	N
661242689470244224	NGC2632B	5830	3.98	+0.09	−0.03	+0.06	+0.04	−0.01	−0.10	−0.08	N	N
661242895630246016	NGC2632A	6266	4.29	+0.20	−0.11	+0.07	−0.01	−0.01	−0.12	+0.02	Y	N
661243273585807872	NGC2632A	5976	4.31	+0.19	−0.08	+0.05	+0.03	+0.00	−0.20	−0.01	Y	N
661243411024757760	NGC2632B	6176	4.19	+0.05	−0.07	+0.06	−0.07	+0.00	−0.30	+0.00	N	N
661244338737678336	NGC2632B	5866	3.89	+0.06	−0.03	+0.08	+0.03	−0.01	−0.25	−0.12	N	N
661245232090878208	NGC2632B	5128	3.89	−0.06	+0.06	+0.01	+0.06	+0.06	+0.06	+0.09	N	N
661245506968786304	NGC2632A	5291	3.51	+0.04	+0.05	+0.02	+0.02	+0.06	−0.10	+0.02	N	N
661245919285629312	NGC2632B	5213	3.78	+0.06	+0.00	+0.01	+0.04	+0.03	+0.09	−0.01	N	N
661247426815874560	NGC2632B	6047	4.09	+0.07	−0.07	+0.07	+0.00	−0.01	−0.39	−0.08	N	N
661247976571685888	NGC2632B	5115	3.29	−0.13	+0.05	+0.00	+0.04	+0.03	−0.11	+0.14	Y	Y
661251210685333120	NGC2632B	6177	5.37	+0.30	−0.09	+0.03	+0.02	−0.01	−0.09	+0.05	Y	N
661251966599576576	NGC2632B	4828	4.52	+0.20	+0.02	+0.01	+0.01	+0.02	+0.12	−0.17	Y	N
661252997391718272	NGC2632A	6136	4.29	+0.12	−0.08	+0.06	+0.02	+0.00	−0.32	+0.02	Y	N
661253027453650432	NGC2632B	6326	5.09	+0.20	−0.10	+0.05	+0.00	−0.01	−0.76	−0.06	Y	N
661253237909888640	NGC2632A	4938	2.94	+0.05	+0.08	+0.01	+0.00	+0.09	−0.10	+0.04	N	N
661254131263080832	NGC2632B	6222	4.31	+0.11	−0.10	+0.05	+0.03	+0.00	−0.22	+0.01	N	N
661254440500722176	NGC2632B	4897	2.89	+0.02	+0.04	−0.02	+0.03	−0.01	−0.02	+0.08	Y	Y
661257154920147072	NGC2632B	6280	5.19	+0.23	−0.10	+0.04	+0.00	−0.01	−0.65	−0.02	Y	N
661257704675956480	NGC2632B	6336	5.15	+0.16	−0.09	+0.05	+0.00	−0.01	−0.96	−0.04	Y	N
661258872906952320	NGC2632B	5048	4.56	+0.20	+0.00	+0.02	+0.00	+0.02	+0.10	−0.10	Y	N
661259079065485440	NGC2632B	5912	4.08	+0.11	−0.04	+0.07	+0.03	−0.01	−0.12	−0.04	N	N
661260144217277568	NGC2632B	6360	4.76	+0.10	−0.09	+0.07	−0.06	+0.00	−0.46	−0.08	N	N
661260316015969920	NGC2632B	6185	4.20	+0.08	−0.08	+0.06	−0.04	+0.00	−0.20	−0.01	N	N
661262515039216000	NGC2632B	5034	3.87	−0.08	+0.07	+0.03	+0.05	+0.06	−0.08	+0.07	N	N

Continued on next page

Table B.1 – Continued

Gaia ID	Cluster	T_{eff} (K)	log g (dex)	[Fe/H] (dex)	[Mg/Fe] (dex)	[Si/Fe] (dex)	[Ni/Fe] (dex)	[Ca/Fe] (dex)	[Na/Fe] (dex)	[V/Fe] (dex)	Member	Mass
661263305313199360	NGC2632B	4691	4.30	+0.12	+0.05	+0.00	+0.02	+0.04	−0.03	−0.14	Y	N
661264439184662016	NGC2632A	6078	4.42	+0.22	−0.11	+0.03	+0.02	+0.00	−0.08	−0.04	Y	N
661264679702825600	NGC2632B	6202	4.42	+0.15	−0.06	+0.03	−0.05	−0.01	−0.21	−0.14	N	N
661266633909627264	NGC2632B	6353	4.28	+0.11	−0.11	+0.06	−0.03	+0.00	−0.10	+0.02	N	N
661270245980334464	NGC2632B	6205	4.15	+0.04	−0.07	+0.07	−0.04	−0.01	−0.28	−0.01	N	N
661270486498500352	NGC2632B	4376	2.24	−0.04	+0.10	−0.04	−0.02	+0.09	+0.19	+0.21	Y	N
661270795736143872	NGC2632B	6145	4.19	+0.10	−0.08	+0.06	−0.01	−0.01	−0.08	+0.00	N	N
661271620369865344	NGC2632B	5090	3.63	−0.20	+0.09	+0.03	+0.06	+0.06	−0.03	+0.17	N	N
661271826528291072	NGC2632B	4715	3.32	−0.32	+0.29	+0.12	+0.09	+0.16	−0.13	+0.06	N	N
661272032686720896	NGC2632B	5884	4.32	+0.13	−0.06	+0.04	+0.01	−0.01	−0.52	+0.02	N	N
661272548082791936	NGC2632B	5272	3.74	−0.16	+0.08	+0.04	+0.06	+0.06	+0.00	+0.15	N	N
661273368419254144	NGC2632B	5353	3.80	−0.01	+0.01	+0.02	+0.04	+0.04	+0.02	+0.07	N	N
661276293294303744	NGC2632B	5028	3.23	−0.42	+0.19	+0.10	+0.07	+0.12	+0.05	+0.18	N	N
661276739971003264	NGC2632B	5823	3.91	+0.11	−0.04	+0.08	+0.03	−0.02	−0.06	−0.04	N	N
661280171647443968	NGC2632B	6355	4.29	+0.11	−0.12	+0.06	−0.03	+0.01	−0.16	−0.02	N	N
661281309816022784	NGC2632B	4802	4.32	+0.12	+0.03	+0.01	+0.01	+0.03	+0.08	−0.11	N	N
661282031370596608	NGC2632B	4713	4.42	+0.17	+0.03	+0.01	+0.01	+0.03	+0.10	−0.15	Y	N
661283199601699328	NGC2632B	4615	4.28	+0.15	+0.05	+0.00	+0.02	+0.03	+0.08	−0.17	Y	N
661283405760129792	NGC2632B	6071	4.19	+0.08	−0.07	+0.06	+0.01	−0.02	−0.40	−0.08	N	N
661283573261540608	NGC2632B	4743	4.39	+0.16	+0.03	+0.01	+0.01	+0.03	+0.13	−0.13	N	N
661284608350960768	NGC2632B	4827	4.22	+0.12	+0.03	+0.01	+0.01	+0.03	+0.07	−0.11	N	N
661287082252140160	NGC2632B	5132	3.29	−0.11	+0.06	+0.01	+0.03	+0.01	−0.09	+0.14	N	N
661287284113283840	NGC2632B	5284	3.54	−0.09	+0.04	+0.01	+0.02	+0.02	−0.12	+0.23	N	N
661287387192498688	NGC2632B	5904	4.01	+0.12	−0.06	+0.07	+0.02	−0.02	−0.24	−0.09	N	N
661287563288471296	NGC2632A	6041	4.17	+0.04	−0.07	+0.03	−0.01	+0.00	+0.04	−0.07	N	N
661287563288471296	NGC2632B	6078	4.09	+0.09	−0.06	+0.08	+0.01	−0.01	−0.14	−0.04	N	N

Continued on next page

Table B.1 – Continued

Gaia ID	Cluster	T_{eff} (K)	log g (dex)	[Fe/H] (dex)	[Mg/Fe] (dex)	[Si/Fe] (dex)	[Ni/Fe] (dex)	[Ca/Fe] (dex)	[Na/Fe] (dex)	[V/Fe] (dex)	Member	Mass
661288903318257536	NGC2632B	6174	4.15	+0.09	−0.10	+0.08	−0.02	−0.04	−0.10	−0.01	N	N
661289315635121152	NGC2632B	5081	3.69	−0.12	+0.09	+0.02	+0.07	+0.04	+0.03	+0.07	N	N
661289521793490944	NGC2632B	6144	4.08	+0.10	−0.08	+0.10	+0.00	−0.03	−0.03	+0.07	N	N
661290071549304320	NGC2632B	4963	3.27	−0.24	+0.16	+0.06	+0.07	+0.09	+0.15	−0.03	N	N
661290964902652672	NGC2632B	6164	4.22	+0.11	−0.09	+0.07	−0.03	−0.02	−0.32	−0.06	N	N
661293537585522816	NGC2632A	5841	4.55	+0.24	−0.08	+0.02	+0.04	+0.00	−0.17	−0.03	Y	N
661293537585522816	NGC2632B	5645	4.45	+0.20	−0.06	+0.01	+0.03	+0.00	−0.18	+0.05	Y	N
661293812462666240	NGC2632B	5186	4.60	+0.20	−0.01	+0.01	+0.02	+0.01	+0.11	−0.09	Y	N
661294052980833792	NGC2632B	4805	4.39	+0.17	+0.02	+0.01	+0.01	+0.02	+0.13	−0.16	Y	N
661294332158553856	NGC2632A	5918	4.55	+0.23	−0.09	+0.01	+0.04	+0.01	−0.12	−0.02	Y	N
661294332158553856	NGC2632B	5939	4.28	+0.22	−0.09	+0.04	+0.03	−0.03	−0.17	−0.07	Y	N
661295156790633344	NGC2632B	4631	3.55	−0.17	+0.15	+0.03	+0.05	+0.11	−0.19	+0.03	N	N
661295324291154816	NGC2632B	5307	4.47	+0.16	−0.02	+0.01	+0.04	+0.02	−0.50	−0.02	Y	N
661295461730107392	NGC2632A	6224	4.35	+0.14	−0.12	+0.02	−0.01	+0.00	−0.04	−0.04	Y	N
661295702248275328	NGC2632B	4941	3.42	+0.06	+0.08	+0.03	+0.02	−0.01	+0.28	−0.27	N	N
661297115295806592	NGC2632B	6169	4.29	+0.22	−0.10	+0.05	+0.04	−0.03	−0.03	−0.03	Y	N
661297458893183232	NGC2632B	5941	5.13	+0.28	−0.07	+0.02	+0.04	+0.01	+0.10	+0.04	Y	N
661298833282624000	NGC2632B	6269	5.12	+0.27	−0.06	+0.03	+0.02	−0.02	+0.19	−0.13	Y	N
661298936361837184	NGC2632B	6246	4.22	−0.02	−0.06	+0.05	−0.04	−0.02	−0.17	−0.06	N	N
661300929226743936	NGC2632B	4841	3.51	−0.23	+0.18	+0.06	+0.07	+0.08	+0.06	+0.04	N	N
661301444622810368	NGC2632A	5957	4.41	+0.18	−0.08	+0.04	+0.02	+0.00	−0.25	−0.04	N	N
661301444622810368	NGC2632B	5943	4.07	+0.18	−0.08	+0.07	+0.04	−0.04	−0.07	−0.08	N	N
661301616421508608	NGC2632B	5771	4.12	+0.12	−0.06	+0.00	+0.02	+0.00	+0.23	−0.13	N	N
661302887731820416	NGC2632B	5455	4.30	+0.16	−0.05	+0.00	+0.04	+0.01	+0.13	−0.08	Y	N
661304296481106048	NGC2632B	6202	4.30	+0.07	−0.10	+0.03	+0.00	−0.05	−0.21	−0.21	N	N
661305361632896512	NGC2632B	5654	3.84	+0.06	+0.01	+0.01	+0.03	−0.03	+0.08	−0.22	N	N

Continued on next page

Table B.1 – Continued

Gaia ID	Cluster	T_{eff} (K)	log g (dex)	[Fe/H] (dex)	[Mg/Fe] (dex)	[Si/Fe] (dex)	[Ni/Fe] (dex)	[Ca/Fe] (dex)	[Na/Fe] (dex)	[V/Fe] (dex)	Member	Mass
661306529864082944	NGC2632B	5921	3.90	−0.04	−0.04	+0.06	−0.06	−0.02	−0.18	−0.11	N	N
661306907821119488	NGC2632B	5237	3.50	−0.01	+0.06	+0.00	+0.04	−0.02	+0.02	−0.06	N	N
661307904253568256	NGC2632B	4923	4.01	+0.07	+0.03	+0.02	+0.02	+0.02	+0.15	−0.10	N	N
661307934315134720	NGC2632B	6179	4.15	+0.07	−0.08	+0.07	−0.01	−0.01	−0.25	−0.04	N	N
661309587880745088	NGC2632B	5789	3.84	−0.01	−0.03	+0.02	−0.02	−0.03	−0.07	+0.00	N	N
661310068917076992	NGC2632B	6021	4.17	+0.11	−0.08	−0.02	−0.02	−0.02	−0.02	−0.12	N	N
661310309435240704	NGC2632B	4938	3.60	−0.19	+0.17	+0.06	+0.09	+0.09	+0.24	−0.07	N	N
661310756111835392	NGC2632B	4737	4.26	+0.11	+0.04	+0.03	+0.00	+0.02	+0.19	−0.22	Y	N
661310790473154560	NGC2632A	5949	4.48	+0.19	−0.08	+0.03	+0.05	+0.02	−0.23	−0.04	N	N
661311713886346752	NGC2632B	6286	4.42	+0.07	−0.13	+0.02	+0.03	+0.02	−0.47	+0.09	N	N
661311752544249088	NGC2632A	6231	4.33	+0.11	−0.12	+0.01	−0.02	+0.01	−0.02	−0.13	Y	N
661311889983198208	NGC2632B	6083	5.11	+0.23	−0.07	+0.03	+0.08	+0.02	+0.04	+0.02	N	N
661313191355096448	NGC2632B	4367	1.99	+0.26	+0.09	+0.01	+0.03	+0.02	−0.08	−0.07	Y	Y
661313917207778304	NGC2632B	6349	5.03	+0.24	−0.08	+0.04	+0.01	−0.03	+0.05	−0.17	Y	N
661314570042801280	NGC2632B	4350	2.37	−0.08	+0.13	−0.05	+0.00	+0.07	+0.14	−0.11	Y	N
661318624491908480	NGC2632B	4764	3.80	+0.08	+0.06	+0.02	+0.01	+0.01	+0.21	−0.22	N	N
661319341748259072	NGC2632B	4627	3.93	+0.06	+0.06	+0.02	+0.00	+0.03	+0.10	−0.19	N	N
661319483485360000	NGC2632A	5874	4.55	+0.22	−0.08	+0.02	+0.05	+0.01	−0.21	−0.08	Y	N
661319998881439232	NGC2632B	5606	3.85	+0.01	+0.01	+0.00	+0.06	−0.03	−0.08	+0.01	N	N
661320548637246848	NGC2632B	6097	4.11	−0.01	−0.06	+0.06	−0.02	−0.05	−0.09	−0.16	N	N
661320960954104448	NGC2632B	5451	3.68	+0.02	+0.01	−0.02	+0.03	−0.03	−0.07	+0.05	N	N
661321304551598464	NGC2632B	5547	3.67	−0.03	+0.03	+0.02	−0.01	−0.05	+0.03	−0.18	N	N
661322335343655424	NGC2632B	6242	4.43	+0.15	−0.11	+0.02	+0.05	+0.01	−0.33	+0.15	N	N
661344188136057984	NGC2632A	6299	4.39	+0.16	−0.14	+0.02	−0.01	+0.00	−0.04	−0.04	Y	N
661344600452915328	NGC2632A	6095	4.26	+0.12	−0.08	+0.05	+0.01	+0.01	−0.16	+0.00	N	N
661347727189029504	NGC2632B	6299	4.84	+0.23	−0.07	+0.03	−0.02	−0.01	+0.07	−0.14	Y	N

Continued on next page

Table B.1 – Continued

Gaia ID	Cluster	T_{eff} (K)	log g (dex)	[Fe/H] (dex)	[Mg/Fe] (dex)	[Si/Fe] (dex)	[Ni/Fe] (dex)	[Ca/Fe] (dex)	[Na/Fe] (dex)	[V/Fe] (dex)	Member	Mass
661397342651227776	NGC2632B	4871	3.56	−0.18	+0.17	+0.05	+0.07	+0.09	+0.06	+0.03	N	N
661397445730441344	NGC2632B	5962	4.12	+0.08	−0.05	+0.03	+0.02	−0.03	+0.14	−0.16	N	N
661401122222444288	NGC2632A	5967	4.48	+0.20	−0.09	+0.04	+0.04	+0.00	−0.37	−0.05	Y	N
664292322407994624	NGC2632B	6247	5.38	+0.30	−0.09	+0.04	+0.01	−0.01	+0.03	+0.00	Y	N
664292322407996032	NGC2632B	6251	5.40	+0.29	−0.09	+0.04	+0.00	−0.01	−0.02	+0.03	N	N
664293387559886464	NGC2632B	4562	3.61	−0.08	+0.12	+0.00	+0.05	+0.08	−0.03	−0.02	Y	N
664297064051880832	NGC2632B	4627	4.26	+0.15	+0.05	+0.01	+0.01	+0.03	+0.13	−0.21	Y	N
664318160931228800	NGC2632B	6025	4.07	−0.01	−0.08	+0.02	−0.07	−0.04	−0.16	−0.08	N	N
664320325594734720	NGC2632B	6277	4.22	+0.15	−0.11	+0.07	+0.00	+0.00	−0.14	+0.02	N	N
664320497393421952	NGC2632B	6140	5.41	+0.30	−0.08	+0.03	+0.03	+0.00	+0.08	+0.00	Y	N
664321218947941632	NGC2632B	5992	4.16	+0.04	−0.07	+0.06	+0.00	−0.01	−0.70	−0.10	N	N
664323349251710848	NGC2632B	4682	4.13	+0.07	+0.04	+0.02	+0.01	+0.03	+0.06	−0.13	N	N
664323761568567808	NGC2632B	4608	3.97	+0.05	+0.08	+0.01	+0.03	+0.05	+0.01	−0.15	Y	N
664324002086740608	NGC2632B	6318	4.44	+0.14	−0.14	+0.03	+0.01	+0.01	−0.21	−0.04	N	N
664325170317925120	NGC2632B	5855	5.10	+0.26	−0.02	+0.02	+0.06	+0.02	+0.32	−0.06	Y	N
664328090895681408	NGC2632B	6197	4.33	+0.04	−0.09	+0.01	+0.03	+0.00	−0.42	+0.08	N	N
664329873304598656	NGC2632B	5781	4.04	+0.07	−0.01	+0.01	+0.03	−0.05	−0.02	−0.10	N	N
664330427357809664	NGC2632B	4852	3.65	−0.17	+0.15	+0.05	+0.08	+0.09	+0.11	+0.02	N	N

Bibliography

Ahumada, R., Prieto, C. A., Almeida, A., Anders, F., Anderson, S. F., Andrews, B. H., Anguiano, B., Arcodia, R., Armengaud, E., Aubert, M., Avila, S., Avila-Reese, V., Badenes, C., Balland, C., Barger, K., Barrera-Ballesteros, J. K., Basu, S., Bautista, J., Beaton, R. L., Beers, T. C., Benavides, B. I. T., Bender, C. F., Bernardi, M., Bershady, M., Beutler, F., Bidin, C. M., Bird, J., Bizyaev, D., Blanc, G. A., Blanton, M. R., Boquien, M., Borissova, J., Bovy, J., Brandt, W. N., Brinkmann, J., Brownstein, J. R., Bundy, K., Bureau, M., Burgasser, A., Burtin, E., Cano-Díaz, M., Capasso, R., Cappellari, M., Carrera, R., Chabanier, S., Chaplin, W., Chapman, M., Cherinka, B., Chiappini, C., Doohyun Choi, P., Chojnowski, S. D., Chung, H., Clerc, N., Coffey, D., Comerford, J. M., Comparat, J., da Costa, L., Cousinou, M.-C., Covey, K., Crane, J. D., Cunha, K., Ilha, G. d. S., Dai, Y. S., Damsted, S. B., Darling, J., Davidson, James W., J., Davies, R., Dawson, K., De, N., de la Macorra, A., De Lee, N., Queiroz, A. B. d. A., Deconto Machado, A., de la Torre, S., Dell'Agli, F., du Mas des Bourboux, H., Diamond-Stanic, A. M., Dillon, S., Donor, J., Drory, N., Duckworth, C., Dwelly, T., Ebelke, G., Eftekharzadeh, S., Davis Eigenbrot, A., Elsworth, Y. P., Eracleous, M., Erfanianfar, G., Escoffier, S., Fan, X., Farr, E., Fernández-Trincado, J. G., Feuillet, D., Finoguenov, A., Fofie, P., Fraser-McKelvie, A., Frinchaboy, P. M., Fromenteau, S., Fu, H., Galbany, L., Garcia, R. A., García-Hernández, D. A., Oehmichen, L. A. G., Ge, J., Maia, M. A. G., Geisler, D., Gelfand, J., Goddy, J., Gonzalez-Perez, V., Grabowski, K., Green, P., Grier, C. J., Guo, H., Guy, J., Harding, P., Hasselquist, S., Hawken, A. J., Hayes, C. R., Hearty, F., Hekker, S., Hogg, D. W., Holtzman, J. A., Horta, D., Hou, J., Hsieh, B.-C., Huber, D., Hunt, J. A. S., Chitham, J. I., Imig, J., Jaber, M., Angel, C. E. J., Johnson, J. A., Jones, A. M., Jönsson, H., Jullo, E., Kim, Y., Kinemuchi, K., Kirkpatrick, Charles C., I., Kite, G. W., Klaene, M., Kneib, J.-P., Kollmeier, J. A., Kong, H., Kounkel, M., Krishnarao, D., Lacerna, I., Lan, T.-W., Lane, R. R., Law, D. R., Le Goff, J.-M., Leung, H. W., Lewis, H., Li, C., Lian, J., Lin, L., Long, D., Longa-Peña, P., Lundgren, B., Lyke, B. W., Ted Mackereth, J., MacLeod, C. L., Majewski, S. R., Manchado, A., Maraston, C., Martini, P., Masseron, T., Masters, K. L., Mathur, S., McDermid, R. M., Merloni, A., Merrifield, M., Mészáros, S., Miglio, A., Minniti, D., Minsley, R., Miyaji, T., Mohammad, F. G., Mosser, B., Mueller, E.-M., Muna, D., Muñoz-Gutiérrez, A., Myers, A. D., Nadathur, S., Nair, P., Nandra, K., do Nascimento, J. C., Nevin, R. J., Newman, J. A., Nidever, D. L., Nitschelm, C., Noterdaeme, P., O'Connell, J. E., Olmstead, M. D., Oravetz, D., Oravetz, A., Osorio, Y., Pace, Z. J., Padilla, N., Palanque-Delabrouille, N., Palicio, P. A., Pan, H.-A., Pan, K., Parker, J., Paviot, R., Peirani, S., Ramŕez, K. P., Penny, S., Percival,

W. J., Perez-Fournon, I., Pérez-Ràfols, I., Petitjean, P., Pieri, M. M., Pinsonneault, M., Poovelil, V. J., Povick, J. T., Prakash, A., Price-Whelan, A. M., Raddick, M. J., Raichoor, A., Ray, A., Rembold, S. B., Rezaie, M., Riffel, R. A., Riffel, R., Rix, H.-W., Robin, A. C., Roman-Lopes, A., Román-Zúñiga, C., Rose, B., Ross, A. J., Rossi, G., Rowlands, K., Rubin, K. H. R., Salvato, M., Sánchez, A. G., Sánchez-Menguiano, L., Sánchez-Gallego, J. R., Sayres, C., Schaefer, A., Schiavon, R. P., Schimoia, J. S., Schlafly, E., Schlegel, D., Schneider, D. P., Schultheis, M., Schwope, A., Seo, H.-J., Serenelli, A., Shafieloo, A., Shamsi, S. J., Shao, Z., Shen, S., Shetrone, M., Shirley, R., Aguirre, V. S., Simon, J. D., Skrutskie, M. F., Slosar, A., Smethurst, R., Sobeck, J., Sodi, B. C., Souto, D., Stark, D. V., Stassun, K. G., Steinmetz, M., Stello, D., Stermer, J., Storchi-Bergmann, T., Streblyanska, A., Stringfellow, G. S., Stutz, A., Suárez, G., Sun, J., Taghizadeh-Popp, M., Talbot, M. S., Tayar, J., Thakar, A. R., Theriault, R., Thomas, D., Thomas, Z. C., Tinker, J., Tojeiro, R., Toledo, H. H., Tremonti, C. A., Troup, N. W., Tuttle, S., Unda-Sanzana, E., Valentini, M., Vargas-González, J., Vargas-Magaña, M., Vázquez-Mata, J. A., Vivek, M., Wake, D., Wang, Y., Weaver, B. A., Weijmans, A.-M., Wild, V., Wilson, J. C., Wilson, R. F., Wolthuis, N., Wood-Vasey, W. M., Yan, R., Yang, M., Yèche, C., Zamora, O., Zarrouk, P., Zasowski, G., Zhang, K., Zhao, C., Zhao, G., Zheng, Z., Zheng, Z., Zhu, G., & Zou, H. 2020, Astrophysical Journal Supplement, 249, 3

Alonso-Santiago, J., Negueruela, I., Marco, A., Tabernero, H. M., González-Fernández, C., & Castro, N. 2017, Monthly Notices of the Royal Astronomy Society, 469, 1330

Bagdonas, V., Drazdauskas, A., Tautvaišienė, G., Smiljanic, R., & Chorniy, Y. 2018, Astronomy and Astrophysics, 615, A165

Beckers, J. M., Ulich, B. L., Shannon, R. R., Carleton, N. P., Geary, J. C., Latham, D. W., Roger, J., Angel, P., Hoffmann, W. F., Low, F. J., Weymann, R. J., & Woolf, N. J. 1981, in Telescopes for the 1980s, Annual Reviews Monograph, ed. G. Burbidge & A. Hewitt, 63–128

Blanton, M. R., Bershady, M. A., Abolfathi, B., Albareti, F. D., Allende Prieto, C., Almeida, A., Alonso-García, J., Anders, F., Anderson, S. F., Andrews, B., & et al. 2017, The Astronomical Journal, 154, 28

Bowen, I. S. & Vaughan, A. H., J. 1973, Applied Optics, 12, 1430

Campante, T. L., Schofield, M., Kuszlewicz, J. S., Bouma, L., Chaplin, W. J., Huber, D., Christensen-Dalsgaard, J., Kjeldsen, H., Bossini, D., North, T. S. H., Appourchaux, T., Latham, D. W., Pepper, J., Ricker, G. R., Stassun, K. G., Vanderspek, R., & Winn, J. N. 2016, The Astrophysical Journal, 830, 138

Cantat-Gaudin, T., Anders, F., Castro-Ginard, A., Jordi, C., Romero-Gómez, M., Soubiran, C., Casamiquela, L., Tarricq, Y., Moitinho, A., Vallenari, A., Bragaglia, A., Krone-Martins, A., & Kounkel, M. 2020, Astronomy and Astrophysics, 640, A1

Carrera, R., Casamiquela, L., Ospina, N., Balaguer-Núñez, L., Jordi, C., & Monteagudo, L. 2015, Astronomy and Astrophysics, 578, A27

Carretta, E., Bragaglia, A., Gratton, R. G., & Tosi, M. 2004a, Astronomy and Astrophysics, 422, 951

—. 2004b, Astronomy and Astrophysics, 422, 951

Christensen-Dalsgaard, J. 1998, in Lecture Notes on Stellar Oscillations (Institut for Fysik og Astronomi, Aarhus Universitet)

da Silveira, M. D., Pereira, C. B., & Drake, N. A. 2018, Monthly Notices of the Royal Astronomy Society, 476, 4907

De Silva, G. M., Carraro, G., D'Orazi, V., Efremova, V., Macpherson, H., Martell, S., & Rizzo, L. 2015, Monthly Notices of the Royal Astronomy Society, 453, 106

Dias, W. S., Alessi, B. S., Moitinho, A., & Lépine, J. R. D. 2002, Astronomy and Astrophysics, 389, 871

Donor, J., Frinchaboy, P. M., Cunha, K., O'Connell, J. E., Allende Prieto, C., Almeida, A., Anders, F., Beaton, R., Bizyaev, D., Brownstein, J. R., Carrera, R., Chiappini, C., Cohen, R., García-Hernández, D. A., Geisler, D., Hasselquist, S., Jönsson, H., Lane, R. R., Majewski, S. R., Minniti, D., Bidin, C. M., Pan, K., Roman-Lopes, A., Sobeck, J. S., & Zasowski, G. 2020, The Astronomical Journal, 159, 199

Donor, J., Frinchaboy, P. M., Cunha, K., Thompson, B., O'Connell, J., Zasowski, G., Jackson, K. M., Meyer McGrath, B., Almeida, A., Bizyaev, D., Carrera, R., García-Hernández, D. A., Nitschelm, C., Pan, K., & Zamora, O. 2018, The Astronomical Journal, 156, 142

Eisenstein, D. J., Weinberg, D. H., Agol, E., Aihara, H., Allende Prieto, C., Anderson, S. F., Arns, J. A., Aubourg, É., Bailey, S., Balbinot, E., & et al. 2011, The Astronomical Journal, 142, 72

Fabricant, D., Fata, R., Roll, J., Hertz, E., Caldwell, N., Gauron, T., Geary, J., McLeod, B., Szentgyorgyi, A., Zajac, J., Kurtz, M., Barberis, J., Bergner, H., Brown, W., Conroy, M., Eng, R., Geller, M., Goddard, R., Honsa, M., Mueller, M., Mink, D., Ordway, M., Tokarz, S., Woods, D., Wyatt, W., Epps, H., & Dell'Antonio, I. 2005, Publications of the Astronomical Society of the Pacific, 117, 1411

Frinchaboy, P. M. & Majewski, S. R. 2008, The Astronomical Journal, 136, 118

Gaia Collaboration, Brown, A. G. A., Vallenari, A., Prusti, T., de Bruijne, J. H. J., Babusiaux, C., Bailer-Jones, C. A. L., Biermann, M., Evans, D. W., Eyer, L., Jansen, F., Jordi, C., Klioner, S. A., Lammers, U., Lindegren, L., Luri, X., Mignard, F., Panem, C., Pourbaix, D., Randich, S., Sartoretti, P., Siddiqui, H. I., Soubiran, C., van Leeuwen, F., Walton, N. A., Arenou, F., Bastian, U., Cropper, M., Drimmel, R., Katz, D., Lattanzi, M. G., Bakker, J., Cacciari, C., Castañeda, J., Chaoul, L., Cheek, N., De Angeli, F., Fabricius, C., Guerra, R., Holl, B., Masana, E., Messineo, R., Mowlavi, N., Nienartowicz, K., Panuzzo, P., Portell, J., Riello, M., Seabroke, G. M., Tanga,

P., Thévenin, F., Gracia-Abril, G., Comoretto, G., Garcia-Reinaldos, M., Teyssier, D., Altmann, M., Andrae, R., Audard, M., Bellas-Velidis, I., Benson, K., Berthier, J., Blomme, R., Burgess, P., Busso, G., Carry, B., Cellino, A., Clementini, G., Clotet, M., Creevey, O., Davidson, M., De Ridder, J., Delchambre, L., Dell'Oro, A., Ducourant, C., Fernández-Hernández, J., Fouesneau, M., Frémat, Y., Galluccio, L., García-Torres, M., González-Núñez, J., González-Vidal, J. J., Gosset, E., Guy, L. P., Halbwachs, J. L., Hambly, N. C., Harrison, D. L., Hernández, J., Hestroffer, D., Hodgkin, S. T., Hutton, A., Jasniewicz, G., Jean-Antoine-Piccolo, A., Jordan, S., Korn, A. J., Krone-Martins, A., Lanzafame, A. C., Lebzelter, T., Löffler, W., Manteiga, M., Marrese, P. M., Martín-Fleitas, J. M., Moitinho, A., Mora, A., Muinonen, K., Osinde, J., Pancino, E., Pauwels, T., Petit, J. M., Recio-Blanco, A., Richards, P. J., Rimoldini, L., Robin, A. C., Sarro, L. M., Siopis, C., Smith, M., Sozzetti, A., Süveges, M., Torra, J., van Reeven, W., Abbas, U., Abreu Aramburu, A., Accart, S., Aerts, C., Altavilla, G., Álvarez, M. A., Alvarez, R., Alves, J., Anderson, R. I., Andrei, A. H., Anglada Varela, E., Antiche, E., Antoja, T., Arcay, B., Astraatmadja, T. L., Bach, N., Baker, S. G., Balaguer-Núñez, L., Balm, P., Barache, C., Barata, C., Barbato, D., Barblan, F., Barklem, P. S., Barrado, D., Barros, M., Barstow, M. A., Bartholomé Muñoz, S., Bassilana, J. L., Becciani, U., Bellazzini, M., Berihuete, A., Bertone, S., Bianchi, L., Bienaymé, O., Blanco-Cuaresma, S., Boch, T., Boeche, C., Bombrun, A., Borrachero, R., Bossini, D., Bouquillon, S., Bourda, G., Bragaglia, A., Bramante, L., Breddels, M. A., Bressan, A., Brouillet, N., Brüsemeister, T., Brugaletta, E., Bucciarelli, B., Burlacu, A., Busonero, D., Butkevich, A. G., Buzzi, R., Caffau, E., Cancelliere, R., Cannizzaro, G., Cantat-Gaudin, T., Carballo, R., Carlucci, T., Carrasco, J. M., Casamiquela, L., Castellani, M., Castro-Ginard, A., Charlot, P., Chemin, L., Chiavassa, A., Cocozza, G., Costigan, G., Cowell, S., Crifo, F., Crosta, M., Crowley, C., Cuypers, J., Dafonte, C., Damerdji, Y., Dapergolas, A., David, P., David, M., de Laverny, P., De Luise, F., De March, R., de Martino, D., de Souza, R., de Torres, A., Debosscher, J., del Pozo, E., Delbo, M., Delgado, A., Delgado, H. E., Di Matteo, P., Diakite, S., Diener, C., Distefano, E., Dolding, C., Drazinos, P., Durán, J., Edvardsson, B., Enke, H., Eriksson, K., Esquej, P., Eynard Bontemps, G., Fabre, C., Fabrizio, M., Faigler, S., Falcão, A. J., Farràs Casas, M., Federici, L., Fedorets, G., Fernique, P., Figueras, F., Filippi, F., Findeisen, K., Fonti, A., Fraile, E., Fraser, M., Frézouls, B., Gai, M., Galleti, S., Garabato, D., García-Sedano, F., Garofalo, A., Garralda, N., Gavel, A., Gavras, P., Gerssen, J., Geyer, R., Giacobbe, P., Gilmore, G., Girona, S., Giuffrida, G., Glass, F., Gomes, M., Granvik, M., Gueguen, A., Guerrier, A., Guiraud, J., Gutiérrez-Sánchez, R., Haigron, R., Hatzidimitriou, D., Hauser, M., Haywood, M., Heiter, U., Helmi, A., Heu, J., Hilger, T., Hobbs, D., Hofmann, W., Holland, G., Huckle, H. E., Hypki, A., Icardi, V., Janßen, K., Jevardat de Fombelle, G., Jonker, P. G., Juhász, Á. L., Julbe, F., Karampelas, A., Kewley, A., Klar, J., Kochoska, A., Kohley, R., Kolenberg, K., Kontizas, M., Kontizas, E., Koposov, S. E., Kordopatis, G., Kostrzewa-Rutkowska, Z., Koubsky, P., Lambert, S., Lanza, A. F., Lasne, Y., Lavigne, J. B., Le Fustec, Y., Le Poncin-Lafitte, C., Lebreton, Y., Leccia, S., Leclerc, N., Lecoeur-Taibi, I., Lenhardt, H., Leroux, F., Liao, S., Licata, E., Lindstrøm, H. E. P., Lister, T. A., Livanou, E., Lobel, A., López, M., Managau, S., Mann, R. G., Mantelet, G., Marchal, O., Marchant, J. M., Marconi, M., Marinoni, S., Marschalkó, G., Marshall, D. J.,

Martino, M., Marton, G., Mary, N., Massari, D., Matijevič, G., Mazeh, T., McMillan, P. J., Messina, S., Michalik, D., Millar, N. R., Molina, D., Molinaro, R., Molnár, L., Montegriffo, P., Mor, R., Morbidelli, R., Morel, T., Morris, D., Mulone, A. F., Muraveva, T., Musella, I., Nelemans, G., Nicastro, L., Noval, L., O'Mullane, W., Ordénovic, C., Ordóñez-Blanco, D., Osborne, P., Pagani, C., Pagano, I., Pailler, F., Palacin, H., Palaversa, L., Panahi, A., Pawlak, M., Piersimoni, A. M., Pineau, F. X., Plachy, E., Plum, G., Poggio, E., Poujoulet, E., Prša, A., Pulone, L., Racero, E., Ragaini, S., Rambaux, N., Ramos-Lerate, M., Regibo, S., Reylé, C., Riclet, F., Ripepi, V., Riva, A., Rivard, A., Rixon, G., Roegiers, T., Roelens, M., Romero-Gómez, M., Rowell, N., Royer, F., Ruiz-Dern, L., Sadowski, G., Sagristà Sellés, T., Sahlmann, J., Salgado, J., Salguero, E., Sanna, N., Santana-Ros, T., Sarasso, M., Savietto, H., Schultheis, M., Sciacca, E., Segol, M., Segovia, J. C., Ségransan, D., Shih, I. C., Siltala, L., Silva, A. F., Smart, R. L., Smith, K. W., Solano, E., Solitro, F., Sordo, R., Soria Nieto, S., Souchay, J., Spagna, A., Spoto, F., Stampa, U., Steele, I. A., Steidelmüller, H., Stephenson, C. A., Stoev, H., Suess, F. F., Surdej, J., Szabados, L., Szegedi-Elek, E., Tapiador, D., Taris, F., Tauran, G., Taylor, M. B., Teixeira, R., Terrett, D., Teyssandier, P., Thuillot, W., Titarenko, A., Torra Clotet, F., Turon, C., Ulla, A., Utrilla, E., Uzzi, S., Vaillant, M., Valentini, G., Valette, V., van Elteren, A., Van Hemelryck, E., van Leeuwen, M., Vaschetto, M., Vecchiato, A., Veljanoski, J., Viala, Y., Vicente, D., Vogt, S., von Essen, C., Voss, H., Votruba, V., Voutsinas, S., Walmsley, G., Weiler, M., Wertz, O., Wevers, T., Wyrzykowski, Ł., Yoldas, A., Žerjal, M., Ziaeepour, H., Zorec, J., Zschocke, S., Zucker, S., Zurbach, C., & Zwitter, T. 2018, Astronomy and Astrophysics, 616, A1

García, R. A. & Ballot, J. 2019, Living Reviews in Solar Physics, 16, 4

García Pérez, A. E., Allende Prieto, C., Holtzman, J. A., Shetrone, M., Mészáros, S., Bizyaev, D., Carrera, R., Cunha, K., García-Hernández, D. A., Johnson, J. A., Majewski, S. R., Nidever, D. L., Schiavon, R. P., Shane, N., Smith, V. V., Sobeck, J., Troup, N., Zamora, O., Weinberg, D. H., Bovy, J., Eisenstein, D. J., Feuillet, D., Frinchaboy, P. M., Hayden, M. R., Hearty, F. R., Nguyen, D. C., O'Connell, R. W., Pinsonneault, M. H., Wilson, J. C., & Zasowski, G. 2016, The Astronomical Journal, 151, 144

Gilliland, R. L., Brown, T. M., Christensen-Dalsgaard, J., Kjeldsen, H., Aerts, C., Appourchaux, T., Basu, S., Bedding, T. R., Chaplin, W. J., Cunha, M. S., De Cat, P., De Ridder, J., Guzik, J. A., Handler, G., Kawaler, S., Kiss, L., Kolenberg, K., Kurtz, D. W., Metcalfe, T. S., Monteiro, M. J. P. F. G., Szabó, R., Arentoft, T., Balona, L., Debosscher, J., Elsworth, Y. P., Quirion, P.-O., Stello, D., Suárez, J. C., Borucki, W. J., Jenkins, J. M., Koch, D., Kondo, Y., Latham, D. W., Rowe, J. F., & Steffen, J. H. 2010, Publications of the Astronomical Society of the Pacific, 122, 131

Gunn, J. E., Siegmund, W. A., Mannery, E. J., Owen, R. E., Hull, C. L., Leger, R. F., Carey, L. N., Knapp, G. R., York, D. G., Boroski, W. N., Kent, S. M., Lupton, R. H., Rockosi, C. M., Evans, M. L., Waddell, P., Anderson, J. E., Annis, J., Barentine, J. C., Bartoszek, L. M., Bastian, S., Bracker, S. B., Brewington, H. J., Briegel, C. I., Brinkmann, J., Brown, Y. J., Carr, M. A., Czarapata, P. C., Drennan, C. C.,

Dombeck, T., Federwitz, G. R., Gillespie, B. A., Gonzales, C., Hansen, S. U., Harvanek, M., Hayes, J., Jordan, W., Kinney, E., Klaene, M., Kleinman, S. J., Kron, R. G., Kresinski, J., Lee, G., Limmongkol, S., Lindenmeyer, C. W., Long, D. C., Loomis, C. L., McGehee, P. M., Mantsch, P. M., Neilsen, Jr., E. H., Neswold, R. M., Newman, P. R., Nitta, A., Peoples, Jr., J., Pier, J. R., Prieto, P. S., Prosapio, A., Rivetta, C., Schneider, D. P., Snedden, S., & Wang, S.-i. 2006, The Astronomical Journal, 131, 2332

Hekker, S. & Christensen-Dalsgaard, J. 2017, The Astronomy and Astrophysics Review, 25

Holtzman, J. A., Hasselquist, S., Shetrone, M., Cunha, K., Allende Prieto, C., Anguiano, B., Bizyaev, D., Bovy, J., Casey, A., Edvardsson, B., Johnson, J. A., Jönsson, H., Meszaros, S., Smith, V. V., Sobeck, J., Zamora, O., Chojnowski, S. D., Fernandez-Trincado, J., Garcia-Hernandez, D. A., Majewski, S. R., Pinsonneault, M., Souto, D., Stringfellow, G. S., Tayar, J., Troup, N., & Zasowski, G. 2018, The Astronomical Journal, 156, 125

Huber, D., Bedding, T. R., Stello, D., Mosser, B., Mathur, S., Kallinger, T., Hekker, S., Elsworth, Y. P., Buzasi, D. L., De Ridder, J., Gilliland, R. L., Kjeldsen, H., Chaplin, W. J., García, R. A., Hale, S. J., Preston, H. L., White, T. R., Borucki, W. J., Christensen-Dalsgaard, J., Clarke, B. D., Jenkins, J. M., & Koch, D. 2010, The Astrophysical Journal, 723, 1607

Jönsson, H., Holtzman, J. A., Allende Prieto, C., Cunha, K., García-Hernández, D. A., Hasselquist, S., Masseron, T., Osorio, Y., Shetrone, M., Smith, V., Stringfellow, G. S., Bizyaev, D., Edvardsson, B., Majewski, S. R., Mészáros, S., Souto, D., Zamora, O., Beaton, R. L., Bovy, J., Donor, J., Pinsonneault, M. H., Poovelil, V. J., & Sobeck, J. 2020, The Astronomical Journal, 160, 120

Kılıçoğlu, T., Monier, R., Richer, J., Fossati, L., & Albayrak, B. 2016, The Astronomical Journal, 151, 49

Kurtz, D., Jeffrey, S., & Aerts, C. 2016, Astronomy & Geophysics, 57, 4.37

Leavitt, H. S. & Pickering, E. C. 1912, Harvard College Observatory Circular, 173, 1

Luck, R. E. 1994, Astrophysical Journal Supplement, 91, 309

Majewski, S. R., Schiavon, R. P., Frinchaboy, P. M., Allende Prieto, C., Barkhouser, R., Bizyaev, D., Blank, B., Brunner, S., Burton, A., Carrera, R., Chojnowski, S. D., Cunha, K., Epstein, C., Fitzgerald, G., García Pérez, A. E., Hearty, F. R., Henderson, C., Holtzman, J. A., Johnson, J. A., Lam, C. R., Lawler, J. E., Maseman, P., Mészáros, S., Nelson, M., Nguyen, D. C., Nidever, D. L., Pinsonneault, M., Shetrone, M., Smee, S., Smith, V. V., Stolberg, T., Skrutskie, M. F., Walker, E., Wilson, J. C., Zasowski, G., Anders, F., Basu, S., Beland, S., Blanton, M. R., Bovy, J., Brownstein, J. R., Carlberg, J., Chaplin, W., Chiappini, C., Eisenstein, D. J., Elsworth, Y., Feuillet, D., Fleming, S. W., Galbraith-Frew, J., García, R. A., García-Hernández, D. A., Gillespie,

B. A., Girardi, L., Gunn, J. E., Hasselquist, S., Hayden, M. R., Hekker, S., Ivans, I., Kinemuchi, K., Klaene, M., Mahadevan, S., Mathur, S., Mosser, B., Muna, D., Munn, J. A., Nichol, R. C., O'Connell, R. W., Parejko, J. K., Robin, A. C., Rocha-Pinto, H., Schultheis, M., Serenelli, A. M., Shane, N., Silva Aguirre, V., Sobeck, J. S., Thompson, B., Troup, N. W., Weinberg, D. H., & Zamora, O. 2017, The Astronomical Journal, 154, 94

Martinez, C. F., Holanda, N., Pereira, C. B., & Drake, N. A. 2020, Monthly Notices of the Royal Astronomy Society, 494, 1470

Martinez-Medina, L. A., Gieles, M., Pichardo, B., & Peimbert, A. 2018, Monthly Notices of the Royal Astronomy Society, 474, 32

Mitschang, A. W., De Silva, G. M., & Zucker, D. B. 2012, Monthly Notices of the Royal Astronomy Society, 422, 3527

Myers, N., Donor, J., Spoo, T., Frinchaboy, P. M., Cunha, K., Price-Whelan, A. M., Majewski, S. R., Beaton, R. L., Zasowski, G., O'Connell, J., Ray, A. E., Bizyaev, D., Chiappini, C., García-Hernández, D. A., Geisler, D., Jönsson, H., Lane, R. R., Longa-Peña, P., Minchev, I., Minniti, D., Nitschelm, C., & Roman-Lopes, A. 2022, The Astronomical Journal, 164, 85

Ness, M., Hogg, D. W., Rix, H.-W., Ho, A. Y. Q., & Zasowski, G. 2015, The Astrophysical Journal, 808, 16

Netopil, M., Paunzen, E., Heiter, U., & Soubiran, C. 2016, Astronomy and Astrophysics, 585, A150

Nidever, D. L., Holtzman, J. A., Allende Prieto, C., Beland, S., Bender, C., Bizyaev, D., Burton, A., Desphande, R., Fleming, S. W., García Pérez, A. E., Hearty, F. R., Majewski, S. R., Mészáros, S., Muna, D., Nguyen, D., Schiavon, R. P., Shetrone, M., Skrutskie, M. F., Sobeck, J. S., & Wilson, J. C. 2015, The Astronomical Journal, 150, 173

Pace, G., Danziger, J., Carraro, G., Melendez, J., François, P., Matteucci, F., & Santos, N. C. 2010a, Astronomy and Astrophysics, 515, A28

Pace, G., Danziger, J., Carraro, G., Melendez, J., François, P., Matteucci, F., & Santos, N. C. 2010b, Astronomy and Astrophysics, 515, A28

Pace, G., Pasquini, L., & François, P. 2008, Astronomy and Astrophysics, 489, 403

Payne, C. H. 1925, PhD thesis, RADCLIFFE COLLEGE.

Peña Suárez, V. J., Sales Silva, J. V., Katime Santrich, O. J., Drake, N. A., & Pereira, C. B. 2018, The Astrophysical Journal, 854, 184

Pinsonneault, M. H., Elsworth, Y., Epstein, C., Hekker, S., Mészáros, S., Chaplin, W. J., Johnson, J. A., García, R. A., Holtzman, J., Mathur, S., García Pérez, A., Silva Aguirre, V., Girardi, L., Basu, S., Shetrone, M., Stello, D., Allende Prieto, C., An, D., Beck, P., Beers, T. C., Bizyaev, D., Bloemen, S., Bovy, J., Cunha, K., De Ridder, J., Frinchaboy, P. M., García-Hernández, D. A., Gilliland, R., Harding, P., Hearty, F. R., Huber, D., Ivans, I., Kallinger, T., Majewski, S. R., Metcalfe, T. S., Miglio, A., Mosser, B., Muna, D., Nidever, D. L., Schneider, D. P., Serenelli, A., Smith, V. V., Tayar, J., Zamora, O., & Zasowski, G. 2014, Astrophysical Journal Supplement, 215, 19

Pinsonneault, M. H., Elsworth, Y. P., Tayar, J., Serenelli, A., Stello, D., Zinn, J., Mathur, S., Garcí a, R. A., Johnson, J. A., Hekker, S., Huber, D., Kallinger, T., Mészáros, S., Mosser, B., Stassun, K., Girardi, L., Rodrigues, T. S., Aguirre, V. S., An, D., Basu, S., Chaplin, W. J., Corsaro, E., Cunha, K., García-Hernández, D. A., Holtzman, J., Jönsson, H., Shetrone, M., Smith, V. V., Sobeck, J. S., Stringfellow, G. S., Zamora, O., Beers, T. C., Fernández-Trincado, J. G., Frinchaboy, P. M., Hearty, F. R., & Nitschelm, C. 2018, The Astrophysical Journal Supplement Series, 239, 32

Ray, A. E., Frinchaboy, P. M., Donor, J., Chojnowski, S. D., & Melendez, M. 2022, The Astronomical Journal, 163, 195

Reddy, A. B. S., Giridhar, S., & Lambert, D. L. 2013a, Monthly Notices of the Royal Astronomy Society, 431, 3338

Reddy, A. B. S., Giridhar, S., & Lambert, D. L. 2013b, Monthly Notices of the Royal Astronomy Society, 431, 3338

Reddy, A. B. S., Giridhar, S., & Lambert, D. L. 2015a, Monthly Notices of the Royal Astronomy Society, 450, 4301

Reddy, A. B. S., Giridhar, S., & Lambert, D. L. 2015b, Monthly Notices of the Royal Astronomy Society, 450, 4301

Reddy, A. B. S., Lambert, D. L., & Giridhar, S. 2016, Monthly Notices of the Royal Astronomy Society, 463, 4366

Sandquist, E. L., Jessen-Hansen, J., Shetrone, M. D., Brogaard, K., Meibom, S., Leitner, M., Stello, D., Bruntt, H., Antoci, V., Orosz, J. A., Grundahl, F., & Frandsen, S. 2016, The Astrophysical Journal, 831, 11

Santos, N. C., Lovis, C., Pace, G., Melendez, J., & Naef, D. 2009, Astronomy and Astrophysics, 493, 309

Stello, D., Huber, D., Sharma, S., Johnson, J., Lund, M. N., Handberg, R., Buzasi, D. L., Silva Aguirre, V., Chaplin, W. J., Miglio, A., Pinsonneault, M., Basu, S., Bedding, T. R., Bland-Hawthorn, J., Casagrande, L., Davies, G., Elsworth, Y., Garcia, R. A., Mathur, S., Di Mauro, M. P., Mosser, B., Schneider, D. P., Serenelli, A., & Valentini, M. 2015, The Astrophysical Journal Letters, 809, L3

Sun, Q., Deliyannis, C. P., Steinhauer, A., Twarog, B. A., & Anthony-Twarog, B. J. 2020, The Astronomical Journal, 159, 220

Ting, Y.-S., De Silva, G. M., Freeman, K. C., & Parker, S. J. 2012, Monthly Notices of the Royal Astronomy Society, 427, 882

Tonry, J. & Davis, M. 1979, The Astronomical Journal, 84, 1511

Villanova, S., Carraro, G., Geisler, D., Monaco, L., & Assmann, P. 2018, The Astrophysical Journal, 867, 34

Wilson, J. C., Hearty, F., Skrutskie, M. F., Majewski, S. R., Schiavon, R., Eisenstein, D., Gunn, J., Holtzman, J., Nidever, D., Gillespie, B., Weinberg, D., Blank, B., Henderson, C., Smee, S., Barkhouser, R., Harding, A., Hope, S., Fitzgerald, G., Stolberg, T., Arns, J., Nelson, M., Brunner, S., Burton, A., Walker, E., Lam, C., Maseman, P., Barr, J., Leger, F., Carey, L., MacDonald, N., Ebelke, G., Beland, S., Horne, T., Young, E., Rieke, G., Rieke, M., O'Brien, T., Crane, J., Carr, M., Harrison, C., Stoll, R., Vernieri, M., Shetrone, M., Allende-Prieto, C., Johnson, J., Frinchaboy, P., Zasowski, G., Garcia Perez, A., Bizyaev, D., Cunha, K., Smith, V. V., Meszaros, S., Zhao, B., Hayden, M., Chojnowski, S. D., Andrews, B., Loomis, C., Owen, R., Klaene, M., Brinkmann, J., Stauffer, F., Long, D., Jordan, W., Holder, D., Cope, F., Naugle, T., Pfaffenberger, B., Schlegel, D., Blanton, M., Muna, D., Weaver, B., Snedden, S., Pan, K., Brewington, H., Malanushenko, E., Malanushenko, V., Simmons, A., Oravetz, D., Mahadevan, S., & Halverson, S. 2012, in Proceedings of the SPIE, Vol. 8446, Ground-based and Airborne Instrumentation for Astronomy IV, 84460H

Yong, D., Carney, B. W., & Friel, E. D. 2012, The Astronomical Journal, 144, 95

Yong, D., Carney, B. W., & Teixera de Almeida, M. L. 2005, The Astronomical Journal, 130, 597

Zinn, J. C., Stello, D., Elsworth, Y., García, R. A., Kallinger, T., Mathur, S., Mosser, B., Hon, M., Bugnet, L., Jones, C., Reyes, C., Sharma, S., Schönrich, R., Warfield, J. T., Luger, R., Vanderburg, A., Kobayashi, C., Pinsonneault, M. H., Johnson, J. A., Huber, D., Buder, S., Joyce, M., Bland-Hawthorn, J., Casagrande, L., Lewis, G. F., Miglio, A., Nordlander, T., Davies, G. R., Silva, G. D., Chaplin, W. J., & Silva Aguirre, V. 2022, The Astrophysical Journal, 926, 191

VITA

Personal Background	Amy Elaine Ray Lexington, TN Daughter of Brad and Nancy Ray
Education	Diploma, Lexington High School, Lexington, TN, 2008 Bachelor of Science, Physics, Mississippi State University, Starkville, MS, 2013 Master of Science, Physics, Mississippi State University, Starkville, MS, 2017
Experience	Staff Astroomer, Hobby-Eberly Telescope, Fort Davis, TX, 2022-Present Lecturer, Texas State University, San Marcos TX, 2021-2022 Research assistantship, Texas Christian University, Fort Worth, TX, 2018-2021 Teaching assistantship, Texas Christian University, Fort Worth, TX, 2016-2018 Research assistantship, Mississippi State University, Starkville, MS, 2013-2015 Summer research assistant, Mississippi State University, Starkville, MS,
Professional Memberships	American Astronomical Society American Association for the Advancement of Science

ABSTRACT

CHEMICAL ABUNDANCES OF OPEN CLUSTERS USING *THE CANNON*: APPLICATION TO IMPROVE CALIBRATION OF ASTEROSEISMIC AGES

by Amy E. Ray, Ph.D., 2022
Department of Physics and Astronomy
Texas Christian University

Research Advisor: Peter M. Frinchaboy III, Professor of Physics & Astronomy

Precise stellar ages for field stars or stars that are not gravitationally bound to other stars are still elusive today. If precise ages were able to be determined, they would have a significant impact on our understanding of the history of stellar formation in the Milky Way. It would also provide a basis for understanding stellar formation in other galaxies as well. More accurate ages of halo stars, thought to be the oldest stars in the Milky Way, could provide an even better limit on the age of the universe itself. Determining these ages with better precision is crucial to our understanding of the universe. Current methods to determine age estimates of stars, such as spectroscopy and asteroseismology, individually have very large uncertainties. Combining these two age estimation methods would significantly reduce this uncertainty. In this dissertation, metallicites and asteroseismology data for a set of open clusters are combined to produce a new asteroseismic age-metallicity-mass relation to reduce the uncertainty in age estimates of stars. Open clusters are the ideal age calibrator, however few have good asteroseismic data. To date, there have been no larger scale surveys of open clusters that compare asteroseismology and spectroscopy estimates of stellar ages, due to the limits of area coverage from the

Kepler mission. The approach of this study is to more than double the number of clusters with high-quality asteroseismology and high-resolution abundance determinations by observing a sample of 10 open clusters. These clusters were chosen as they overlapped with *Kepler* 2 (K2) campaign fields to utilize the asteroseismology observations of giant stars in the K2 fields. We analyze the clusters and use *The Cannon* to measure abundances of [Fe/H], [Mg/Fe], [Si/Fe], [Ni/Fe], [Ca/Fe], [Na/Fe],and [V/Fe] and determine cluster membership. Using this smaple, we present a new asteroseismic age-metallicity-mass relation that improves the age precision for Mily Way disk field stars using asteroseismology.